# GENERAL AVIATION OMEGA NAVIGATION IN THE NATIONAL AIRSPACE SYSTEM

MIT

DEPARTMENT OF AERONAUTICS & ASTRONAUTICS

FLIGHT TRANSPORTATION LABORATORY
Cambridge, Mass. 02139

June 1976

FTL R76-7

# GENERAL AVIATION OMEGA NAVIGATION IN THE NATIONAL AIRSPACE SYSTEM

by

C. Edward Wischmeyer

ACKNOWLEDGMENTS

This thesis work was performed under a wide variety of circumstances, and with the assistance of many people. Most outstanding among these are my advisor, Professor Walter M. Hollister, without whose constructive criticisms, positive encouragement and wisdom this thesis would not have been accomplished; Mr. Anthony E. Scandora, who supplied invaluable technical help; and Mr. Peter V. Hwoschinsky, whose work on closely related topics gave us many opportunities to work together. Many other people provided cooperation, time, hardware, assistance, ideas, and inspriration. I was fortunate to work with many fine and worthwhile people, whose omission by name here in no way reflects my lack of gratitude. My doctoral committee consisted of Professors Robert W. Simpson, Alan S. Willsky, and Walter Wrigley, who introduced me to the concept of graduate education as a uniquely wonderful opportunity.

The second appendix of this thesis was written for another report under NASA Contract NAS1-13644, coauthored by Hwoschinsky and others. Thus, the text of the appendix reflects the editing of various people. Similarly, the data base on which the analysis of Chapter VI is based was performed under that same contract.

Typing of this thesis was done by Deborah Buenz, Donna Baldwin, and Clare Walker, of Systems Control, Inc., whose assistance is gratefully acknowledged.

Lastly, this thesis was supported by NASA under the Tri-University program, Grant No. NGL-22-009-640, and I am most grateful for their support.

TABLE OF CONTENTS

## List of Figures

List of Figures (Continued)

## List of Figures (Continued)

## List of Figures (Concluded)

## List of Tables

## List of Tables (Concluded)

# CHAPTER I

## INTRODUCTION

Omega navigation (33) has great potential as a navigation sensor for general aviation aircraft. Advantages of Omega navigation include signal availability at all altitudes, and no need for overflying of various stations. Also, because Omega coverage is not localized to small geographic areas, area navigation is an implicit capability of airborne Omega receivers. For use in the National Airspace System, several questions arise: How accurate is Omega navigation? How do you use the measurements made to give navigation information? What are the noise sources? How can these noise sources be eliminated or minimized? How do you use Omega in the National Airspace System?

This thesis attempts to answer these questions based upon a 70-hour flight test program, mathematical models, analysis of the literature, and the author's experience as a commercially licensed, instrument-rated pilot. The thesis rather naturally divides into two parts: the first, Chapters II through VIII, attempts to answer the questions of Omega accuracy and operational characteristics. The second part of the thesis, Chapters IX through XVI, considers the questions of Omega implementation, including regulatory aspects and details required by good operating practice.

The first part of the thesis, Chapters II through VIII, concerns Omega accuracies and the results of a 70-hour flight test program. Omega noise sources discussed in the literature were used for mathematical models, and a noise source not considered in the literature is discussed and measured. This is "short-term Omega noise", which is the noise in phase between successive measurements. For long time constant receivers, this noise is not important, but

for light aircraft navigation, this is an important noise source. Analysis of the Weibull distribution showed little applicability of this distribution to Omega navigation errors, based upon the experience acquired in this program with a low-cost, commercially available Omega receiver. This flight test is also discussed in Refs. 16 and 17. In addition, four approaches were flown using Omega navigation, with surprisingly good results. Based upon the flight test data and the short-term noise measurements, mathematical models were made to determine RMS error of differential Omega with variations in update rate, and path-following accuracies available using Omega.

The second part of the thesis concerns Omega implementation. The various configurations of Omega receivers are discussed. These configurations differ in what information is processed and how this information is used to give position information. Present regulations for Omega receivers are discussed, and future requirements for airborne Omega receivers, such as self-test and fail-soft capabilities, are discussed. Problems of waypoint setting errors with area navigation systems are discussed, and an easy method of error detection is shown which is compatible with Omega waypoint definition and which will allow use of standard aeronautical charts with minimal changes. Differential Omega is discussed in terms of message content and uplink medium.

The results of the thesis are boiled down into the last chapter, the Conclusions. All of the meaty points are discussed briefly. Appendices include data on the approaches flown with the Omega receiver; the data collection and reduction for the flight evaluation program; and copyright agreement restrictions on reproduction of certain figures in the thesis based upon copyrighted approach plates.

# CHAPTER II

# OMEGA NOISE PHENOMENA

## 2.1 Introduction

Omega "noise" phenomena can be fitted into two broad categories: propagation anomalies and short-term noise. Propagation anomalies are those factors which cause the phase of the received Omega signal to vary, whereas short-term noise refers to the variations in this received phase from measurement to measurement. Propagation anomalies include Sudden Ionospheric Distrubances (SID), Polar Cap Absorption (PCA), diurnal variations of received phase, and local phase anomalies, if any. Short-term noise is induced by lightning noise, 60 Hz interference, 400 Hz interference, modal interference, reradiated Omega signals, and precipitation static. These phenomena are discussed below.

## 2.2 Propagation Anomalies

Propagation anomalies induce changes in received phase which will be observed by all Omega receiver front ends and phase detectors. Omega signals travel in the waveguide formed by the earth's surface and the ionosphere, and are prone to waveguide phenomena. Primarily, phase shifts are caused by changes in the height of the ionosphere, but other factors are important.

Sudden Ionospheric Disturbances are one form of unpredictable phase anomaly. These events are caused by X-rays emitted by solar flares striking the ionosphere, lowering its height. Typically, these SIDs last 49 minutes, with the first six minutes inducing a phase shift in Omega signals of 15 cec (centicycles) followed by a linear recovery. The largest on record caused a phase shift of 97 cec, and lasted for two hours. Figure 2-1 shows the effects of a SID on a receiver phase.

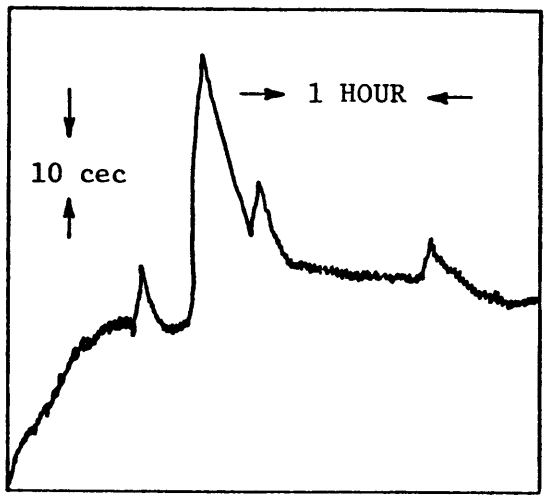


Figure 2-1. Sudden Ionospheric Disturbance (Ref. 3)

Some solar flares emit protons which are funneled into high latitude regions by a complex mechanism involving the earth's magnetosphere. These protons cause Polar Cap Absorption events, which can cause severe signal attenuation and phase shifts on high latitude propagation paths. PCAs are not characterized by a well defined shape like SIDs, and can last for several days. The largest on record caused a phase shift of 87 cec.

Diurnal variations in Omega signals are caused by the daily changes in the height of the ionosphere. These changes are well correlated from day to day and depend upon sunlight striking the ionosphere. Thus, seasonal variations are also noted. Diurnal corrections are included in the so-called skywave correction tables in Ref. 1, which also include phase anomalies induced by the differing surface conductivities of the earth with ice, water, and land. Figure 2-2 shows a typical diurnal variation pattern with skywave correction and residual error.

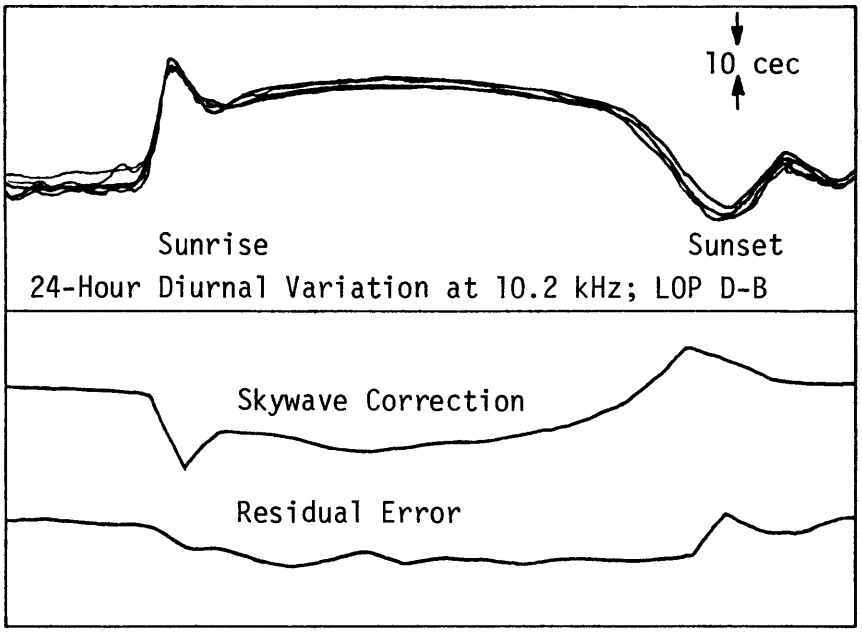


Figure 2-2. Diurnal Variation in Received Phase (Ref. 3)

Local phase anomalies are theoretically possible with changes in local surface conductivities, such as along shorelines. Based upon the experience of the flight test program, however, their effects, if any, are negligible.

## 2.3 Short-Term Noise

Short-term noise is the error of the phase detectors caused by noise added to the Omega signal. This noise can include lightning noise and various sorts of interference.

Lightning noise is discussed more fully in Chapter 4.4. This noise is correlated over a period of about one millisecond, and is impulsive in nature. This noise also travels in a waveguide mode, and should, therefore, display good correlation in distance. Ref. 13 describes the mechanisms of this noise in detail.

The 10.2 kHz Omega frequency is used by virtually all Omega receivers. However, 10.2 kHz is a multiple of 50, 60 and 400 Hz, which are common AC power supply frequencies. Hence, any nonlinearities which would generate the appropriate harmonics would also cause signals at the 10.2 kHz Omega frequency.

Omega signals themselves can cause interference. Near the Omega antennae, various waveguide modes of propagation are present, with differing rates of attentuation with distance. If the receiver is too close to the antenna, modes other than the primary can cause interference. Another interesting phenomenon occurs on the ground. It has been found (2) that trees can re-radiate Omega signals, causing local interferences.

# CHAPTER III

## THE WEIBULL DISTRIBUTION FOR DESCRIBING NAVIGATION ERRORS

### 3.1 Introduction

The Weibull distribution has been advocated in the literature as a suitable distribution for describing radial errors (4,5). Special cases of the Weibull distribution include the Rayleigh and the exponential distributions. However, the estimation of the parameters of a Weibull distribution is shown to be extremely sensitive to errors near zero, and the Weibull distribution is shown not to describe radial errors of two dimensional Gaussian distributions, except in the case of circular contours of equal probability. Furthermore, using information theory to describe the mutual information between where the aircraft is and where the receiver says it is with additive Gaussian noise, the Weibull distribution is shown again not to be useful.

### 3.2 Weibull Distribution and Parameter Estimation

The Weibull distribution, the effects of the parameters, and statistics of the distribution are discussed. Parameter estimation with the use of plots and numerical methods and the effects of data points near zero are discussed.

In its most general form, the density function of the Weibull distribution is

$$f(x) = \frac{C}{B}\left(\frac{x-A}{B}\right)^{C-1} \exp - \left(\frac{x-A}{B}\right)^{C} \quad \text{for} \quad x \geq 0 \tag{3.1}$$

where $A$ is a (real valued) location parameter, $B$ is the (positive) scale parameter, and $C$ is the (positive) shape parameter. The $A$ parameter shifts the distribution along the $x$ axis, and the $B$ parameter scales

the distribution along the x axis. The C parameter effects are less clear.

Various Weibull distributions are shown in Figure 3-1, with location parameter A = 0 and B = 2. Observe the density function at x = 0 is 0 for C > 1, is $\frac{1}{B}$ for C = 1, and is unbounded for C < 1. Various statistics for the Weibull distribution are listed in Table 3-1.

Parameter estimation of Weibull distributions can be done either graphically or numerically. Graphical methods are described by Refs. 4 and 5, and numerical methods by Refs. 6 and 7.

An example of a graphical estimation of parameters is shown in Figure 3-2. Position error is plotted against the cumulative distribution of the

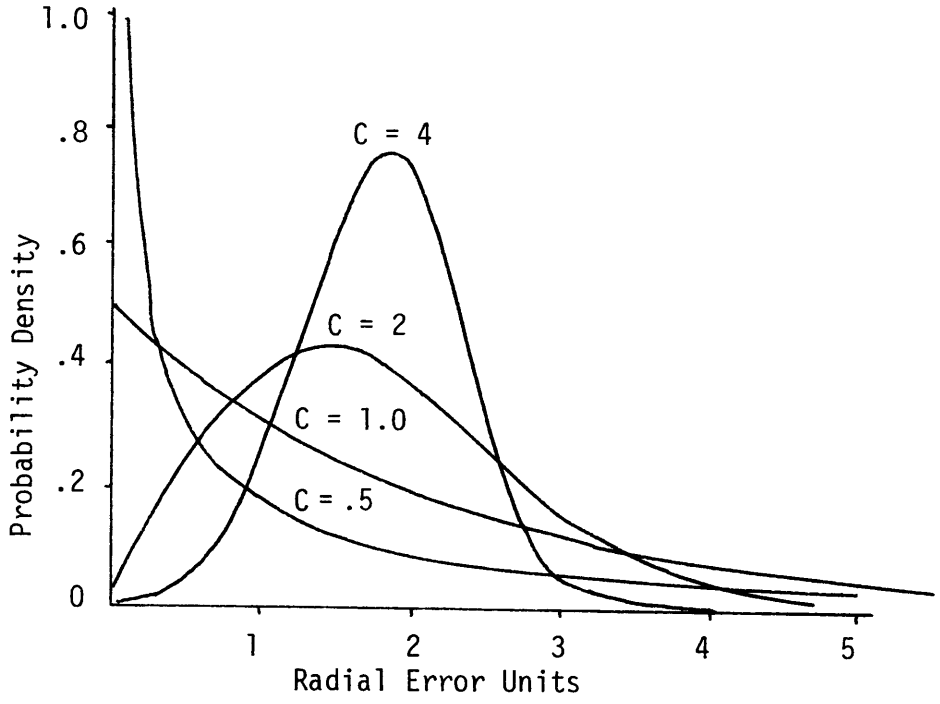


Figure 3-1. Weibull Distribution for A=0, B=2. (Ref.4)

Table 3-1. Statistics of the Weibull Distribution with A = 0 (4)

$$pdf(R) = \frac{C}{B}\left(\frac{R}{B}\right)^{C-1} e^{-\left(\frac{R}{B}\right)^{C}}$$

and the corresponding cumulative distribution function is

$$CDF(R) = \int_0^{\infty} pdf(R)dR = 1 - e^{-\left(\frac{R}{B}\right)^{C}}$$

The mean value of radial error is

$$H_R = \int_0^{\infty} R \ pdf(R) \ dR = B\,\Gamma\left(1 + \frac{1}{C}\right)$$

where the Gamma function

$$\Gamma(z) = \int_0^{\infty} t^{z-1} e^{-t} \, dt$$

is available in tabular form. The RMS value of radial error is

$$RMS_R = \sqrt{\int_0^{\infty} R^2 \ pdf(R) \ dR} = B\sqrt{\Gamma\left(1 + \frac{2}{C}\right)}$$

The variance of radial error is $\sigma_R^2 = RMS_R^2 - \mu_R^2 = B^2\left[\Gamma\left(1+\frac{2}{C}\right) - \Gamma^2\left(1+\frac{1}{C}\right)\right]$

Most probable error $= B\left(1 - \frac{1}{C}\right)^{1/C}$ for $C > 1$

$= 0$ for $0 < C \leq 1$

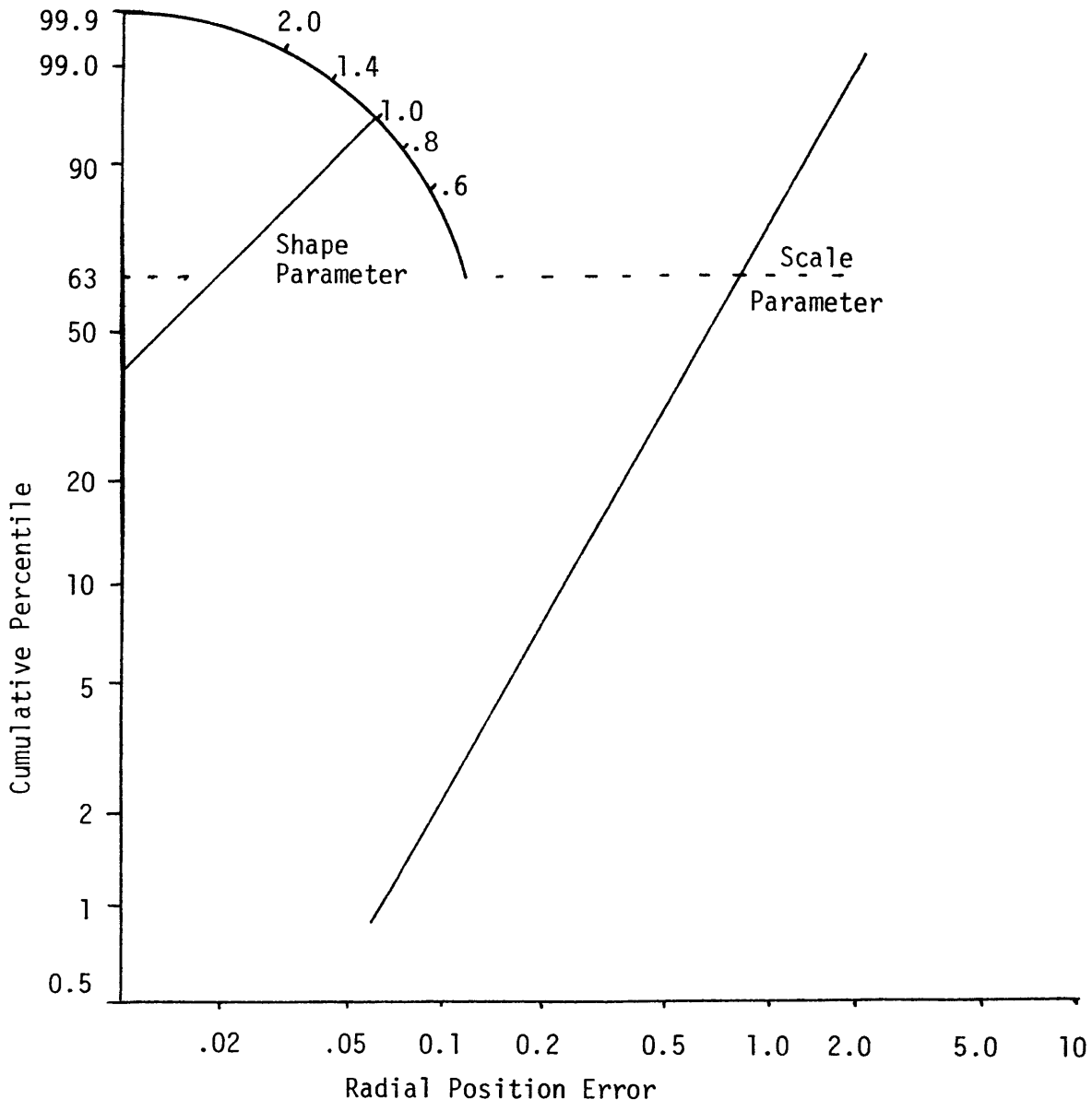


Figure 3-2. Graphical Estimation of Weibull Parameters (Ref. 4)

errors on special graph paper. A straight line is then fitted to the data points, with appropriate weighting for overlapping data points. This method is fairly straightforward, but requires that the data points be ordered, and a distribution function be determined. The scale factor $B$ is the abcissa of the 63rd percentile of the straight line fitted to the data points, and the shape parameter $C$ is determined from the slope of the line fitted to the data points.

A numerical method for estimating the $B$ and $C$ parameters is discussed in Ref. 6. The methods specified are suitable for implementation on data processing equipment, and were used for some of the calculations in this thesis.

Both the numerical and the graphical parameter estimation schemes are subject to extreme sensitivity to data near zero. In the numerical method, parameter estimation functions on the sum of logs of radial error, sum of squares of logs of radial error, and number of data points. For small radial errors, the ratio of measurement error to actual error can be relatively large, and can be accentuated by taking the logarithm. Using graphical methods, radial errors are plotted on a logarithmic scale and encounter the same phenomena. In either scheme, errors observed as zero are unacceptable data points.

Recall that the value of the density function at zero for a Weibull distribution is $0$ for $C > 1$, $\frac{1}{B}$ for $C = 1$, and unbounded for $C < 1$. For data with many points of near zero error, any measurement error can severely effect the estimate of the shape parameter. If data points with radial error measured as zero or "small" are present, the assignment of an

(arbitrary) radial error to the data points can force the parameter estimation to a value of $C < 1$.

A simple example of the effects of measurement error is shown in Figure 3-3. In Case 1, n data points at both 1.0 and 2.0 nm are observed, with an equal number of data points assigned the value of 0.1 nm. In Case 2, n data points each are observed at 1.0 and 2.0 nm, with n data points at 0.01 nm. The discrepancy between the slopes of the two lines, and hence of the shape parameter C, is apparent. For Case 1, C is estimated as 1.1. For Case 2, C is estimated to be 0.6.

### 3.3 Weibull Distribution With C = 2

With shape parameter $C = 2$, the Weibull distribution reduces to the Rayleigh distribution with parameter $\frac{1}{B}$, which describes the radial error of two dimensional samples with a zero mean Gaussian distribution and variances equal along both axes. It is shown that Gaussian distributions which generate ellipses of equal probability are not Weibull distributed. This result carries over to the mutual information between receiver indication of position and actual position in the presence of additive Gaussian noise, where the Weibull distribution does not fit the distribution unless the lines of equal probability are circular.

Omega position errors due to short-term noise, as will be discussed in Chapter IV, can be assumed to be Gaussian along each line of position, uncorrelated in time, and possibly correlated between lines of position if a particular station is used to generate both lines of position. Depending upon the relative standard deviations, an error ellipse can be determined. Analysis was done to attempt to define radial error distributions.

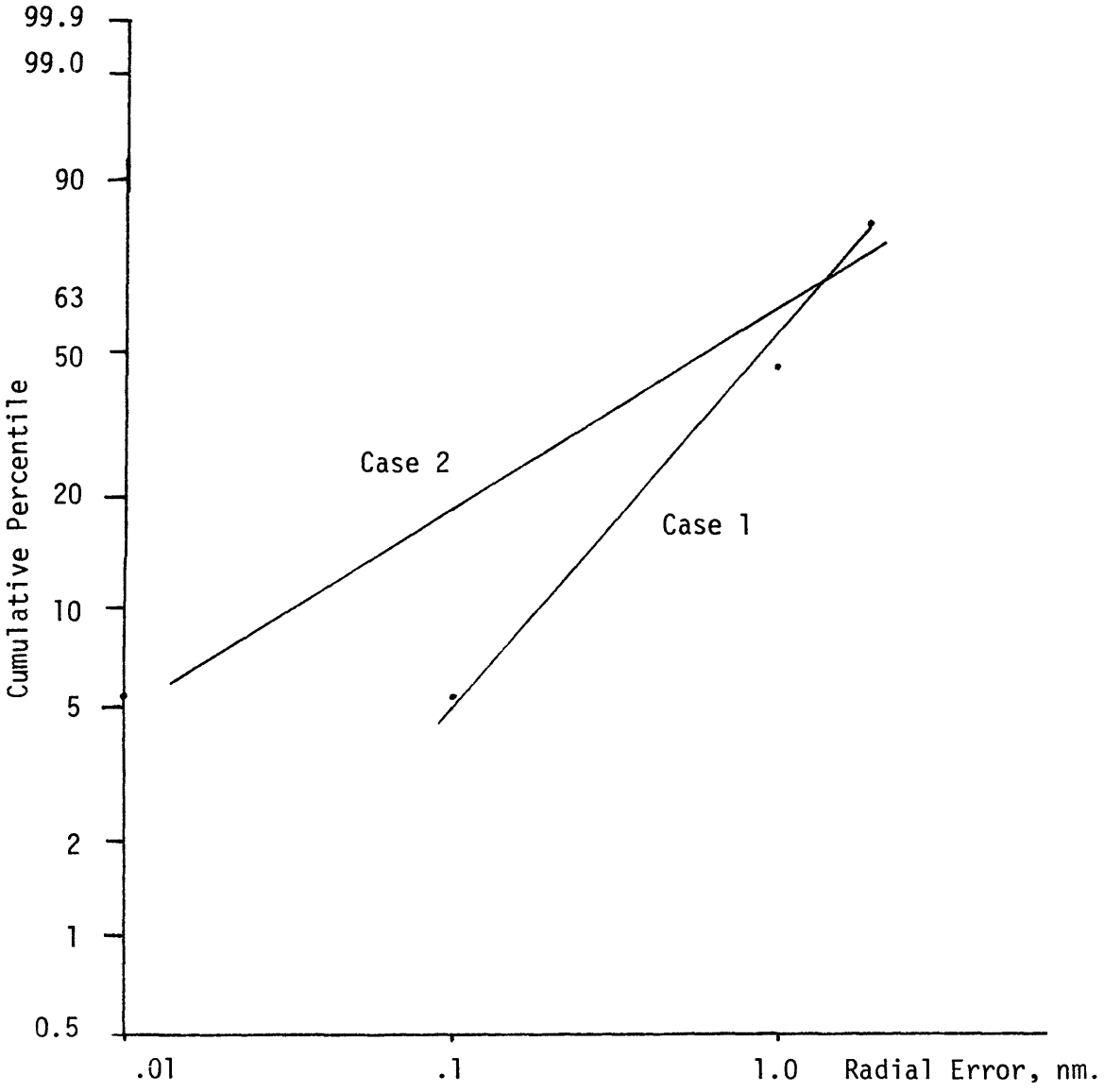


Figure 3-3. Weibull Parameter Estimation with Points near Zero

It can be demonstrated that radial errors in an ellipse are not Weibull distributed unless the major and minor axes are equal. Any error ellipse is described by

$$p(x,y) = \frac{1}{2\pi\ \sigma_1\sigma_2}\ e^{-\left(\frac{x^2}{2\sigma_1^2} + \frac{y^2}{2\sigma_2^2}\right)} \tag{3.2}$$

where the $x$ and $y$ axes are orthogonal but possibly rotated. Without loss of generality, assume $\sigma_1^2 > \sigma_2^2$, and let us convert to polar coordinates using $x = r\cos\theta$, $y = r\sin\theta$.

$$p(r,\theta) = \frac{1}{2\pi\ \sigma_1\sigma_2}\ e^{-\left(\frac{r^2}{2\sigma_1^2} + \frac{r^2\sin^2\theta}{2}\,\frac{\sigma_1^2 - \sigma_2^2}{\sigma_1^2\ \sigma_2^2}\right)} \tag{3.3}$$

Recall that the case $\sigma_1^2 = \sigma_2^2$ is not under consideration.

The radial error distribution is

$$\int_0^{2\pi} p(r,\theta)\ r\,d\theta = \int_0^{2\pi} \frac{r}{2\pi\ \sigma_1\sigma_2}\ e^{-\left(\frac{r^2}{2\sigma_1^2} + \frac{r^2\sin^2}{\sigma_1^2\ \sigma_2^2}(\sigma_1^2 - \sigma_2^2)\right)}\ d\theta \tag{3.4}$$

Assume this distribution is Weibull with parameters $B = s$ and $C = c$.

Let us then find any relationships between $s$, $c$, $\sigma_1$, and $\sigma_2$.

$$\frac{c}{s}\left(\frac{R}{s}\right)^{c-1}\ \exp^{-\left(\frac{R}{s}\right)^c} = \int_0^{2\pi} \frac{r}{2\pi\ \sigma_1\sigma_2}\ e^{-\left(\frac{r^2}{2\sigma_1^2} + \frac{r^2\sin^2\theta}{\sigma_1^2\ \sigma_2^2}(\sigma_1^2 - \sigma_2^2)\right)}\ d\theta \tag{3.5}$$

If we differentiate the left side with respect to $\theta$, assuming $R = Rf(\theta)$, and match this with the integrand, we obtain:

$$G(\theta) = \text{left hand side} = \frac{c}{s}\left(\frac{Rf(\theta)}{s}\right)^{c-1} e^{-\left(\frac{Rf(\theta)}{s}\right)^{c}} \tag{3.6}$$

$$\frac{dG}{d\theta} = \frac{c(c-1)}{s}\left(\frac{R}{s}\right)^{c-1} f(\theta)^{c-2} f'(\theta)\ e^{-\left(\frac{Rf(\theta)}{s}\right)^{c}}$$

$$- \frac{c^2}{s}\left(\frac{R}{s}\right)^{2c-1} f(\theta)^{2c-2} f'(\theta)\ e^{-\left(\frac{Rf(\theta)}{s}\right)^{c}} \tag{3.7}$$

To match powers of $R$ in the exponents of equations 3.5 and 3.6, $c = 2$. This mismatches coefficients, however. Thus, the Weibull distribution does not describe radial errors of elliptical Gaussian error distributions.

Another interesting phenomenon is observable when the shape parameter $C = 2$. Let $X$ be the position of the Omega receiver, and let $Y$ be the indicated position of the Omega receiver, where $Y = X + N$, $N$ being a zero mean Gaussian random variable. The average mutual information between $X$ and $Y$, $I(X;Y)$, is a measure of how much information the receiver supplies about its position. If $H(Y)$ is the entropy of the position estimate, and $H(Y|X)$ is the conditional entropy of the position estimate,

$$I(X;Y) = H(Y)-H(Y|X) \tag{3.8}$$

Since

$$H(Y|X) = H(N) \tag{3.9}$$

and

$$I(X;Y) = H(Y) - H(N) \tag{3.10}$$

Let us calculate $H(N)$.

For convenience, let us assume that the variance of $N$ is 0.5, and let us consider the case where $N$ is one dimensional.

$$H(N) = \int_{-\infty}^{\infty} p(x) \log p(x)\, dx \tag{3.11}$$

$$= \int_{-\infty}^{\infty} \frac{1}{\sqrt{\pi}} \exp(-x^2)\ (-x^2 \log \frac{e}{\sqrt{\pi}})\, dx \tag{3.12}$$

$$= k \int_{0}^{\infty} x^2 \exp(-x^2)\, dx \tag{3.13}$$

for an appropriate constant $K$.

Let us now consider the two dimensional case where the noise is zero mean Gaussian and the two noise sources act in orthogonal directions.

$$p(x,y) = \frac{1}{2\pi\ \sigma_1\sigma_2} \exp -\frac{1}{2}^{(x,y)} \begin{bmatrix} \sigma_1^2 & 0 \\ 0 & \sigma_2^2 \end{bmatrix} \begin{bmatrix} x \\ y \end{bmatrix}$$

$$= \frac{1}{2\pi\sigma_1\sigma_2} \exp - \left( \frac{x^2}{2\sigma_1^2} + \frac{y^2}{2\sigma_2^2} \right) \tag{3.14}$$

$$H(N) = \iint_{-\infty}^{\infty} p(x,y) \log p(x,y)\, dx\, dy \tag{3.15}$$

$$= k \iint_{-\infty}^{\infty} \exp \left( - \frac{x^2}{2\sigma_1^2} \right) \exp \left( - \frac{y^2}{2\sigma_2^2} \right) \left( \frac{x^2}{2\sigma_1^2} + \frac{y^2}{2\sigma_2^2} \right) dx\, dy \tag{3.16}$$

$$= k\int_{-\infty}^{\infty} \frac{x^2}{2\sigma_1^2} \exp\left(-\frac{x^2}{2\sigma_1^2}\right) dx + k\int_{-\infty}^{\infty} \frac{y^2}{2\sigma_2^2} \exp\left(-\frac{y^2}{2\sigma_1^2}\right) dy \qquad (3.17)$$

for appropriate constants $k$. For the case $\sigma_1 = \sigma_2$, with appropriate changes of variables, this can be rewritten in the form of Eq. 3.13 using the fact that the integrands are even functions.

Let us now compute the mean radial error for a Weibull distribution with $C = 2$.

$$\bar{r} = \int_0^{\infty} r\, p(r)\, dr \qquad (3.18)$$

$$= \int_0^{\infty} r \frac{2}{B} \left(\frac{r}{B}\right)^{2-1} \exp - \left(\frac{r}{B}\right)^2 dr \qquad (3.19)$$

$$= k' \int_0^{\infty} \left(\frac{r}{B}\right)^2 \exp - \left(\frac{r}{B}\right)^2 dr \qquad (3.20)$$

for an appropriate constant $k'$. It is clear that Eqs. 3.13 and 3.20 are of the same form. Since $N$ is a position error, $x$ will have units of distance, as will $r$. Thus, the entropy of additive Gaussian noise with covariance $\begin{bmatrix} \sigma^2 & 0 \\ 0 & \sigma^2 \end{bmatrix}$ in position measurement is a constant multiple of the mean radial error when the radial errors are Weibull distributed with $C = 2$.

## 3.3 Conclusions

The Weibull distribution has been shown to have several characteristics which tend not to make it suitable for use in describing radial errors. Firstly, parameter estimation is sensitive to points with radial errors near zero. Secondly, radial errors of zero mean two variable Gaussian distributions are shown not to be Weibull distributed except in the special case of circular lines of equal probability.

# CHAPTER IV

# SHORT-TERM OMEGA NOISE STATISTICS

## 4.1 Introduction

Short-term Omega noise was defined in Chapter 2.3 to be the changes in phase observed at the output of the phase detector circuitry of the Omega receiver between successive measurements. This is in effect noise sampled every ten seconds, and is within the bandwidth of the pilot/aircraft system when navigating using Omega. Based on experimental data, this noise was modeled as Gaussian, uncorrelated noise.

## 4.2 Experiment Setup and Data Collection

The experiment performed consisted of recording deflections of the Course Deviation Indicator of the Omega receiver on a strip chart recorder. These data were then keypunched and processed numerically.

The Omega receiver was set up in an office, powered by a standard lab power supply. A six foot whip antenna was installed on the roof of the building with an antenna coupler, which supplied signals to the Omega receiver through a 75' cable. The autopilot output of the Omega receiver, which is identical to the signal driving the CDI, was connected to a Russ-trak recorder.

A sample of the recorded data is shown in Figure 4-1. This data shows the effects of the sampling of the recorder at a rate of about 2/sec, and also shows the noise on the needle deflection over the course of the ten second Omega cycle. The recorded data were manually filtered to provide one data point every ten seconds, as shown by the arrows in Figure 4-1.

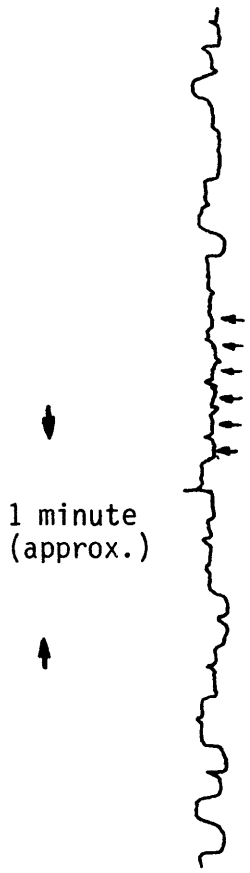


Figure 4-1. Strip Chart Recording of Needle Deflections.
Needle Deflection Showing Only B-D LOP Variations.

Four hundred five data points were recorded, corresponding to about 1.1 hours of data. The 300 central data points were used as a sliding "window" to calculate the autocorrelation function of the ensemble of data points.

4.3 Experimental Results

The experimental data shows that the short-term Omega noise observed can be modeled as Gaussian, uncorrelated noise with a standard deviation of 4 cel (centilanes).

Figure 4-2 shows a histogram of the observed data points. Excluded from consideration in the histogram are 29 points which are off scale, and are apparently the result of 60 Hz interference from the high concentration of electrical machinery in the vicinity of the antenna. Of the 376 points comprising the histogram, 89.8% are within the central 20 cec,

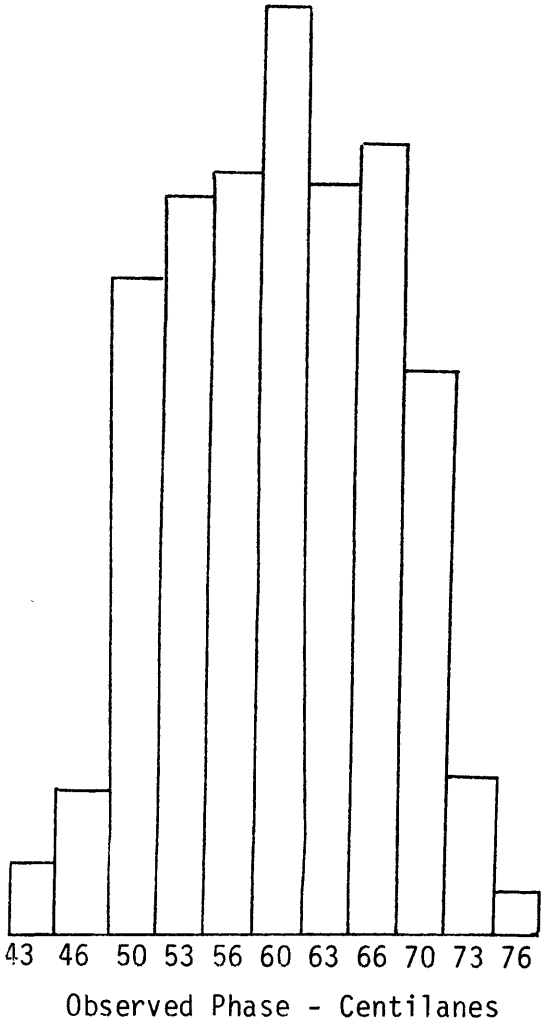


Figure 4-2. Histogram of Observed Omega Short Term Noise

and the distribution is roughly Gaussian. The standard deviation can be computed as 5 cel, since a ±2 sigma distribution is about 95%.

However, the data shown in the histogram reflects a drift in the observed data. Table 4-1 shows statistics on all data points, divided into four groups for analysis. The distribution of points within each group was roughly Gaussian. Based on these individual smaller samples, a more reasonable estimate of sigma is 4 cel.

Table 4-1. Data Point Statistics in Four Consecutive Groups

| No. Pts. | Mean | % Pts. in ±7 cel |
|---|---|---|
| 109 | 66.4 | 90.0 |
| 112 | 63.1 | 94.5 |
| 112 | 56.0 | 92.7 |
| 72 | 51.5 | 97.0 |

The autocorrelation function of all observed data points was calculated by taking a 300 point sample from the center of the 405 data point sample. This 300 point sample was then multiplied term by term with the large sample at 105 different locations to generate the autocorrelation function of Figure 4-3. It should be noted that the autocorrelation function does not go to zero because the random variable is not zero mean.

The autocorrelation function is shown enlarged in Figure 4-4. The autocorrelation function in two samples (20 seconds) drops off to a value which reflects the bias of the data and the correlation due to the observed drift in the mean value of smaller samples within the 405 point sample.

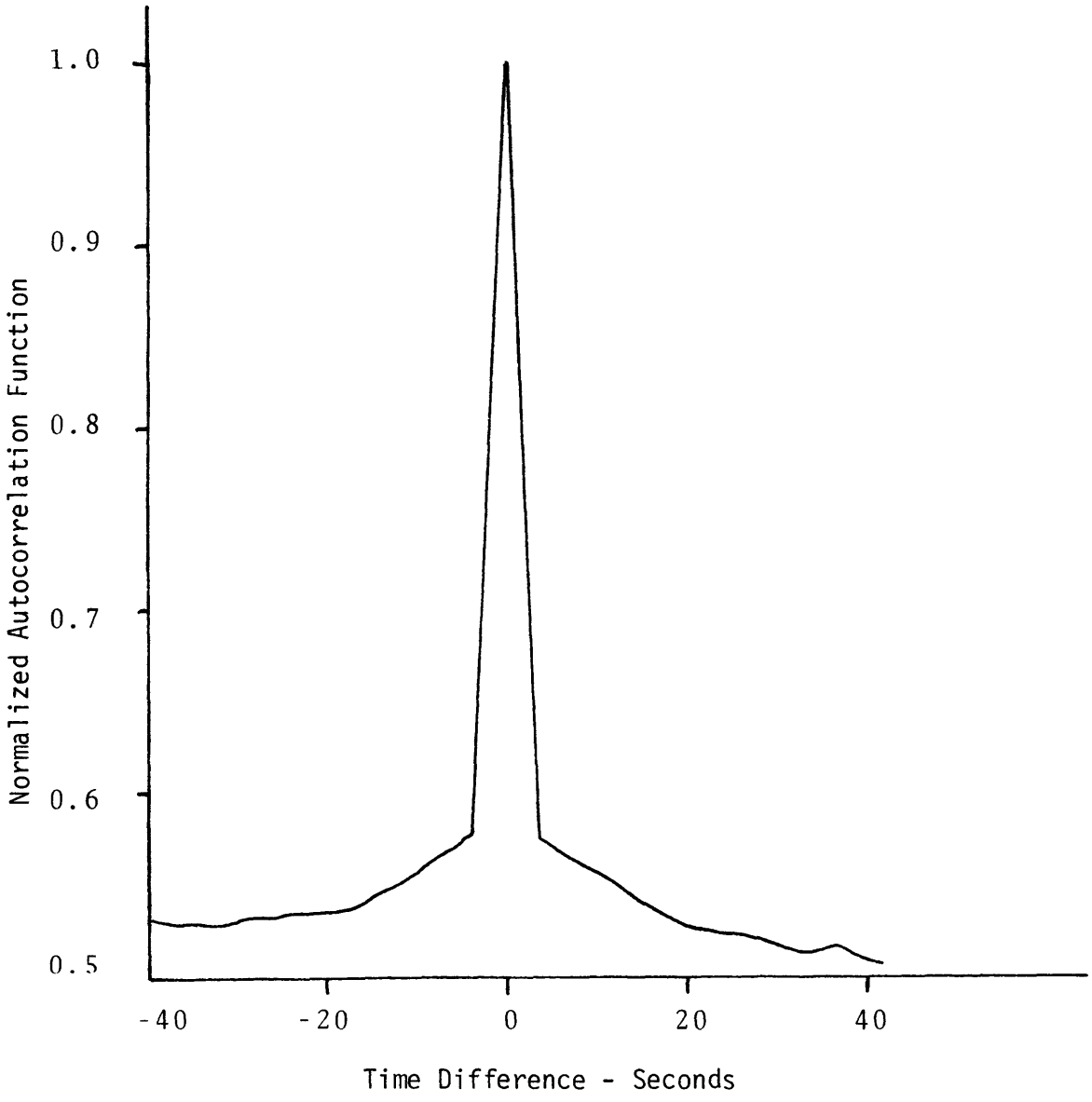


Figure 4-3. Normalized Autocorrelation Function of Observed Omega Short Term Noise

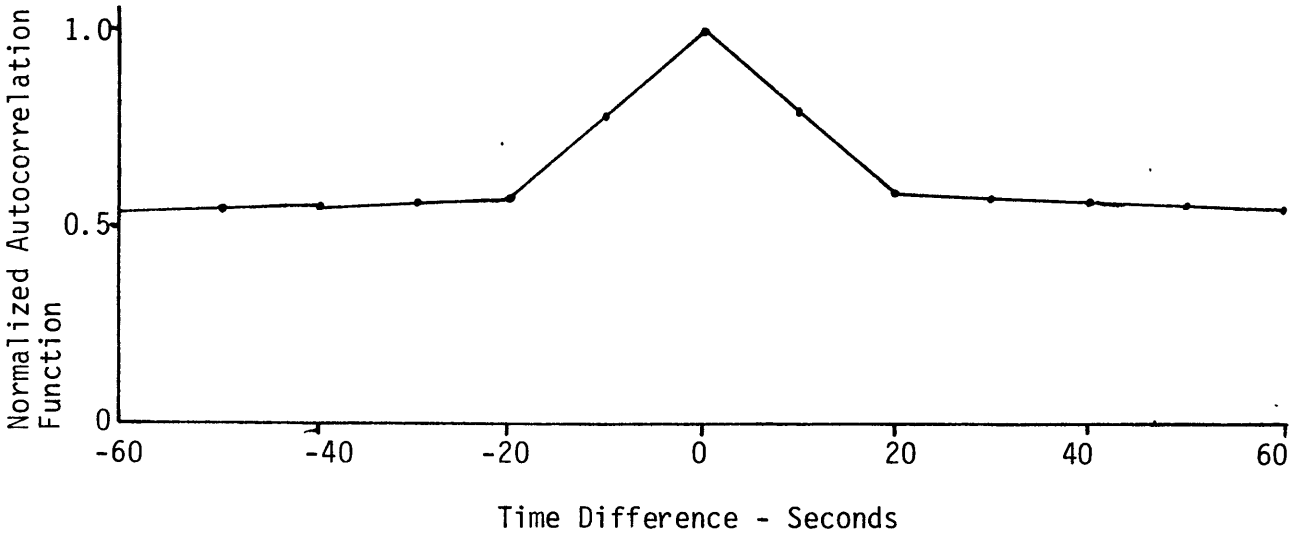


Figure 4-4. Normalized Autocorrelation Function of Observed Omega Short Term Noise

Based on this data, the correlation coefficient between successive samples is about 0.48, corresponding to a time constant of 7.5 seconds, assuming that the noise is exponentially correlated. Based on these data, however, exponential correlation is not a good model, and the noise is modeled as uncorrelated between samples. The correlation observed is apparently due to the phase lock loop, which has a time constant short compared to path following dynamics and is ignored.

## 4.4 Expected Experimental Results

Simple analysis of receiver front end design and phase lock loop design indicate that the observed short-term Omega noise should have a Gaussian distribution, correlated between successive measurements only by the filtering of the phase lock loop.

Typical general aviation Omega receivers (11,12) have front end receiver designs consisting of successive stages of filtering and gain. For those receivers using an E-field antenna, a preamplifier is used to amplify the signal from the highly reactive wire antenna and provide some impedance matching to send the signal to the receiver itself, usually through several feet of coaxial cable. At the receiver, the signal is amplified and fed through filters of successively narrower bandwidth until the bandwidth is 100 Hz or less. In addition, hard limiting or noise blanking is employed to reduce the effects of atmospheric noise, which is impulsive and caused by lightning.

Atmospheric noise can be modeled by the Hall model (13) as

$$y(t) = n(t) \times A(t) \tag{4.1}$$

where $n(t)$ is Gaussian noise, and $A(t)$ is low pass filtered Gaussian noise. $A(t)$ has a correlation time of about 1 ms. Even though this noise distribution is not normal, and even though the receiver front end design is nonlinear with the noise limiters, the received phase should be Gaussian because more than 8,000 phase measurements will be made by a phase lock loop while an Omega station is broadcasting. The shortest Omega broadcast time is 800 ms, or 800 times longer than the correlation time of $A(t)$. By the Central Limit Theorem, the observed phase should be Gaussian.

Let us compare these results with those obtained in the preceding section. A Gaussian or near Gaussian distribution was observed, and this correlates well with our prediction. Successive measurements were predicted to be uncorrelated, but instead, some correlation was observed. This

correlation time is small compared to that of the pilot/aircraft system following, as will be discussed in detail in Chapter VIII of this thesis.

## 4.5 Summary

Short-term Omega noise as measured by the phase detectors can be modeled as uncorrelated Gaussian noise with a standard deviation of 4 cel. No information was taken from which the correlation between short-term noise standard deviation and Omega station signal to noise ratios could be determined.

# CHAPTER V

## DESCRIPTION OF FLIGHT TESTS

Voluminous flight test data was available for analysis of various Omega characteristics. Most of the flight test data used in this thesis was recorded in a 60-hour flight test program accomplished by Aerospace Systems, Incorporated (ASI) (16), for which the author did the data reduction. This data base is not unique to this thesis.

ASI conducted a flight evaluation of a low-cost Omega receiver in a general aviation aircraft under NASA Contract NAS1-13644, with the MIT Flight Transportation Laboratory as subcontractor. This flight evaluation was to serve two purposes: firstly, to provide information on Omega suitability as a navigation sensor for low altitude commercial VTOL operations in the Northeast Corridor in comparison with previous results in a VOR/DME flight evaluation program (10); secondly, informally stated, to ensure that in an upcoming NASA/FAA differential Omega evaluation program in the Wallops area, no surprises indigenous to the Omega system would be encountered in the evaluation of the differential Omega system. Accomplishment of this second objective was accomplished by analysis of signal and phase characteristics observed in the Wallops area. Because only minimal experience was gained flying approaches using the Omega receiver, an additional flight was accomplished for this thesis to provide this information.

The objectives of the ASI flights are stated in detail in Appendix B, which contains Section 3 of Ref. 16.

On the flights in the Wallops area, radar tracking was to have been available using the FPS-16 tracking radar. Information was supplied from

this radar, but the information could not be correlated with the Omega position indications due to hardware difficulties with the Omega test equipment. In order to provide in-flight information on short-term Omega noise, the additional flight was scheduled to be tracked with the Lincoln Laboratory DABS radar. Unfortunately, the flight was not accomplished when the radar was available. Thus, no flights were accomplished with tracking radar when the Omega test hardware was completely functional.

The designing of the ASI flights was primarily by P.V. Hwoschinsky (17), who provides additional information on the ASI flight test program. Selection of flight profile parameters was done primarily by J.D. Howell of ASI and P.V. Hwoschinsky.

# CHAPTER VI

# FLIGHT TEST EXPERIENCE AND RESULTS

## 6.1 Introduction

In addition to the ground test experiments described in Chapter IV, 70 hours of flight testing was performed. The majority of this flight testing was done under subcontract to ASI of Burlington, MA, and is described in Ref. 16. This data base was also used in a thesis by P.V. Hwoschinsky (17). Additional flight test data consisted of a series of approaches flown to the Bedford, MA, airport, L.G. Hanscom Field. The complete data from the ASI flight tests are included in Ref. 17.

Chapter 6.2 describes various operational factors encountered in the operation of the Dynell Mark III Omega receiver. Many of these factors are described by Hwoschinsky in his thesis. Chapter 6.3 discusses statistical inferences drawn from the flight test data, and Chapter 6.4 discusses the approaches flown using the Omega receiver.

## 6.2 Operational Experience

The flight test program conducted for ASI provided an invaluable opportunity for hands on experience with an airborne Omega receiver appropriate for general aviation. This experience validates mathematical models discussed in other sections of the thesis, and is especially useful in the analysis of Omega applications to the air traffic control environment. The various operational factors discussed are receiver reset bias, VHF power supply interference, lane jumps, precipitation static, Omega transmitter power effects noted, and variations in recorded track. Many of these obser-

vations are peculiar to the receiver used, and many can be reasonably considered endemic to the Omega system.

The Dynell Mark III Omega receiver is prone to a random bias in position estimates depending apparently upon local noise when the receiver is reset. This bias can be explained in the following way. The manufacturer quotes a maximum aircraft speed of 400 knots for utilization of this receiver, which corresponds to a maximum lane slew rate of 80° per Omega transmission cycle, or 40° of phase slew (11). With this relatively fast phase tracking, and no subsequent filtering in the receiver, the Omega short-term noise is not heavily filtered by the receiver. "Resetting" the receiver in fact consists of clearing the lane accumulators which record present phase less phase observed when the receiver was reset. Hence, because the Omega short-term noise is incorporated into the receiver estimate of reset position, all subsequent measurements of phase are biased according to the amount of phase error present at reset.

A phenomenon peculiar to the installation of this Omega receiver was S/N degradation due to the power supplies of the aircraft VHF radios. These radios, dual Narco Mk 12's, incorporate vacuum tubes in their circuitry, which require power supplies. As shown in Figure 6-1, one power supply was mounted aft of the aircraft luggage compartment, and one was mounted behind the instrument panel on the lower right side. The Omega antenna coupler was mounted behind the instrument panel on the upper right side, adjacent to the back end of the ADF. The Omega receiver itself was suspended from the VHF power supply under the right hand side of the instrument panel, as discussed in Appendix B. The result of this installation was S/N degradation of approximately 10-15 dB on Omega Stations A, B and C, and noticeable degrada-

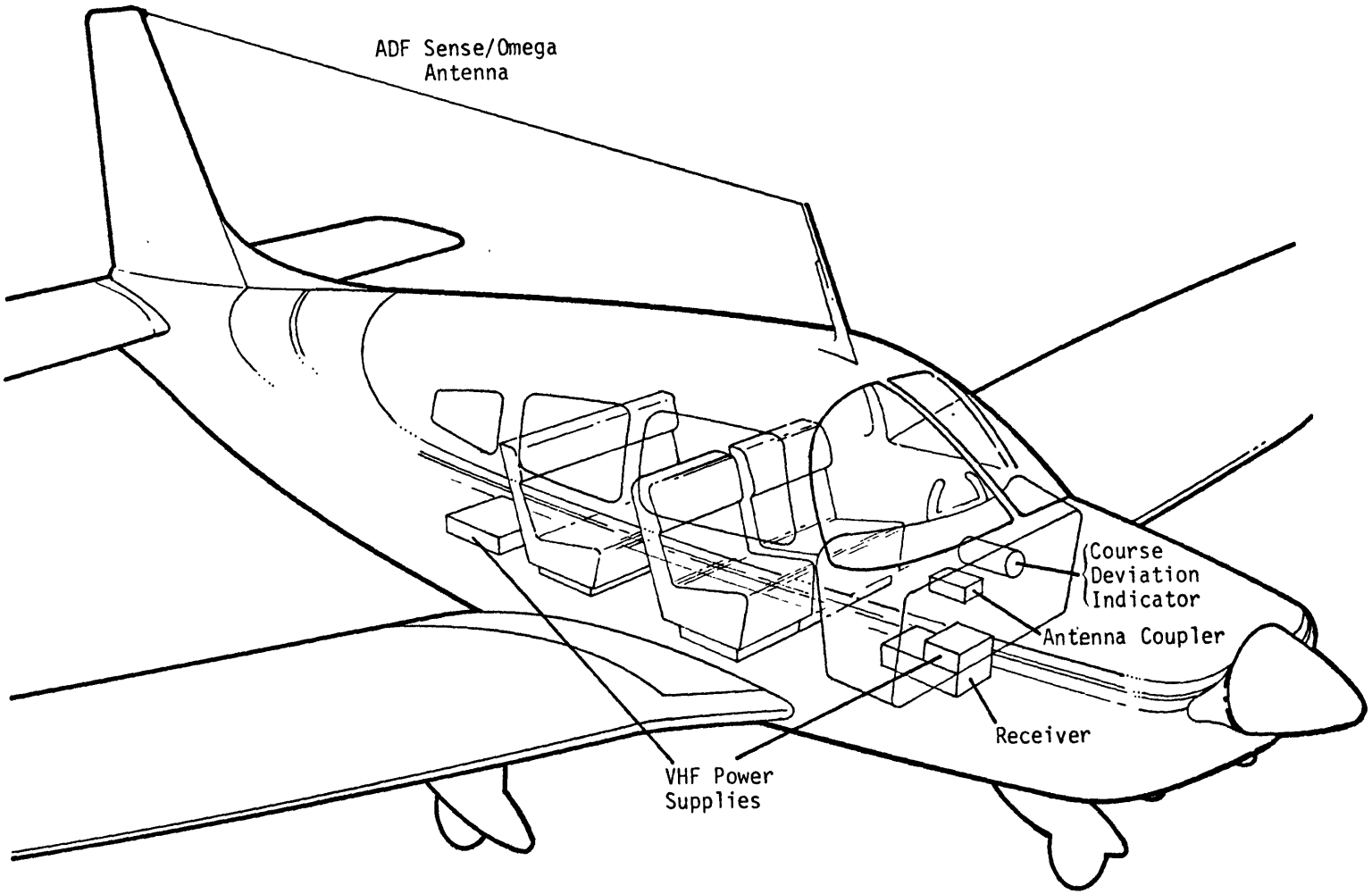


Figure 6-1. Omega Installation in Test Aircraft

tion on Station D. However, over a period of an hour or more, the degradation in S/N diminished, apparently due to thermally induced evacuation of the vacuum tubes in the power supplies, as discussed in Ref. 17.

Lane jumps were observed on three occasions. These lane jumps were confirmed by resetting the front panel waypoint selection on the Omega receiver, which caused the position readouts to indicate the known aircraft position. In all cases, these lane jumps reflected a failure of the receiver to navigate, and did not indicate that the receiver had accrued sufficient errors to track Omega signals with an ambiguity of eight miles as a bias. On flight O-1-6, poor S/N ratios on Station A are suspect as the cause of the lane jumps. During the first part of flight O-2-44, lane jumps occurred, again due to poor Station A S/N ratios. (Although no failure of Station A was reported, an aurora was reported that night, which may indicate PCA.) Later in the same flight, lane jumps were observed with good Station A S/N (-5 dB). These lane jumps were attributed to a receiver malfunction. As will be discussed in Chapter 6.3, receiver operation was apparently not degraded by poor S/N ratios unless the S/N ratios were so bad that navigation was impossible. No intermediate accuracies were observed.

For economic reasons, low-cost Omega receivers have been designed to use E field antennas. These antennas require only a simple preamplifier, and can double as ADF sense antennas. By comparison, H field antennas must be "steered" to receive Omega signals, due to their inherent directionality. This "steering" requires knowledge of the relative bearing to the Omega station currently broadcasting, which in turn requires knowledge of aircraft position in latitude and longitude, and aircraft heading. The advantages of H field antenna include a relative freedom from precipitation static.

Although no precipitation static was observed flying through rain showers, including heavy rain during flight O-1-21, precipitation static was observed on flight O-2-11, resulting in serious degradation of S/N ratios on all stations, as shown in Figures 6-2 and 6-3. (Note that the VHF radios were on during this flight.) During the portion of the flight in which precipitation static was incurred, the outside air temperature was an indicated -16°C. "It is concluded from the above described flights into weather at mid-latitudes and tropical systems that Omega navigation systems equipped with E field antennas will yield poor navigation results when severe weather is encountered. Further, if the aircraft is operating at altitudes where the temperature if below 0°C temperature [sic], it is almost a certainty that an Omega system will lose its reception of the signals for extended periods in clouds." (18)

Reports of Omega transmitter power variations from day to day are not available from the U.S. Coast Guard. Thus, the possible nonlinear effects, if any, of transmitter power could not be observed. During flight O-2-44, however, a sudden increase in Station D S/N ratio was observed, as shown in Figure 6-4. Because no variation in S/N ratios was observed on any other stations, it is reasonable to conclude that this phenomenon is due to a sudden increase in Station D effective radiated power. Subjective experience suggests power variations are not uncommon, which makes station reliability an important issue for Omega use by the aviation community. However, information to confirm or deny these feelings is not available.

A plot of Omega position indication is shown in Figure 6-5. This plot was made by converting the readings of the lane accumulators (information not displayed to the pilot but available via the data recording circuitry)

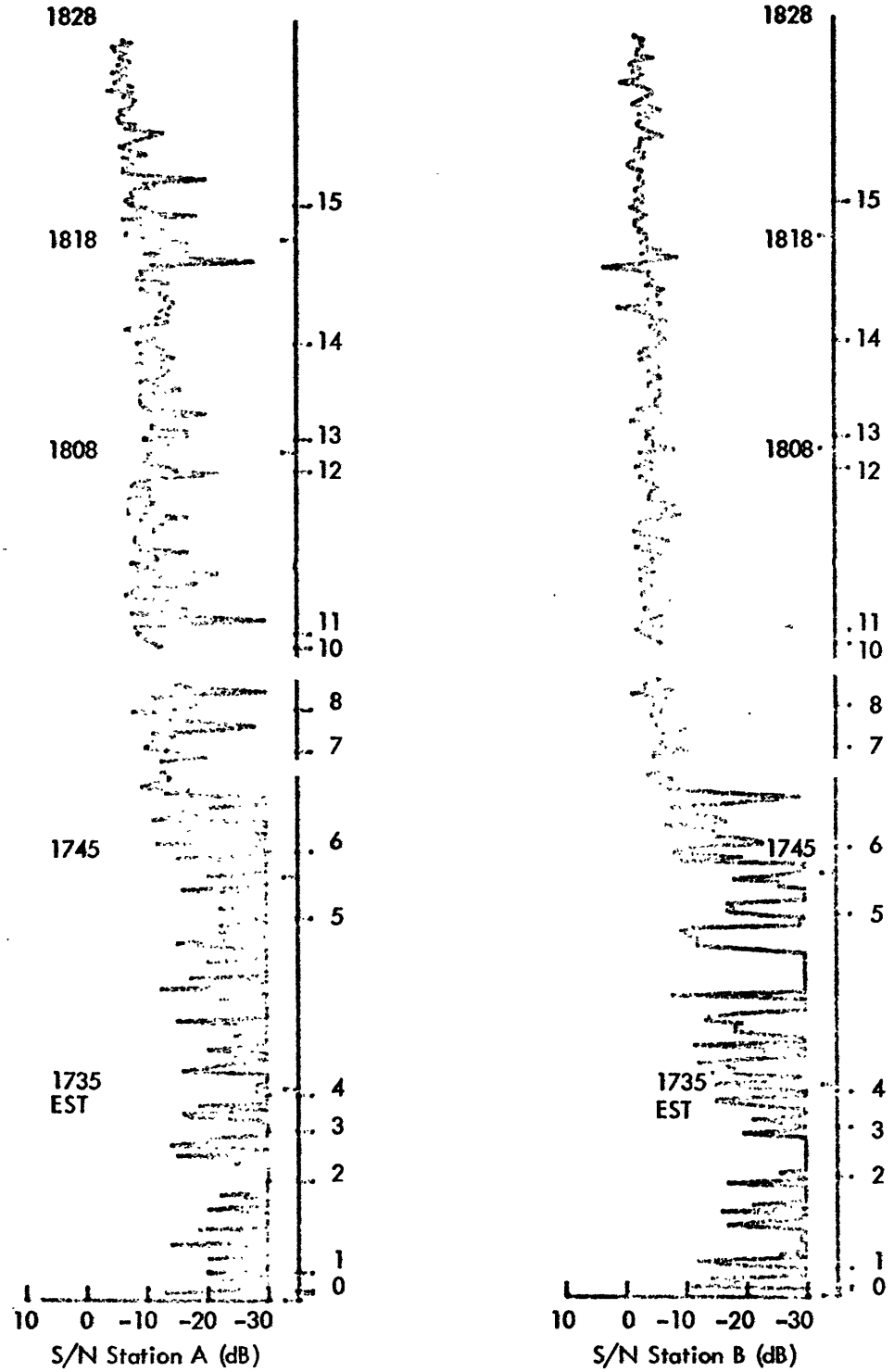


Figure 6-2. S/N Degradation During Precipitation Static, Stations A and B

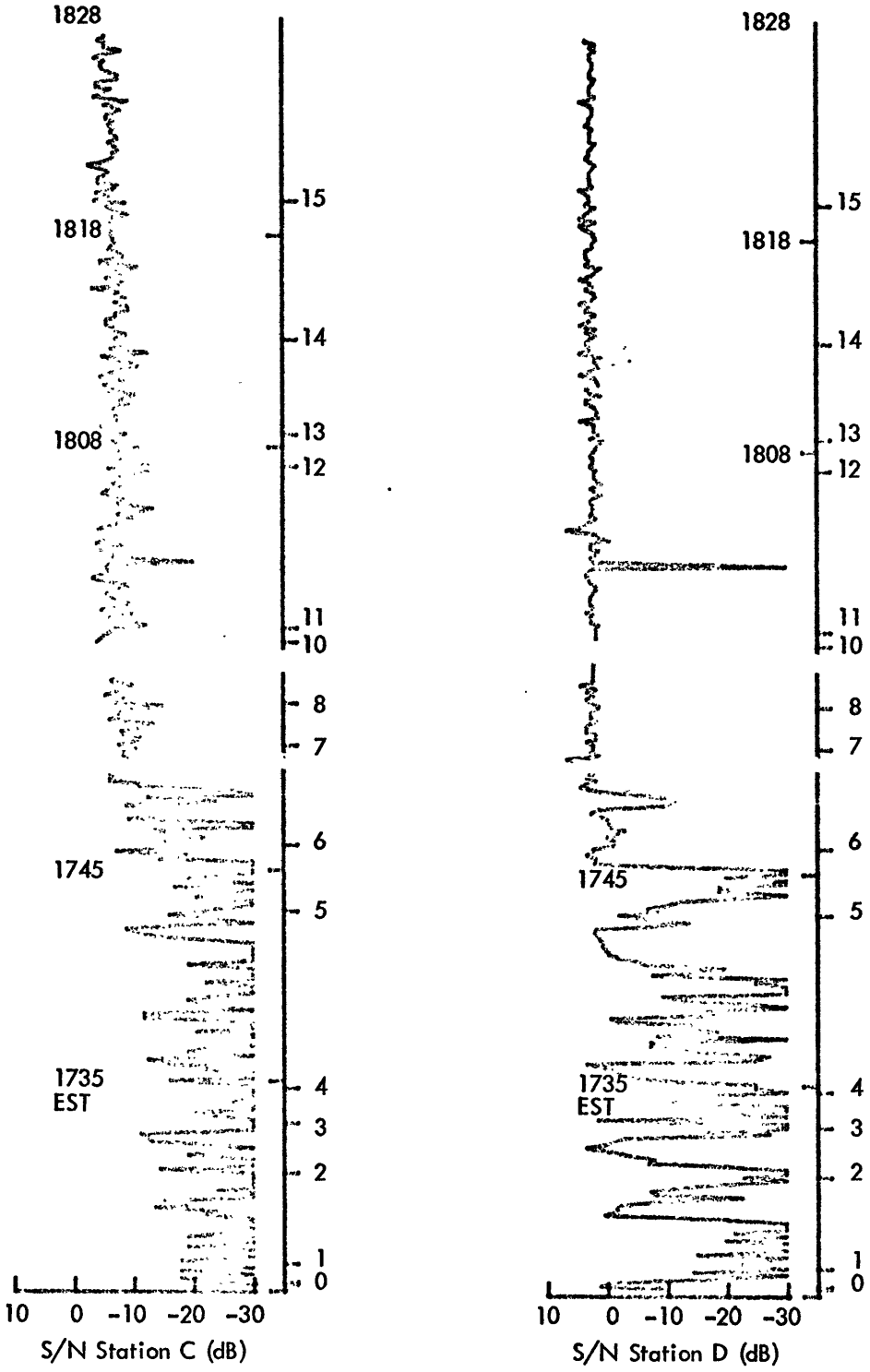


Figure 6-3. S/N Degradation During Precipitation Static, Stations C and D

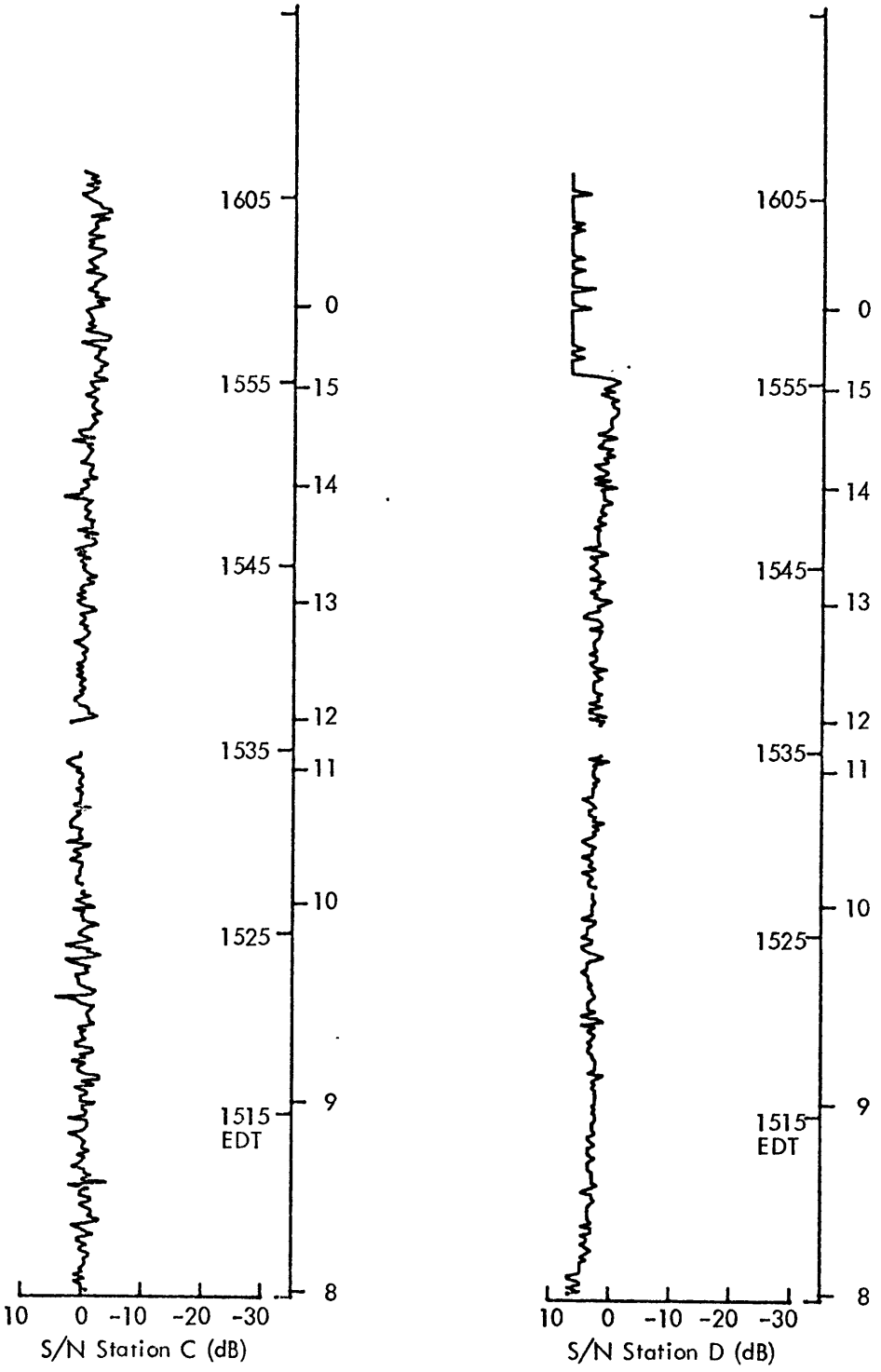


Figure 6-4. Increase in Station D S/N Attributed to Transmitter Power Increase. (Ref. 16, Fig. B-92)

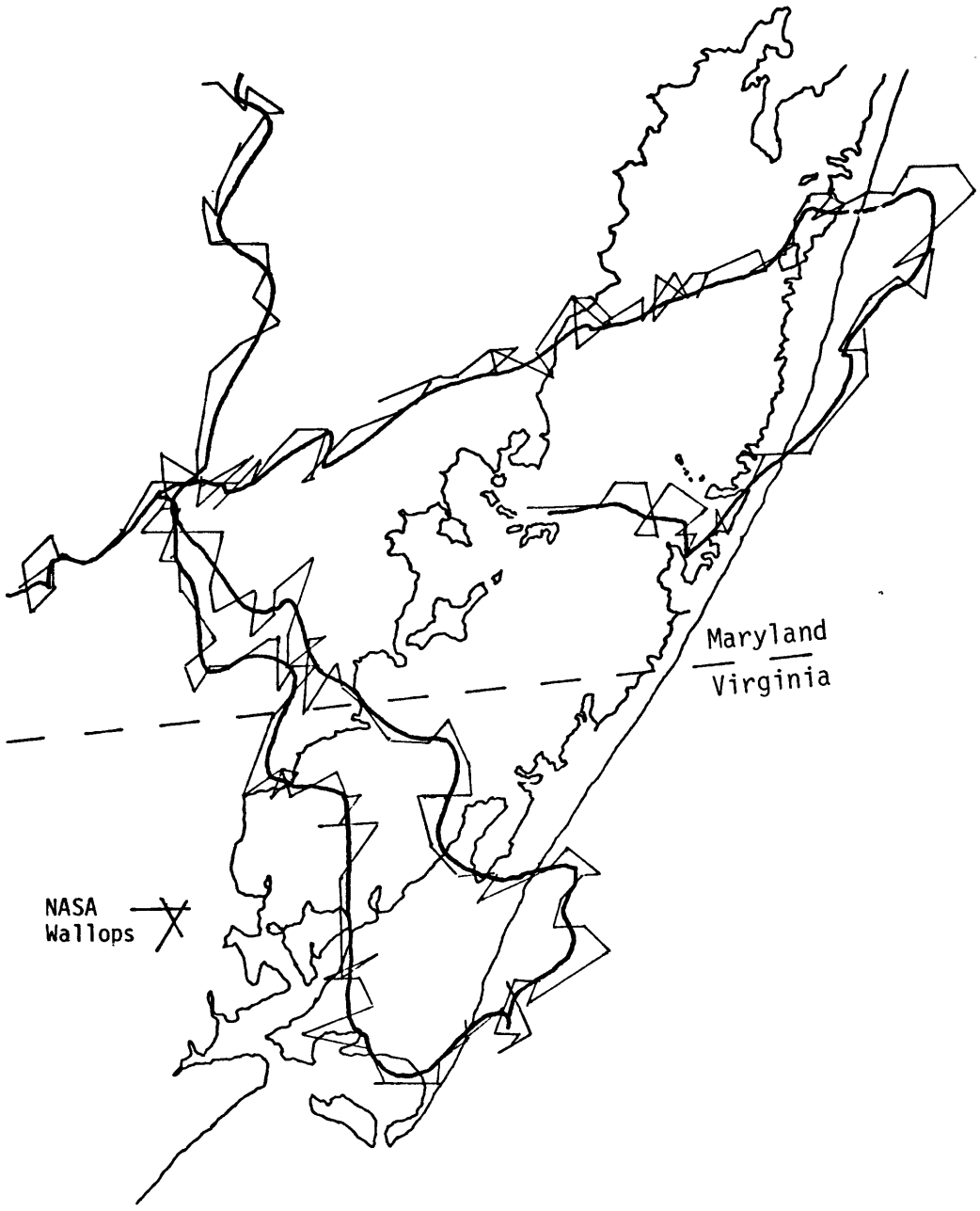


Figure 6-5 Omega Position Plot with Raw and Smoothed Data

to difference in latitude and longitude from the reset point. This information was then plotted on an X-Y plotter. When the plot was made, resolution in LOP 1 was limited to 4 bits/lane due to a hardware failure. This loss of resolution quantizes the data to a half mile, or about a half inch along a line roughly parallel to the coastline. This partial hardware failure does not explain the apparent scalloping in the recorded flight path, scalloping which is not indicative of the route actually flown. Although it is tempting to attribute some of this scalloping to a coastline effect, several factors contradict this conclusion. First, the scalloping is much less than one wavelength in magnitude. Second, scalloping appears on all plots of flights in the Wallops area, and is not always readily discernible over coastlines. Third, variations in propagation speed over land and sea are not sufficient to explain any coastline effect. Table 6-1 shows ratios of propagation speeds to the speed of light for a north/south path during daylight conditions, and the ratio of these two propagation speeds. Because the Delaware and New Jersey coasts lie along the direct line to Station A, it is tempting

Table 6-1. Phase Velocity v Variations (19)

| | |
|---|---|
| $\frac{v}{c}$ sea, N/S, day | 1.00428 |
| $\frac{v}{c}$ land, N/S, day | 1.00394 |
| $\frac{v_{land}}{v_{sea}}$, N/S, day | 1.00034 |

to assume that a shore line affect may be present due to different propagation speeds over land and sea. However, for a scallop of 0.5 nm, the difference in path length over land and sea would have to be approximately 1500 nm.

6.3 Statistical Analysis of Data

Statistical analysis was done on S/N ratios and observed accuracies. The measuring processes are described, and the results discussed.

S/N ratios for each Omega station are measured by the Dynell receiver and recorded by the test apparatus. S/N is estimated by measuring the edge jitter of the received Omega signal while the 10.2 kHz clock pulse is high. By counting edge jitter, which is the result of additive impulsive noise as discussed in Chapter 4.4, an estimate of S/N ratio is provided. The actual data recorded was an S/N count number, defined by

$$\text{S/N Count} = 128 + 100 \times (\text{broadcast time of Omega station}) \times \text{erf}\ \sqrt{\text{S/N power through 100 Hz}} \qquad (6.1)$$

where erf is the error function. The count number had a range of 0-225, and values below 128 indicated that the S/N ratio was less than -30 dB. Because station D was strong enough to saturate the S/N estimator, any count numbers of 255 were interpreted as a S/N ratio $\geq$ 10 dB.

The observed plots of S/N show great variations in S/N from sample to sample. These variations were not analyzed. However, it was noted that individual "spikes" of increased or decreased S/N ratio occurring during the same 10 second Omega transmission cycle were not correlated. In order to interpret the accumulated data, an "eyeball" average of the S/N data plots

was done. This allowed easy filtering of anomalies such as VHF radio interference and precipitation static.

Station S/N ratios are tabulated in Tables 6-2 and 6-4, with accompanying flight descriptions in Tables 6-3 and 6-5. These station S/N ratios were then superimposed on plots of flights and time of day, and are shown in Figures 6-6, 6-7, 6-8, and 6-9. It was observed that station A S/N ratios were higher after local noon by about 10 dB during the Wallops flights, and with the exception of two flights, by about 10 dB in the Northeast corridor flights. T-tests, with the null hypothesis that S/N varied by 10 dB, assuming the variance of S/N was equal for flights after noon and flights before noon, showed that the hypothesis could not be rejected (20). Bortz (21) plots -10 dB contours of S/N ratios of various Omega stations expected at various times throughout the world, and the observed increase in station A S/N ratio is in agreement with the trend of his predictions.

A linear regression of S/N ratios for stations A and B with observed position errors was performed, yielding coefficients of determination less than 0.01. Thus, no conclusions on linear component of relationships between station S/N ratios and position error was made. This result reflects both the fact that position errors depend upon more than S/N ratio, and also the inconsistent quality of position error measurements.

Position error measurements were made in several ways. By far the most common method involved visually estimating the radial position error when the Omega receiver To/From flag flipped. At higher altitudes, these visual estimates of position error were subject to errors greater than those incurred at lower altitudes. Another method involved comparison of VOR indication of waypoint passage and elapsed time until Omega indication of waypoint

Table 6-2. Averaged S/N Ratios for Wallops Flight.

| FLIGHT | PART | DATA (MIN.) | S/N (dB THROUGH 100 Hz) | | | | NAV/COMM ON CONTINUOUSLY? |
|---|---|---|---|---|---|---|---|
| | | | A | B | C | D | |
| 1-1 | 1 | 62 | -10 | 0 | -2 | 5 | On |
| | 2 | 50 | -10 | 0 | 0 | 5 | On |
| 1-2 | -- | 20 | -12 | -2 | -3 | 7,10 | On |
| 1-3 | 1 | 47 | -12 | -2 | 0 | 7,10 | On |
| | 2 | 75 | -10 | -2 | 0 | 7,10 | On |
| 1-4 | -- | 50 | -3 | 0 | 2 | 7 | Off |
| 1-5 | -- | 70 | -7 | -2 | 2 | 4 | On |
| 1-6 | 1 | 89 | -20 | -2 | 0 | 7,10 | On |
| | 2 | 66 | -20 | -2 | 0 | 7,10 | On |
| 1-7 | -- | 5 | -20 | -10 | 7 | 0 | On |
| 1-8 | -- | 90 | -2 | 0 | -2 | 5 | On |
| 1-9 | -- | 80 | 0 | 0 | 0 | 5 | On |
| 1-10 | -- | 70 | -20 | 0 | 0 | 7,10 | On |
| 1-20 | -- | 16 | -20 | -6 | -7 | 3 | On |
| 1-21 | -- | 60 | -10 | 0 | -2 | 5 | Off |
| 1-22 | 1 | 81 | -20 | -3 | -4 | 7,10 | On |
| | 2 | 80 | -10 | 0 | -4 | 7,10 | On |
| 1-23 | 1 | 50 | -23 | -12 | -12 | 2 | On |
| | 2 | 60 | -14 | -4 | -4 | 4 | On |
| 1-24 | 1 | 60 | -20 | -6 | -6 | 4 | On |
| | 2 | 60 | -14 | -4 | -6 | 6 | On |
| | 3 | 50 | -14 | -2 | -6 | 6 | On |

Table 6-3. Wallops Flight Descriptions.

| FLIGHT NUMBER | FLIGHT DESCRIPTION |
|---|---|
| 1-0 | Ferry Flight SBY-WAL (7500') |
| 1-1 | Low Altitude Star Pattern Around Wallops Area (5000', 4000', 3000', 2000') with Radar Tracking |
| 1-2 | Ferry Flight WAL-SBY (1000') |
| 1-3 | High Altitude Star Pattern Around Wallops Area (10,000') with Radar Tracking |
| 1-4 | Ferry Flight WAL-ORF (1000') |
| 1-5 | Night VOR Flight, ORF-SBY-WAL (3000') |
| 1-6 | Modified Snake Route (2000'), WAL-MFV-SBY |
| 1-7 | Ferry Flight SBY-WAL (1500') |
| 1-8 | Day Race Track Route with Radar (3000') |
| 1-9 | Night Race Track Route with Radar (3000') |
| 1-10 | SWL VOR Constant Radial Flight (6000', 5000', 4000', 3000', 2000'), WAL-SBY |
| 1-20 | Ferry Flight SBY-WAL Using AC, BD, LOPs at 2000' |
| 1-21 | Railroad Flight to Kellam in Heavy Rain at 1000', AB/BD, AC/BD, WAL-SBY |
| 1-22 | Constant LOP Flight using AD, AC, AB, BD, BC, LOPs SBY-SWL-SBY (2000') |
| 1-23 | VOR Cloverleaf 30° Cardinal Headings (3000'), SBY-SWL-SBY |
| 1-24 | VOR Cloverleaf 30° Cardinal Headings plus 15° (3500'), Constant CD LOP AB/BC, CD/BD, AB/BD |

Table 6-4. Averaged S/N Ratios for Northeast Corridor Flights.

| FLIGHT | PART | DATA (MIN.) | S/N (dB THROUGH 100 Hz) | | | | NAV/COMM ON CONTINUOUSLY? | LANE JUMP |
|---|---|---|---|---|---|---|---|---|
| | | | A | B | C | D | | |
| 2-3 | -- | 80 | -10 | -8 | 6 | 4 | Off | |
| 2-21-1 | -- | 70 | 0 | 0 | 0 | 7,10 | Off | |
| 2-21-2 | -- | 80 | -4 | -2 | -8 | 0 | Off | |
| 2-4 | -- | 30 | -20 | -22 | Off | -4 | On | |
| 2-5 | -- | 40 | -20 | -12 | -17 | 4 | On | |
| 2-6 | 1 | 40 | -2 | 0 | -4 | 5 | Off | |
| | 2 | 40 | -2 | -2 | -4 | 5 | Off | |
| 2-8 | 1 | 60 | -8 | 0 | 0 | 4 | Off | |
| 2-10 | 1 | 6- | -18 | -8 | -12 | ** | On | |
| | 2 | 6- | -22 | -4 | -10 | ** | | |
| | 3 | 90 | -15 | 0 | 0 | ** | Off | |
| 2-11 | 1 | 60 | -20 | -12 | -10 | 2 | On | |
| | 2 | 30/30 | -25/ -12* | -25/ -5* | -20/ -10* | -20/ 0* | On | |
| | 3 | 61 | -5 | -3 | -5 | 3 | On | |
| 2-12 | 1 | 61 | -5 | 0 | 0 | 7,10 | On | |
| | 2 | 60 | -15 | 0 | 0 | 7,10 | On | |
| | 3 | 87 | -12 | -2 | 0 | 7,10 | On | |
| 2-13 | 1 | 47 | -10 | 3 | 5 | 7,10 | On | |
| | 2 | 58 | -7 | 0 | 5 | 7,10 | On | |
| | 3 | 54 | -5 | 0 | 2 | 7,10 | On | |
| 2-21 | -- | 60 | 2 | 0 | -5 | 7,10 | On | |
| 2-41 | 1 | 61 | -7 | 0 | 2 | 7,10 | On | |
| | 2 | 60 | -9 | 0 | 0 | 7,10 | On | |
| 2-44 | 1 | 80 | -25 | -5 | -7 | 5 | On | ✓ |
| | 2 | 62 | -10 | 0 | 0 | 5 | On | |
| | 3 | 41 | -5 | 0 | 0 | 7,10 | On | ✓ |

*Precipitation Static

**Not Recorded

Table 6-5. Northeast Corridor Flight Descriptions.

| FLIGHT NUMBER | FLIGHT DESCRIPTION |
|---|---|
| 0-2-1 | Local Check Flight |
| 0-2-2 | Ferry Flight to Farmingdale, N.Y. |
| 0-2-3 | Farmingdale to Bedford: First Flight With Custom Interface Unit |
| 0-2-Z1-1 | Farmingdale to Bedford |
| 0-2-Z1-2 | Farmingdale to Bedford after Receiver Repairs |
| 0-2-4 | Local Night Flight |
| 0-2-5 | Bedford to Farmingdale for Receiver Repairs |
| 0-2-6 | Farmingdale to Bedford, Direct |
| 0-2-7 | Local Flight |
| 0-2-8 | Flight to Washington, D.C. Terminated at Flushing, N.Y. Due to Station D Outage |
| 0-2-9 | Return from Flushing Using Other Stations |
| 0-2-10 | Zulu Route Flight to Washington |
| 0-2-11 | IFR Return Flight from Washington |
| 0-2-12 | Zulu Route Towards Washington; Landing Salisbury, MD. |
| 0-2-13 | Zulu Route Return from Wallops Area |
| 0-2-21 | Repeat of 0-2-7 After Hardware Repairs |
| 0-2-31 | Ferry Flight for Aircraft Maintenance |
| 0-2-41 | Bedford to Wallops Area |
| 0-2-44 | Return from Wallops Area at 5500' and 7500' |

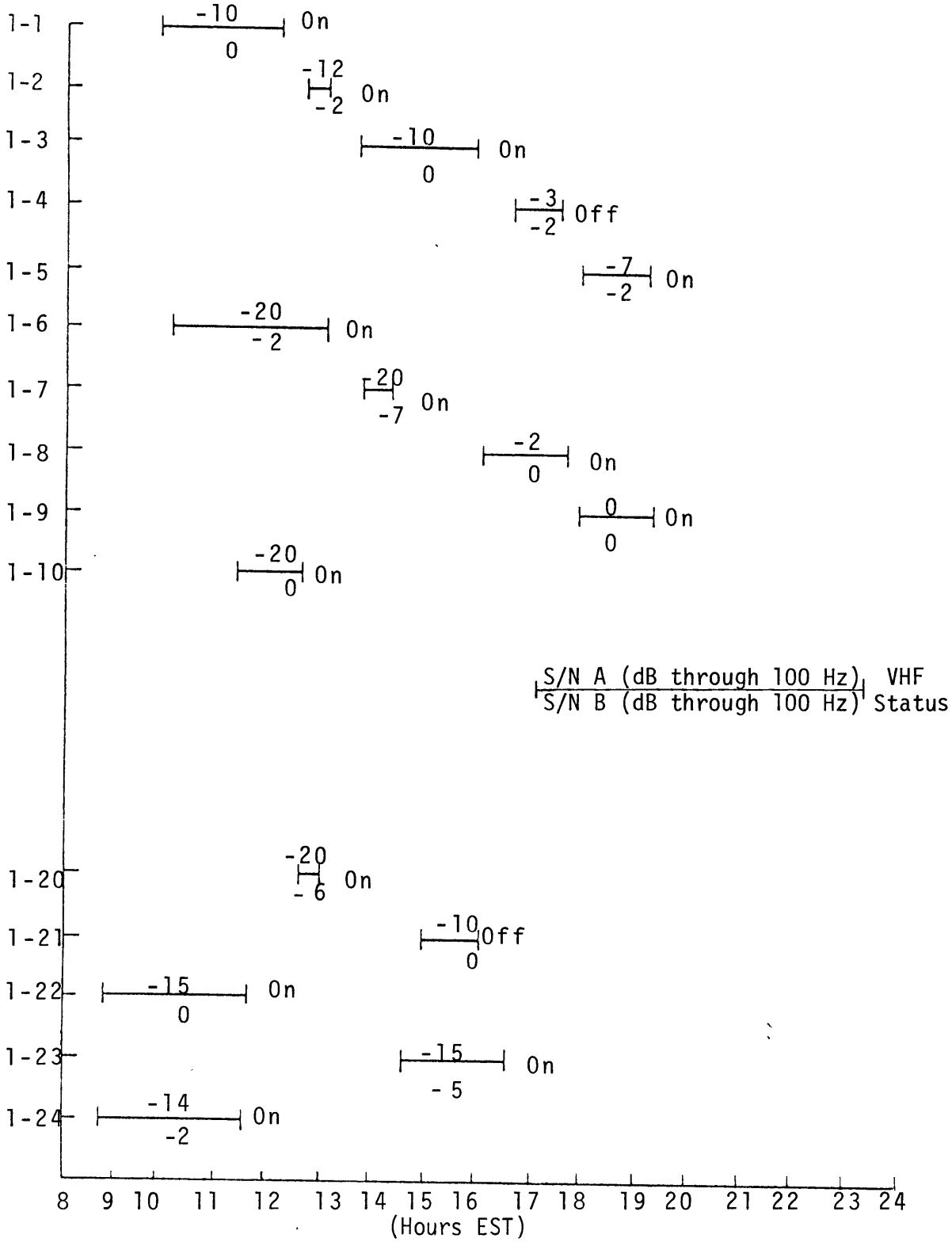


Figure 6-6. Station A and B S/N on Wallops Flights and Time of Day

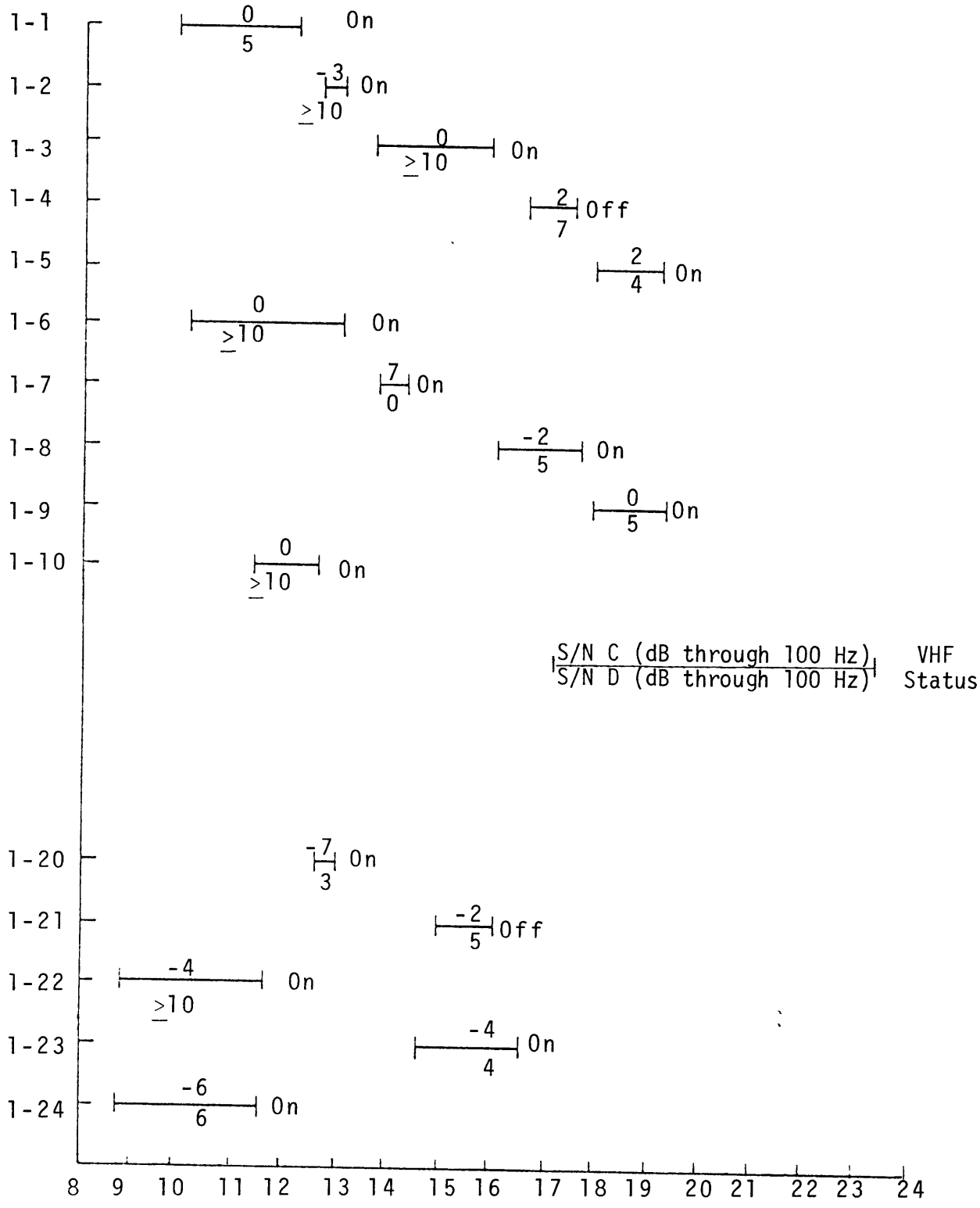


Figure 6-7. Station C and D S/N on Wallops Flights and Time of Day

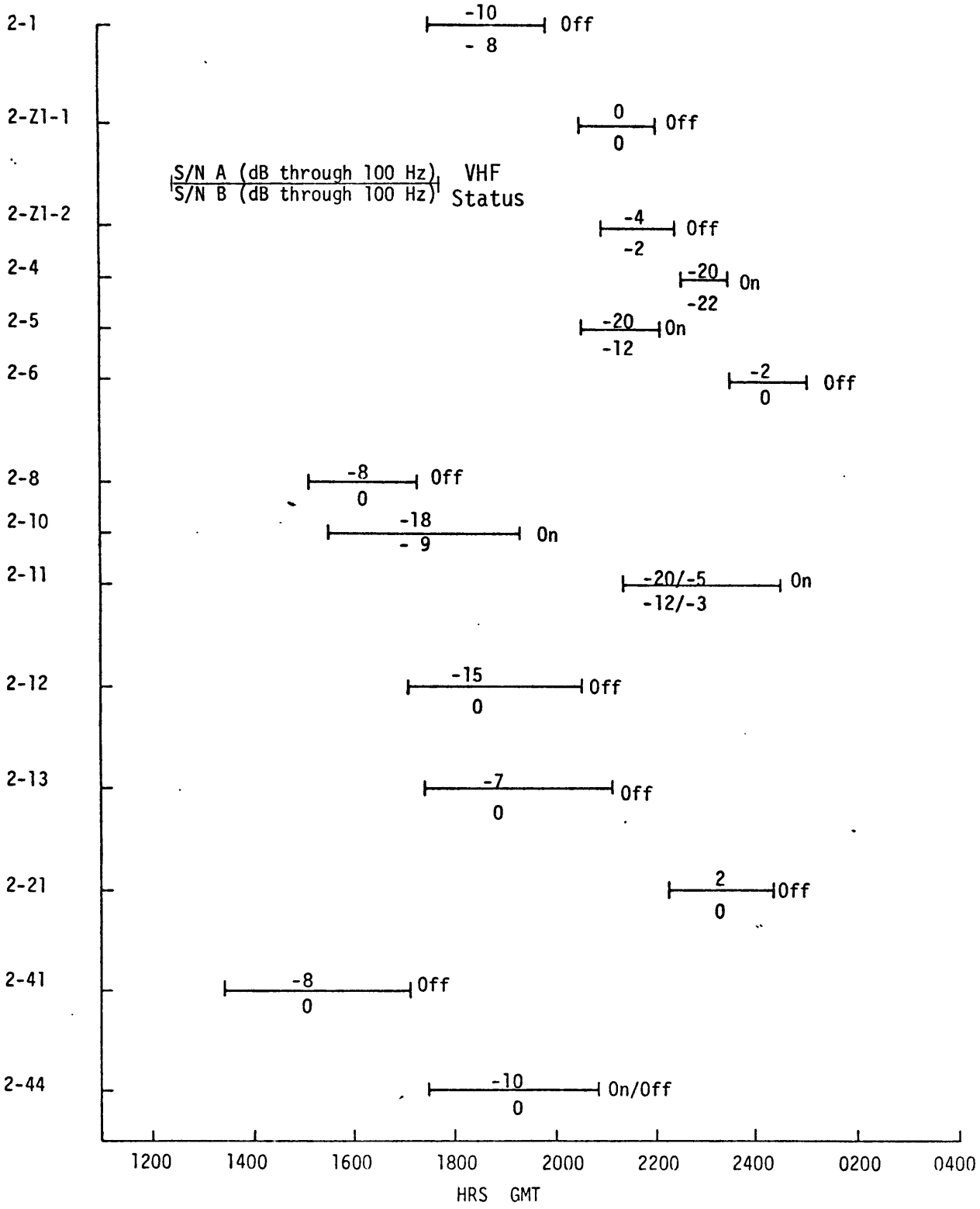


Figure 6-8. Stations A & B S/N on NE Corridor Flights and Time of Day

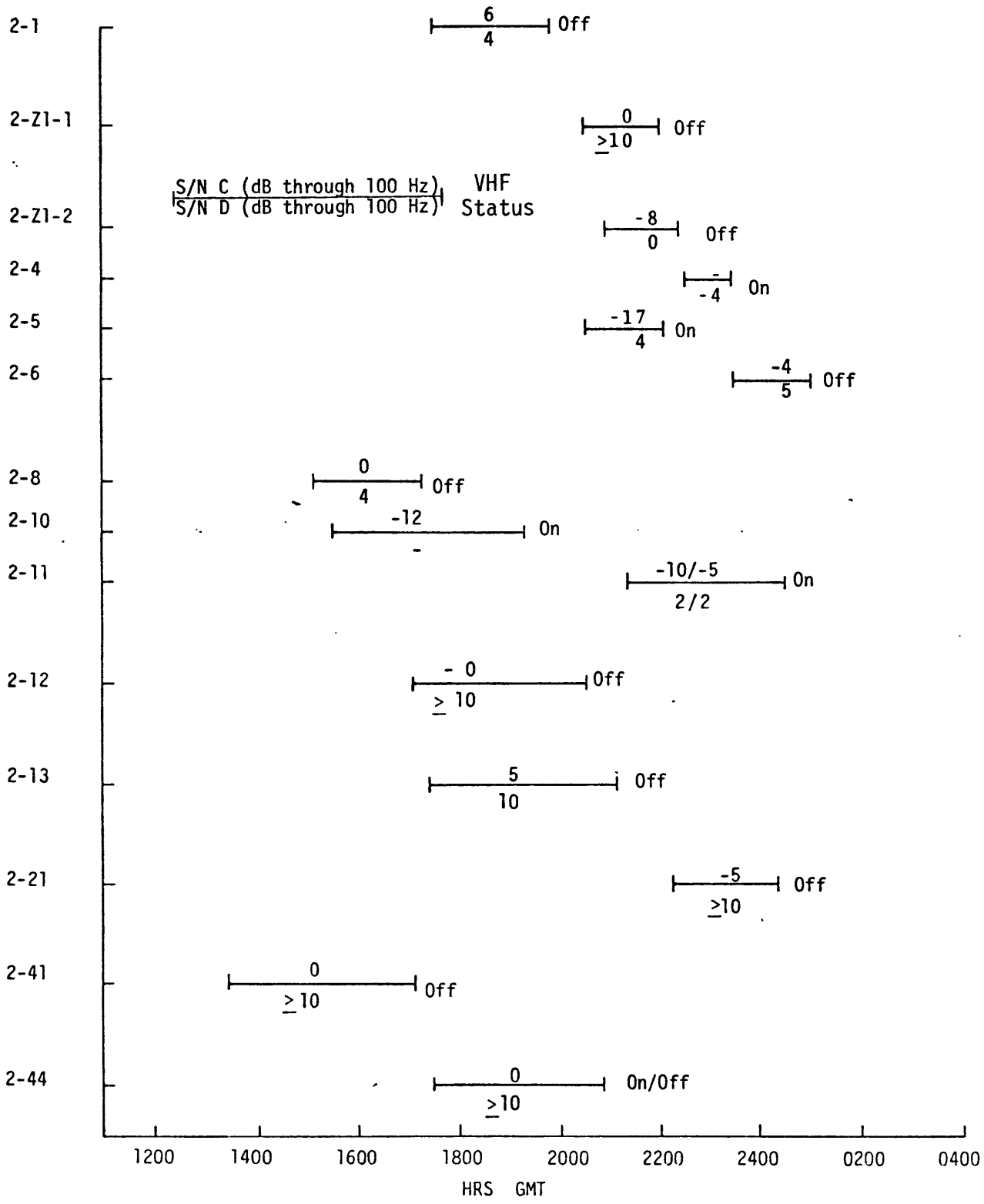


Figure 6-9. Stations C & D S/N on NE Corridor Flights and Time of Day

passage and elapsed time until Omega indication of waypoint passage. As discussed in Chapter V, no position error measurements were available with radar tracking.

Radial errors for the ASI flight test program were compiled and statistics tabulated. These statistics and a histogram of observed errors are shown in Figure 6-10. No distribution was fitted to these data points due to the great number of points with zero indicated error.

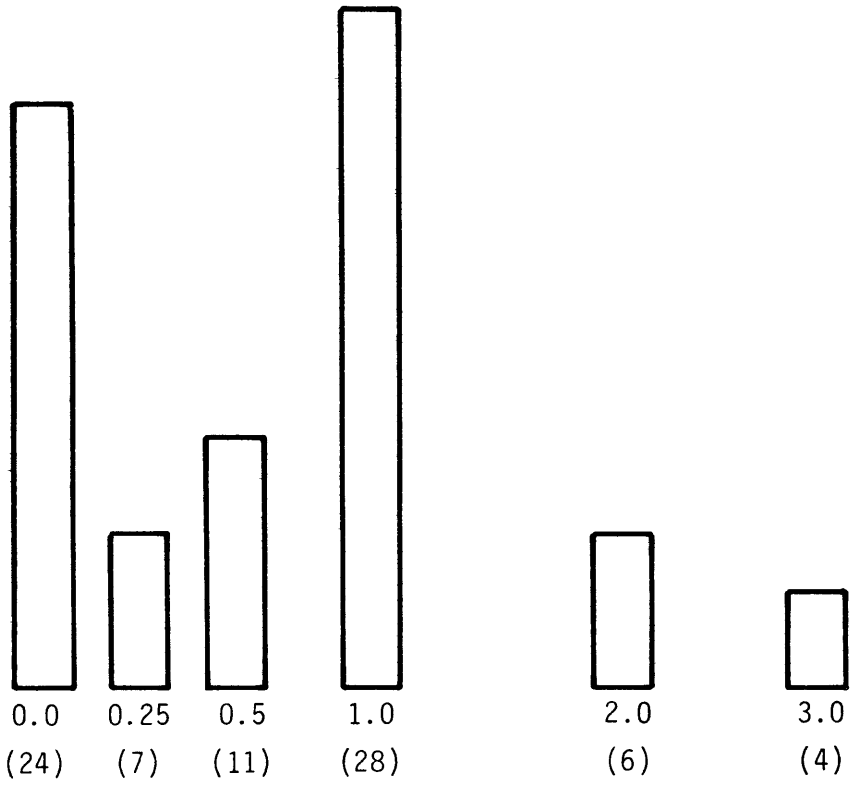


Figure 6-10. Observed Radial Errors, nm., and Number of Data Points ( )

## 6.4 Results of Flying Omega Approaches

Four approaches were flown to the Bedford, MA, airport using the Omega set as the only navigational aid. The aircraft VHF radios were turned off to minimize signal degradation due to the noise from the power supplies, and communication with approach control and Bedford tower was maintained on a portable solid state VHF transceiver. Two localized S/N ratio degradations were observed in flying the various procedures. Most interesting was the accuracy achieved in flying the approaches, as it was possible to fly fairly accurate approaches to the airport, with the receiver twice supplying guidance signals to allow the aircraft to be maneuvered to within 100 yards of the reset point.

With the Dynell receiver, the accumulated phase difference is referenced to the phase difference observed by the receiver when last reset. Hence, if this phase error at reset is large, all subsequent phase measurement will be biased by this same amount. This phenomenon was observed on the first approach, wherein the receiver indications were to fly parallel to the ILS course at Bedford with a bias of one mile. Approach control was unwilling to let the flight continue with this error, so the runway centerline was visually tracked in from the outer marker. Over the center of the airport, the receiver was again reset, and a somewhat smaller bias was observed on the second approach. The receiver was again reset, and no bias was observed on the last two approaches.

The technique for flying these approaches with the very noisy course deviation indicator was to consistently alter the aircraft heading to chase the needle. A gain of approximately 10 degrees of heading change per fifth of full scale deflection was used, resulting in approaches that matched a

beginner's attempts to fly a conventional ILS approach. This technique was used deliberately, using the aircraft itself as a low pass filter. Pilot workload was unacceptably high, and the approach could never be stabilized. However, the final accuracy of these approaches, excluding the biases, was quite good, with a standard deviation visually estimated to be several hundred feet.

These approaches are included in Appendix A, plotted to the same scale as the modified Jeppesen approach plates used for these approaches. The plots also include simulations of various filters described in Appendix A. Vertical tic marks along the path flown indicate position estimates by the simulated filter spaced every two minutes. The effects of various filter lags are apparent.

Localized degradation of S/N ratios was observed in the vicinity of the outer marker on the third approach, but was not encountered on the other approaches. Also, S/N degradation was encountered flying in the vicinity of several TV antennas on Route 128, as seen in Figure A-8. These S/N phenomena were not observed on other occasions, and their occurrence here is not explained.

# CHAPTER VII

# DIFFERENTIAL OMEGA ERROR MODELS

## 7.1 Introduction

Differential Omega is a system modification in which a ground monitor station is used to broadcast phase correction information to system users. RMS error models are constructed analyzing variations in update rate and receiver time constants. SIDs, diurnal variations, and short-term Omega noise are modeled. Errors due to separation of monitor and user are discussed in the literature (2,23).

## 7.2 Models of Diurnal Variations and SID's

Diurnal variations and SIDs are both modeled as ramp functions over a period of up to 15 minutes. SIDs are also modeled as a step function for a conservative error estimate. Phase lock loop (PLL) response to these phenomena are discussed.

Figure 7-1 shows representative diurnal variations in an LOP during disturbed solar conditions. Note the rather linear change in observed LOP at sunrise. Figure 7.2 shows an SID, again with a rather linear change in observed LOP on the leading edge. These are both modeled as ramp functions, with slopes of 70 cel/hr and 43 cel/12 min, or 215 cel/hr, respectively. These add to form a ramp with slope of 285 cel/hr, 0.07917 cel/sec equivalent to about 22.8 mph, even though SID's are a daytime phenomenon.

For a first order phase lock loop with a transfer function of $\frac{1}{\tau s+1}$, the response to a ramp of slope $M$ is

$$y(t) = M[t-\tau + \tau e^{-t/\tau}] \qquad (7.1)$$

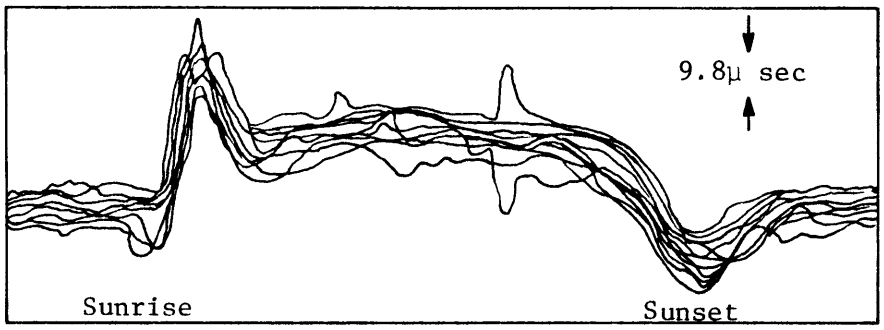


Figure 7-1. Typical Diurnal Variation of Received LOP During Disturbed Solar Conditions. Ref. 22.

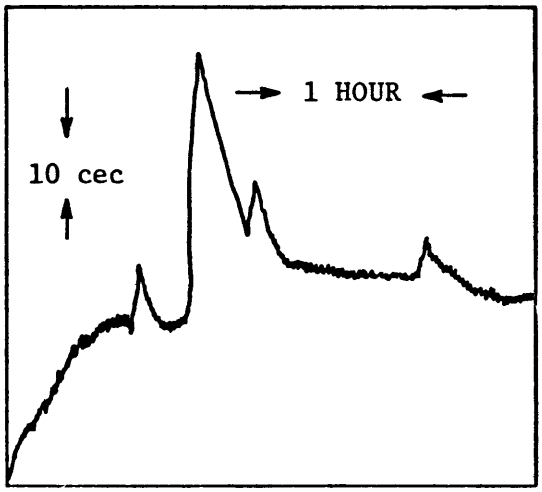


Figure 7-2. Sudden Ionospheric Disturbance. Ref. 22.

Observe that the exponential term is transient. For updates every $T$ seconds, the maximum error is $MT$ cel if both aircraft and monitor receivers have the same time constants. If the two receiver time constants differ by $\Delta\tau$ seconds, the observed error as a function of $T$ is

$$\varepsilon(T) = MT + M\Delta\tau \tag{7.2}$$

Now model the SID as a step function. Although the ionospheric height and received phase cannot, of course, vary instantaneously, this provides a conservative model. As shown in Figure 7-3, the difference in response to a step input $U(s)$ between two first order lags is described by

$$Y(s) = \frac{-(\tau_1-\tau_2)s}{(\tau_1 s+1)(\tau_2 s+1)}\, U(s) \tag{7.3}$$

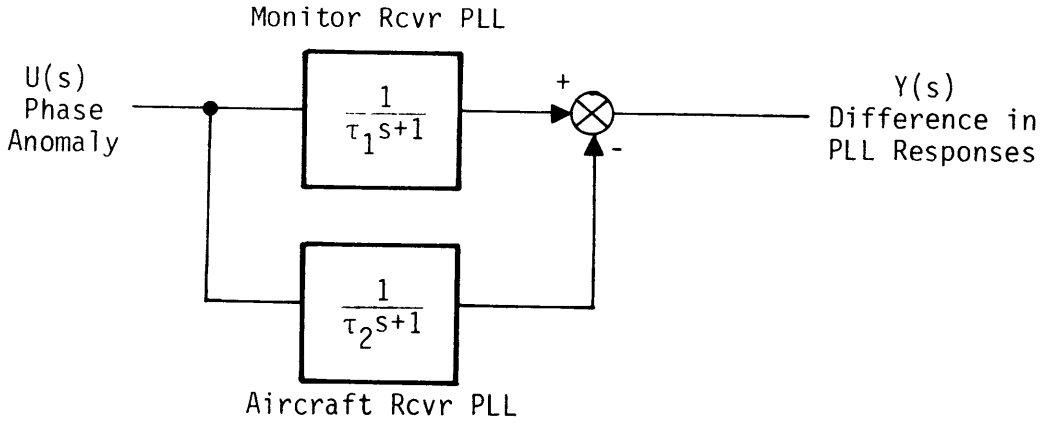


Figure 7-3. Model for Difference in Response to Phase Anomalies

For a unit step, the maximum is

$$\max y(t) = \max \left( e^{-t/\tau_1} - e^{-t/\tau_2} \right) , \qquad (7.4)$$

For $\tau_1$ = 300 sec, $\tau_2$ = 30 sec, and 43 cel step input, a maximum of 29.96 cel occurs at t = 76.75 seconds.

Numerical results of this section are summarized in Table 7-1. Note that the model of the SID as a square wave is more conservative only up to t = 143.75 seconds.

Table 7-1. Differential Omega Errors Due to Diurnal Variations and SIDs for Uplink Intervals T.

| $\tau_1$ | $\tau_2$ | SID MODEL | MAX ERROR $\varepsilon$(T) (T IN SECS) |
|---|---|---|---|
| EQUAL | | RAMP | 0.7917 T cel |
| 300 | 30 | RAMP | 0.7917 T + 21.375 cel |
| 300 | 30 | STEP | 0.01944 T + 29.96 cel |

## 7.3 Short-Term Omega Noise Models in Differential Omega

In Chapter IV, short-term Omega noise was modeled as white Gaussian noise. The effect of passing this noise through a first order phase lock loop with time constant $\tau$ is colored noise with variance varying as $\frac{1}{2\tau}$. The effects of different time constants in the ground monitor and in the aircraft receiver will be examined in view of effects on short-term noise.

For the Dynell receiver used in the measurement of the Omega short-term noise in Chapter IV, a maximum aircraft speed of 400 knots was specified. Interpreting this as the speed at which the phase lock loop lags the true

phase reading by one-half lane, we obtain an estimate of 72 seconds for the time constant of the receiver phase lock loop. However, this analysis makes no allowance for noise in the phase measurements, so a more conservative estimate of 30 seconds was made for the time constant of the Dynell receiver phase lock loop.

Assume that the ground monitor station has a time constant of 300 seconds to reduce the effects of short-term noise on the differential Omega update. In this case, the short-term noise at the output of the ground receiver will be only slightly correlated with the noise at the aircraft receiver. Analysis shows that the short-term noise observed by the aircraft receiver after a differential update will have a standard deviation of about 4.2 cec, which is only a small increase.

For differential Omega updates in less than real time, the short-term Omega noise at the aircraft receiver will be uncorrelated with the short-term noise effects incorporated into the differential Omega update. Thus, the variance observed due to short-term noise will be the sum of variances of the ground and airborne receivers.

For real time differential Omega updates, short-term noise should be reduced. Short-term noise is caused by lightning and other effects which can travel in a waveguide mode similar to the Omega signals. Thus, correlation of short-term noise over short distances should be good, and real time differential Omega using ground and aircraft receivers with identical time constants should substantially reduce short term noise effects. Effects which would not be reduced would be those effects which are not distance correlated, such as local interference from noise sources on the ground and noise sources in the aircraft.

## 7.4 Plots of Errors vs. Differential Update Rates

Chapter 7.2 discussed variations in errors with changes in phase lock loop time constants and update rates due to diurnal variations and SIDs, both of which were modeled as ramp functions. Similarly, Chapter 7.3 discussed various errors observed due to short term noise. These effects are combined in Figures 7-4 through 7-6, with root mean square errors $[(\text{bias}^2 + \text{variance})^{\frac{1}{2}}]$ plotted versus update interval. Note that different receiver time constants on the ground and in the air can cause unacceptable errors due to ramp inputs such as SIDs, even with real time differential uplinks. Real time differential uplinks can reduce short-term noise to the extent that the noise is correlated bewteen ground monitor and aircraft receiver, as well as eliminating propagation anomalies. Thus, real time differential Omega shows the greatest possibility for accuracy enhancement.

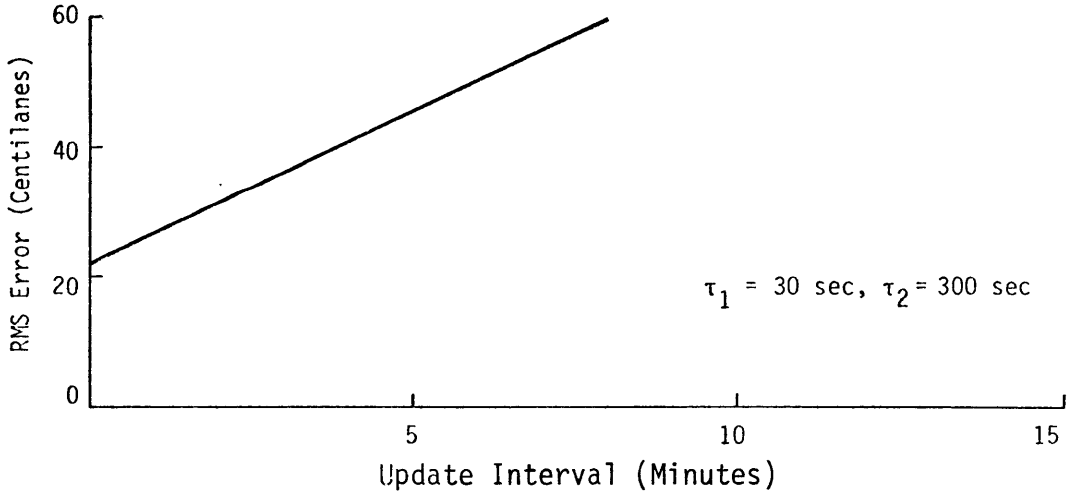


Figure 7-4. RMS Error for Differential Omega (SID as Ramp Error)

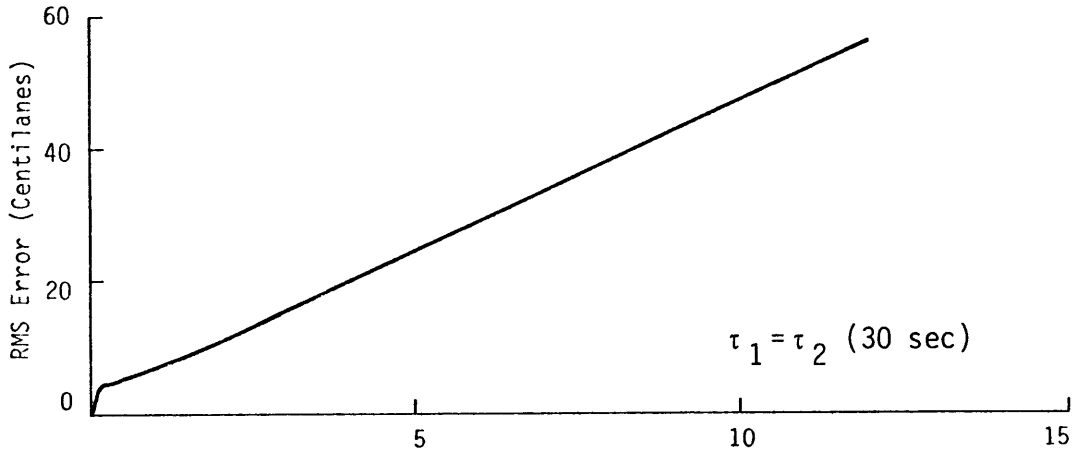


Figure 7-5. RMS Error for Differential Omega

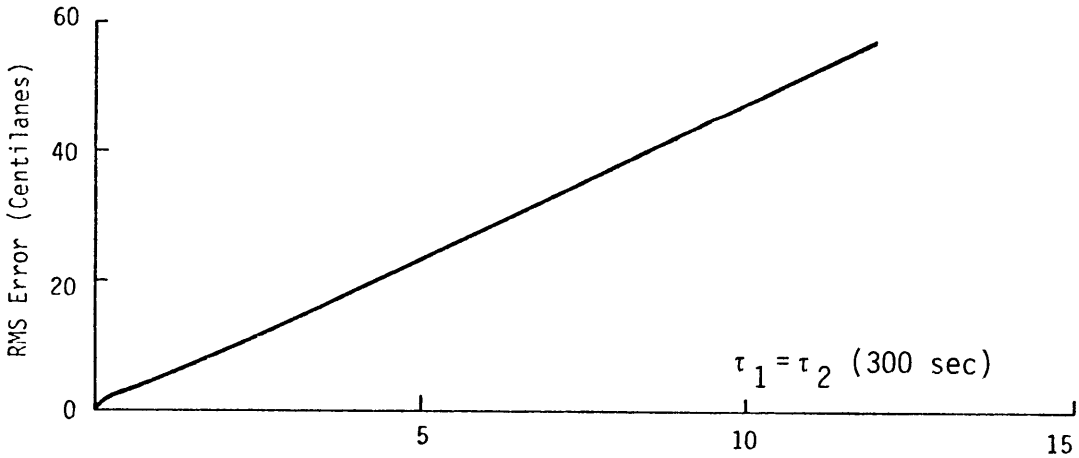


Figure 7-6. RMS Error for Differential Omega

## 7.5 Conclusions

For aircraft navigation, large mismatches in receiver phase lock loop time constants (e.g., a factor of ten) can cause errors in differential Omega on the order of 20-30 cec in the presence of SIDs, regardless of update rates. If aircraft and receiver time constants have identical time constants, differential Omega updates spaced no more than one minute apart should be acceptable, with advantages to be had with real time differential Omega reducing short-term noise effects.

CHAPTER VIII

# PATH FOLLOWING MODELS USING OMEGA

## 8.1 Introduction

For aviation applications, most navigational information is used for determination of either the proper heading for the aircraft to fly or estimated time enroute. In Chapter VI, it was shown by flight test that Omega navigation appears to have a capability for providing guidance information of sufficiently good quality to allow approaches to be flown, at least under some conditions. In this chapter, various models of path following using Omega navigation will be discussed to answer the question, "How well can an aircraft follow a track using differential Omega?"

Figure 8-1 shows the basic configuration of the path following models. Starting from the top left and going across, heading noise is the yaw

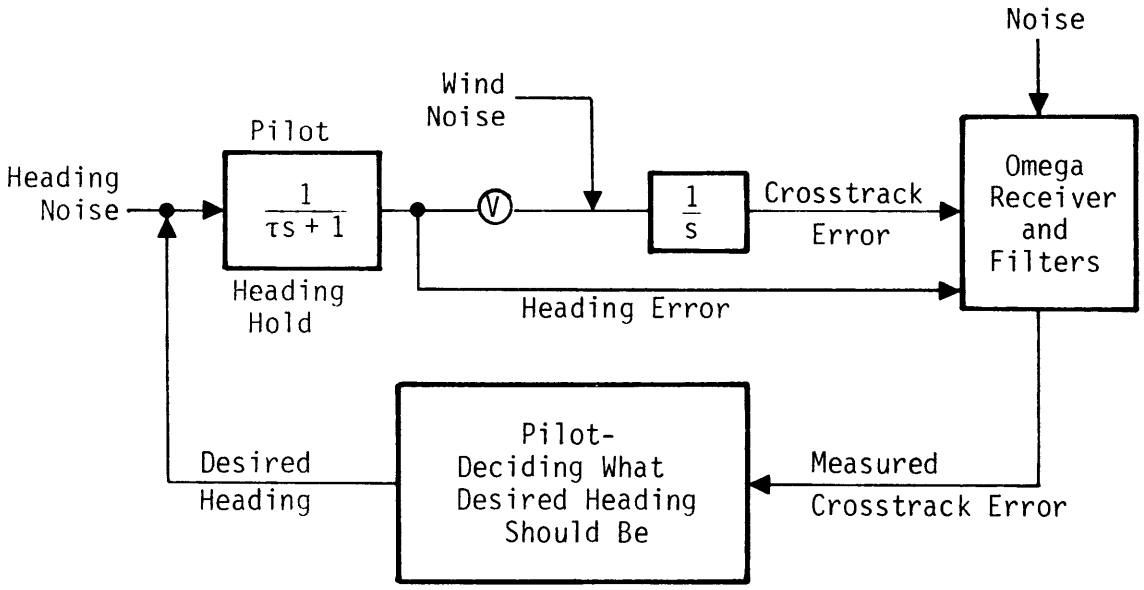


Figure 8-1. Basic Path Following Model

response of the aircraft to turbulence. In other words, heading noise reflects the fact that the aircraft does not hold heading by itself. This heading noise is fed into a first order lag which represents the pilot acting to hold the heading that he has decided is appropriate for the approach. This lag also serves to color the white heading noise. The output of the lag is heading error, which is one possible measurement to be used in the filter which estimates crosstrack error.

The heading error is assumed to be small, so that the sine of the angle is nearly equal to the angle itself (in radians). Thus, by multiplying by the aircraft groundspeed V, the heading error is converted into actual crosstrack error rate. Wind noise is added as a velocity and integrated along with the crosstrack error rate to give the actual crosstrack error. This error is measured by the Omega receiver, along with some Omega noise of various types. It is assumed that differential Omega will be utilized at a high uplink rate to eliminate biases and unpredictable propagation anomalies, as discussed in Chapter VII. For the models of this chapter, Omega noise is modeled as short-term noise as measured in Chapter IV.

The crosstrack error information, heading error information, and Omega noise are combined and processed by various linear system models representing the pilot and the filtering done to the data before presentation to the pilot. Several different models were used, ranging from simple gains to Kalman filters to integral feedback controllers. From the feedback loop, a heading error signal is generated which is fed back into the heading hold lag.

## 8.2 Preliminary Analysis

### 8.2.1 Introduction

In the preliminary analysis of the path following model, the various noise sources will be discussed in detail. In addition, one simple model of path following, using the pilot as a pure gain, will be discussed.

### 8.2.2 Noise Sources in the Path Following Model

In the path following model, there are three noise sources: heading noise, wind noise, and Omega noise. Each of these is discussed in turn.

Heading noise represents the yaw response of the aircraft to turbulence, and also reflects the pilot's inability to precisely hold a heading. The heading noise itself is modeled as white driving noise, so that the noise at the output of the heading hold lag is colored Gaussian noise, correlated over the time constant of the heading hold lag, and with a variance equivalent to $(3°)^2$. It will be shown that heading noise is small compared to other noise sources, and can be neglected.

Wind noise was modeled in three different ways. In the preliminary analysis, wind noise was modeled as variations in wind about the steady state velocity, and very modest values of wind noise were used. Later models of wind represent the effect as a random walk in either position or velocity to account for wind shear effects. For the case of random walk in velocity, white driving noise was fed into an integrator with finite time constant of 50 seconds to give an output with variance of $(50\ \text{ft/sec})^2$. Although the use of a finite time constant means that this is not really a random walk, two advantages accrue: the variance of the system reaches steady state and can therefore be studied with the linear steady state Riccati equation; and the finite variance allows the model results to be correlated with wind

shears of various amounts. For example, the $(50\ ft/sec)^2$ variance represents the mean square value of a wind shear (change in wind velocity) of 50 ft/sec, or about 30 knots. The strength of the driving noise is then $100\ ft^3/sec^2$.

For wind shear modeled as a random walk in position, the situation is somewhat different. The integration producing the random walk is the integration of crosstrack error rate to give crosstrack error, and there is feedback around this integrator, namely, the path following circuitry. Thus, modeling the wind shear as a random walk in position is equivalent to modeling the wind as white noise in velocity. A strength of $(50\ ft/sec^2)$ x (50 sec) was used. The 50 sec is used to model a shear of 50 ft/sec encountered over 50 seconds of flying the approach.

Omega noise was discussed in detail in Chapter IV. For continuous time models, Omega noise is modeled as white noise with a strength of $(2000\ ft)^2$ x (10 sec). Ten seconds represents the sampling time of the Omega system, and thus was chosen to be the time term in the strength of the noise. Two thousand feet is approximately four cel, and is thus the standard deviation of the noise as measured in Chapter IV.

### 8.2.3 Simple Path Following Model

Figure 8-2 shows a simple path following model. In this model, Omega data is filtered with a time constant T and linearly combined with integrated heading error times estimated speed. The integrated heading provides higher frequency response than would be possible with just the filtered Omega data, as the Omega data filter would have to be longer than ten seconds in order to reduce the Omega noise. With this long time

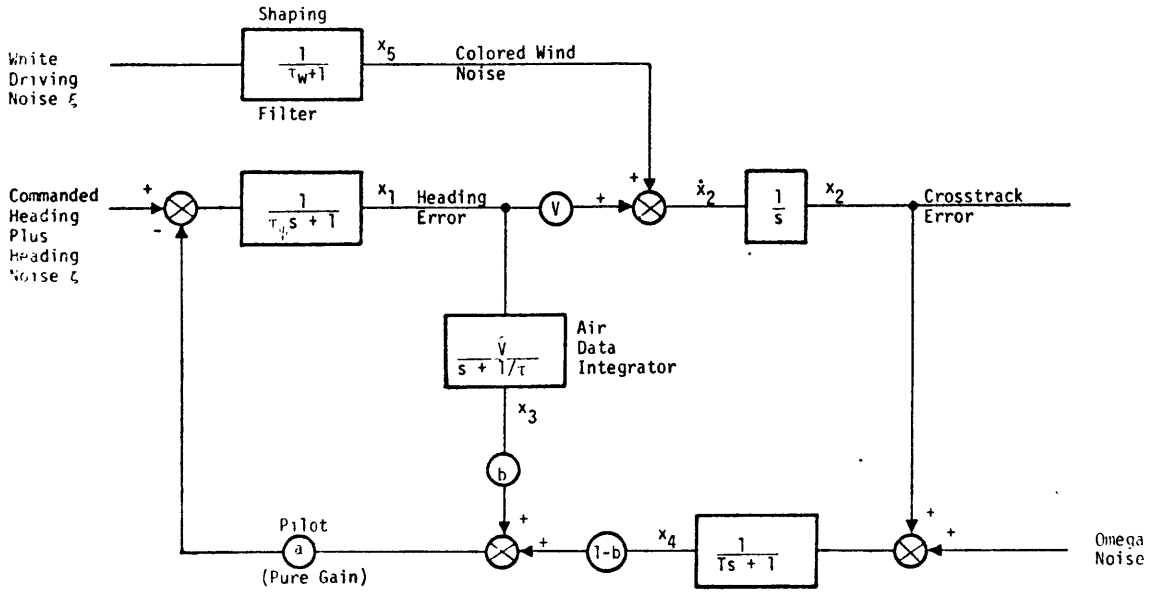


Figure 8-2. Simple Path Following Model (see also Table 8-1).

constant, system response to a wind shear input, modeled as a ramp input, could be excessively sluggish.

In this path following model, the primary feedback path is through the Omega filter, and has a time constant of approximately $\frac{1}{(1-b)aV}$. As the time constant gets longer, the system gets progressively less sensitive to Omega noise and more sensitive to wind noise. Numerical analysis of this system was done by solving the algebraic Riccati Equation 8.1,

$$0 = \dot{\Sigma} = A\Sigma + \Sigma A' + C \equiv C' \; ; \quad \Sigma = E(xx'): \equiv = E(\xi\xi') \tag{8.1}$$

where the A and C matrices define the system dynamics as shown in Eqs. 8.2 and 8.3.

$$\begin{bmatrix} \dot{x}_1 \\ \dot{x}_2 \\ \dot{x}_3 \\ \dot{x}_4 \\ \dot{x}_5 \end{bmatrix} = \begin{bmatrix} -\frac{1}{\tau_\psi} & 0 & -\frac{ab}{\tau_\psi} & -\frac{a}{\tau_\psi}(1-b) & 0 \\ +v & 0 & 0 & 0 & 1 \\ +\hat{v} & 0 & -\frac{1}{\tau} & 0 & 0 \\ 0 & \frac{1}{T} & 0 & -\frac{1}{T} & 0 \\ 0 & 0 & 0 & 0 & -\frac{1}{\tau_w} \end{bmatrix} \begin{bmatrix} x_1 \\ x_2 \\ x_3 \\ x_4 \\ x_5 \end{bmatrix}$$

$$+ \begin{bmatrix} \frac{1}{\tau_\psi} & 0 & 0 \\ 0 & 0 & 0 \\ 0 & 0 & 0 \\ 0 & \frac{1}{T} & 0 \\ 0 & 0 & \frac{1}{\tau} \end{bmatrix} \begin{bmatrix} \zeta \\ \omega \\ \xi \end{bmatrix} \tag{8.2}$$

$$\underline{\dot{x}} = \underline{A}\,\underline{x} + \underline{C}\,\underline{\xi} \tag{8.3}$$

Definitions of states and nominal values of parameters are shown in Table 8-1.

The poles of the system were determined by solving the characteristic equation of the system matrix, and the characteristic equation is 8.4.

$$0 = \left(\lambda + \frac{1}{\tau_w}\right)\left[\lambda^4 + \lambda^3\left(\frac{1}{T} + \frac{1}{\tau} + \frac{1}{\tau_\psi}\right) + \lambda^2\left(\frac{1}{\tau_\psi \tau} + \hat{v}\,\frac{ab}{\tau_\psi} + \frac{1}{T\tau_\psi} + \frac{1}{T\tau}\right)\right.$$

$$\left. + \lambda\left(\frac{1}{T\tau\tau_\psi} + \hat{v}\,\frac{ab}{T\tau_\psi} + \frac{av}{T\tau_\psi}(1-b)\right) + \frac{av}{T\tau\tau_\psi}\,(1-b)\right] \tag{8.4}$$

Table 8-1. Variables of Simple Path Following Model.

| SYMBOL | VARIABLE | UNITS OR NOMINAL VALUE |
|---|---|---|
| $x_1$ | State variable of heading follower | radians |
| $x_2$ | Crosstrack error | feet |
| $x_3$ | State variable of air data integrator | feet |
| $x_4$ | State variable of Omega filter | feet |
| $x_5$ | State variable of wind shaping filter | ft/sec |
| $\tau_w$ | Time constant of wind shaping filter | 2 sec |
| $\tau$ | Time constant of air data integrator | 1 sec |
| $\tau_\psi$ | Time constant of heading follower | 3 sec |
| T | Time constant of Omega data filter | 30 sec |
| a | Pilot, acting as a gain of | 1°/500' |
| b | Air data filter parameter | 0.5 |
| v | Aircraft velocity ($\sim$ 120 kt) | 200'/sec |
| $\hat{v}$ | Estimate of v | 200'/sec |
| $\xi$ | Wind filter driving noise of strength | $(5'/sec)^2$ x 2 sec |
| $\zeta$ | Heading noise of strength | $(2°)^2$ x 3 sec |
| $\omega$ | Omega noise (4 cec $\sim$ 2000 ft) of strength | $(2000')^2$ x 10 sec |

This equation was solved numerically, with results shown in Table 8-2. The poles of the wind shaping filter, the heading hold lag, and the air data integrator were found to be essentially invariant to changes in T and b, so their time constants are not listed in Table 8-2. Note that system time constants are fairly long, and get longer as b decreases. However, this preliminary model assumes that the pilot acts strictly as a gain, which is one weakness of the model. Crosstrack standard deviations are shown in Table 8-3 for various values of T and b. These values are fairly small, and reflect the long time constant filtering effect of the small feedback gain.

With T = 0 sec, and b = 0, the system effectively reduces to third order. With no filtering of the Omega data, crosstrack standard deviations increase as shown in Table 8-4. Note that the use of air data does not supply information to the pilot that is really new. The information is an estimate of crosstrack error based upon heading error, and the pilot can derive this information for himself from his instruments at some expense in workload. Furthermore, the use of air data requires integration of a compass system into the Omega navigation system, with attendant economic penalties for general aviation.

This preliminary analysis has several flaws, however. Most importantly, susceptibility to wind shear has not been measured, and it remains to be shown that the impressive accuracies theoretically obtainable are not severely degraded in the presence of wind shear. Also, the effects of the sampling in the Omega system have been totally ignored. This is not too serious, however, as the time constant of the path following loop is much

Table 8-2. Simple Path Following Model System Time Constants with Variations in b and T. (Other Parameters at Nominal Values of Table 8-1).

| OMEGA FILTER TIME CONSTANT T = 30 SECONDS | |
|---|---|
| FILTER PARAMETER b | SYSTEM TIME CONSTANTS (Seconds) |
| 0.4 | 31,224 |
| 0.45 | 31,251 |
| 0.5 | 30,283 |
| 0.55 | 29,323 |
| 0.6 | 28,392 |
| OMEGA FILTER TIME CONSTANT T = 60 SECONDS | |
| FILTER PARAMETER b | SYSTEM TIME CONSTANTS (Seconds) |
| 0.4 | 68,207 |
| 0.45 | 63,243 |
| 0.5 | 60,284 |
| 0.55 | 57,332 |
| 0.6 | 54,391 |

Table 8-3. Omega Crosstrack Standard Deviations with Filter Data (Unspecified Gains and Noise Strengths at Nominal Values of Table 8-1).

| OMEGA FILTER TIME CONSTANT T = 30 SECONDS | | | | |
|---|---|---|---|---|
| FILTER PARAMETER | CROSSTRACK DEVIATIONS WITH VARIOUS NOISES (FT) | | | |
| b | Heading Noise | Wind Noise | Omega Noise | All Sources |
| 0.4 | 140.1 | 100.8 | 290.7 | 338.1 |
| 0.45 | 145.6 | 104.8 | 278.2 | 331.0 |
| 0.5 | 151.9 | 109.4 | 265.1 | 324.0 |
| 0.55 | 159.3 | 114.7 | 251.3 | 318.9 |
| 0.6 | 168.1 | 121.1 | 236.8 | 314.6 |
| OMEGA FILTER TIME CONSTANT T = 60 SECONDS | | | | |
| FILTER PARAMETER | CROSSTRACK DEVIATIONS WITH VARIOUS NOISES (FT) | | | |
| b | Heading Noise | Wind Noise | Omega Noise | All Sources |
| 0.4 | 147.7 | 106.3 | 290.8 | 343.1 |
| 0.45 | 152.9 | 110.1 | 278.3 | 336.1 |
| 0.5 | 159.0 | 114.4 | 265.1 | 329.6 |
| 0.55 | 166.1 | 117.6 | 251.4 | 324.1 |
| 0.6 | 174.5 | 125.7 | 236.8 | 319.1 |

Table 8-4. Crosstrack Standard Deviation of Simple Model (T = 0, b = 0)

| NOISE SOURCE(S) | STANDARD DEVIATION (FT) |
|---|---|
| All | 401.1 |
| Omega Only | 373.7 |
| Heading Noise | 102.3 |
| Wind Noise | 103.9 |

longer than the sampling time of the system. However, the faster system dynamics are not all faster than the sampler, so this assumption is of limited validity.

## 8.3 Models Using Kalman-Bucy Filtering

### 8.3.1 Introduction

In this section, two models of path following will be studied. In the first model, wind noise is modeled as a random walk in position, and in the second model, as a random walk in velocity. Dynamics of the heading hold lag are neglected to make analytical solutions of the filter equations feasible, and this is justified on the grounds that these dynamics are fast compared to the rest of the system. Also based upon economic reasons discussed above, air data is not assumed to be available for use in the filters.

### 8.3.2 Path Following With Wind As Random Walk In Position

Figure 8-3 shows the model of path following with wind as a random walk in position, or equivalently, a white driving noise in velocity. Omega

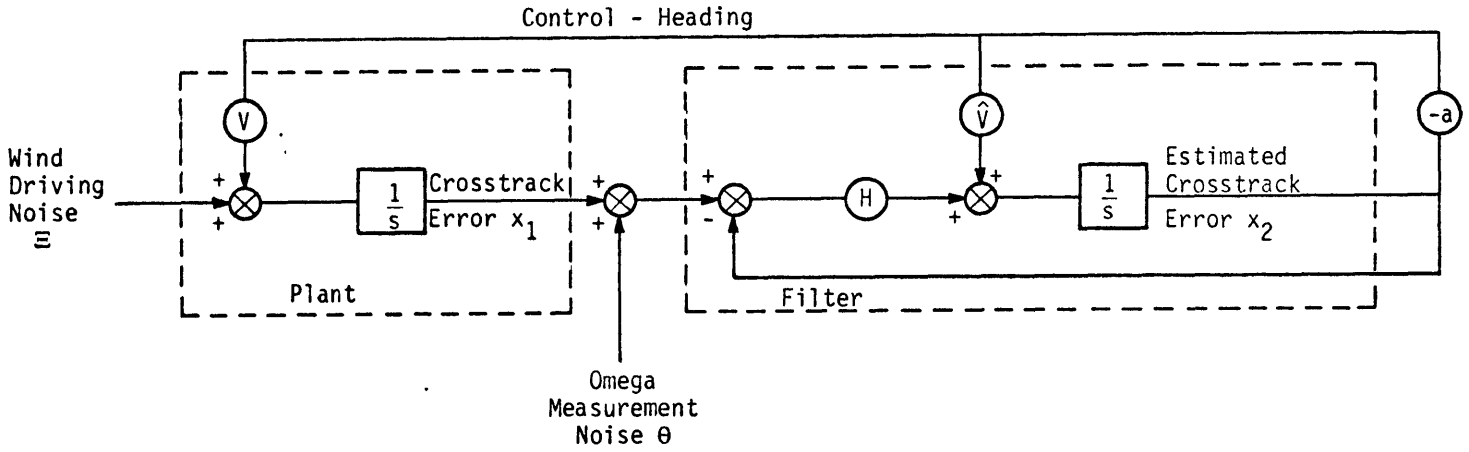


Figure 8.3. Path Following Model with Wind as Random Walk in Position

noise is measurement noise, and heading noise is neglected because in previous anlaysis, with a very small wind noise, the heading noise and wind noise contributed almost equally to standard deviations cross track. In this analysis, the wind noise has been tremendously augmented to represent wind shear.

For a linear state estimator, the error of the estimate is described by Eq. 8.5 where $\Sigma$ is the covariance of the estimation error, $A$ is the system dynamics matrix, $\Xi$ is the strength of the driving noise, $\Theta$ is the strength of the measurement noise, and $C$ is the system output matrix.

$$\dot{\Sigma} = A\Sigma + \Sigma A' + \Xi - \Sigma C'\Theta^{-1} C\Sigma \tag{8.5}$$

The optimal gain matrix $H$ is given by Eq. 8.6.

$$H = \Sigma C'\Theta^{-1} \tag{8.6}$$

For the system under consideration, in steady state, Eq. 8.5 reduces to Eq. 8.7, where all matrices are 1 by 1 (scalars). The solution to this

$$0 = \dot{\Sigma} = \Xi - \Sigma^2 \Theta^{-1} \tag{8.7}$$

equation is given by Eq. 8.8. Thus, $H$ can be obtained by combining the

$$\Sigma = \sqrt{\Xi\Theta} \tag{8.8}$$

results of Eq. 8.8 with Eq. 8.6 to obtain Eq. 8.9.

$$H = \sqrt{\Xi/\Theta} \tag{8.9}$$

Solving for the optimal control is not straightforward, because the criterion is minimization of the crosstrack error. Because there is no cost on the control, assumptions on positive definiteness of matrices which are to be inverted are violated. Therefore, viewing the system as a linear time invariant system (as in Eq. 8.3), the algebraic Riccati Eq. 8.10 was solved for $\sigma^2$, the variance of the crosstrack error (Eq. 8.11).

$$\dot{\Sigma} = A\Sigma + \Sigma A' + C \equiv C' \tag{8.10}$$

$$\sigma^2 = \frac{Hav}{2(H+av)}\,\Theta + \left(\frac{1}{2(H+av)} + \frac{H+av}{2Hav}\right)\Xi \tag{8.11}$$

Differentiating Eq. 8.11 with respect to av and substituting in the value of H from Eq. 8.9, setting the derivative to zero and performing the algebra yields Eq. 8.12. Solving then for $\sigma^2$,

$$av = \sqrt{\Xi/\Theta} \tag{8.12}$$

$$\sigma^2 = \sqrt{\Xi\Theta} \tag{8.13}$$

Using the noise sources in Chapter 8.2.2, we obtain a crosstrack standard deviation of about 1495.35 ft, with system path following time constant of $\frac{1}{av}$ or approximately 17.89 seconds.

It is interesting to note from Eq. 8.12 that as the wind noise increases, the effective time constant of the system should decrease, and as the wind decreases, the system time constant should increase to more heavily filter the Omega noise. The computed value of 17.89 seconds roughly approximates the time constant of the phase lock loop in the Dynell receiver flight tested.

8.3.3 Path Following with Wind as Random Walk in Velocity

Figure 8-4 shows a model of path following using wind modeled as a random walk in velocity as described in Chapter 8.2.2. Observe that the Kalman filter and optimal control law each involve two gains. The Kalman filter gains were solved analytically, but the control laws were not solved, as this involved solution of ten simultaneous linear equations. Although the equation could easily have been solved numerically, an analytic solution was sought to provide insight into the workings of the system.

Solving Eq. 8.5 for the covariance of the estimator error, the variance $\sigma_{22}$ of the estimate of the state $x_2$ is given by Eq. 8.14.

$$0 = -\tau^2\sigma_{22}^4 - 4\Theta\tau\sigma_{22}^3 - 4\frac{\Theta^2}{\tau}\sigma_{22}^2 + 4\Xi\Theta^3\tau \tag{8.14}$$

Knowing that there is exactly one positive solution (by uniqueness theorems and also because there is exactly one change of sign in the coefficients of the equation), and using the substitution $x = \sigma_{22} + \frac{\Theta}{\tau}$, the variance $\sigma_{22}$ is found to be

$$\sigma_{22} = \left(\frac{\Theta^2}{\tau^2} + \sqrt{\Xi\Theta^3}\right)^{1/2} \tag{8.15}$$

The cross covariance between estimation errors is given by Eq. 8.16 as a result of solving Eq. 8.5. These two terms are the only ones required to

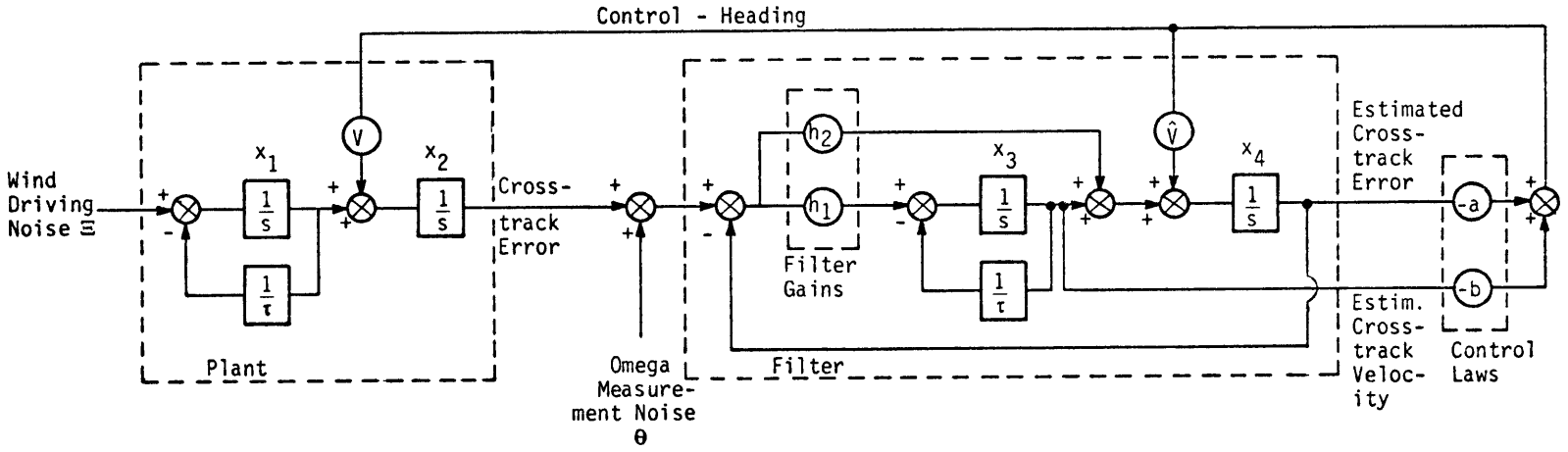


Figure 8-4. Path Following Model with Wind as Random Walk in Velocity

$$\sigma_{21} = \frac{\sigma_2^2}{2\Theta} \tag{8.16}$$

determine the steady state Kalman gains. Involing Eq. 8.6 again, the (optimal) Kalman gain matrix is

$$H = \begin{bmatrix} \frac{\sigma_{21}}{\Theta} \\ \frac{\sigma_{22}}{\Theta} \end{bmatrix} \tag{8.17}$$

Again, positive definiteness of the control cost matrix was not realized and the plant is not completely controllable, so optimal control techniques were not used. Viewing the system as a fourth order linear time invariant system, an attempt was made to analytically solve the steady state covariance matrix. The problem became very involved, however, with such long intermediate expressions that it was doubtful whether the analytic solution would yield meaningful insight into the problem. Therefore, another model of the problem was studied.

## 8.4 Path Following with Integral Control

Figure 8-5 shows a path following model using a gain and an integrator in parallel in the feedback loop. The plant has two state variables, and the estimator has one state. Although the gain configuration is not in a standard form, this filter is a suboptimal linear filter. Considering the states of the two integrators on the right and their feedback loops, a damped second order system is equivalent to a first order filter in the feedback path.

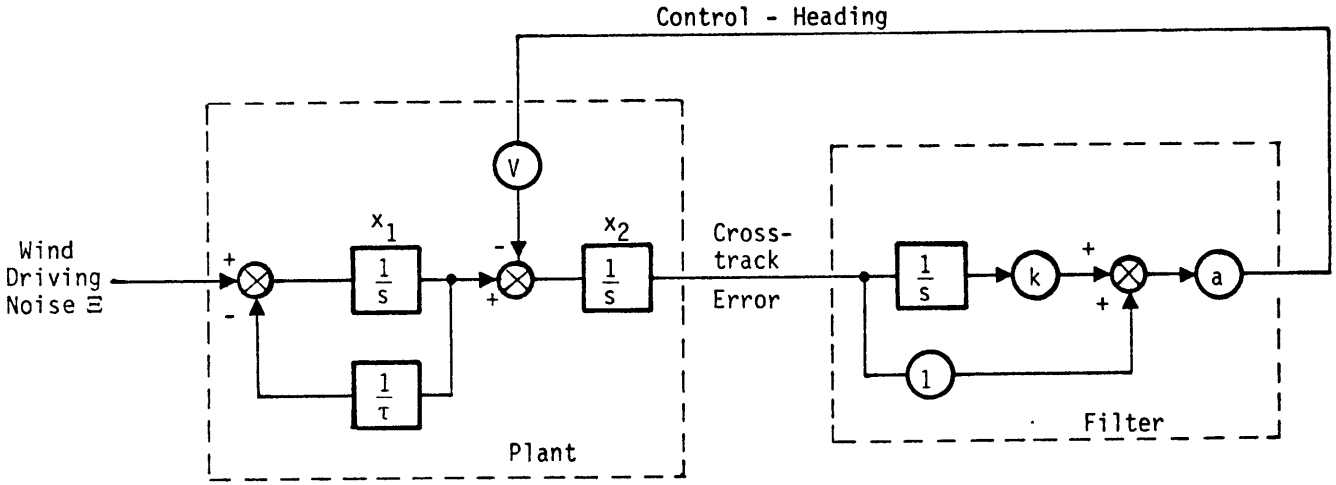


Figure 8-5. Path Following Model with Integral Control

The steady state covariance Eq. 8.10 was solved analytically for this system, and the solution of this equation for the crosstrack error is given by

$$\sigma_{22} = \left(\frac{av}{2} + \frac{k}{2}\right)\theta + \frac{\tau}{2av\ (kav\tau + av\ +\ 1/\tau)}\ \Xi \tag{8.18}$$

Observe that as $k$ and $av$ increase, the Omega noise term in $\theta$ increases monotonically, and the wind noise term decreases monotonically. Thus, it is seen that the tradeoff between Omega noise and wind noise determines optimal values of $k$ and $av$.

Differentiating $\sigma_{22}$ with respect to $k$ and setting the derivative to zero, the value of $k$ to minimize $\sigma_{22}$ is as shown in Eq. 8.19.

$$k = \frac{1}{av}\sqrt{\Xi/\Theta} - \frac{1}{\tau^2} - \frac{1}{av\tau^2} \tag{8.19}$$

Using this $k$, and again differentiating $\sigma_{22}$ but with respect to $av$, we obtain Eq. 8.20.

$$a = \frac{1}{v}\left[2\sqrt{\Xi/\Theta} - \frac{1}{\tau^2}\right]^{\frac{1}{2}} \tag{8.20}$$

Numerically, for the wind and Omega noise values of Table 8-1, this gives $k = 0.00247/sec$, and $av = 0.0525/sec$. The crosstrack standard deviation of this configuration is about 1304.72 feet.

Eq. 8.21 is the state space equation for this system, with variables defined in Table 8-5. The characteristic equation for this system, Eq. 8.22,

$$\begin{bmatrix} \dot{x}_1 \\ \dot{x}_2 \\ \dot{x}_3 \end{bmatrix} = \begin{bmatrix} -\frac{1}{T} & 0 & 0 \\ 1 & -av & -kav \\ 0 & 1 & 0 \end{bmatrix} \begin{bmatrix} x_1 \\ x_2 \\ x_3 \end{bmatrix} + \begin{bmatrix} 1 & 0 \\ 0 & -av \\ 0 & 1 \end{bmatrix} \begin{bmatrix} \xi \\ \theta \end{bmatrix} \tag{8.21}$$

$$0 = \left(\lambda + \frac{1}{T}\right)\left(\lambda^2 + \lambda av + kav\right) \tag{8.22}$$

was solved for the poles of the system, and these have time constants of 20.02 seconds and 384.30 seconds. The residues of these poles are 1.05 for the 20-second pole, and -0.055 for the 384-second pole. Thus, the 20-second response dominates, and has response of opposite sign to the longer time constant response.

In practice, optimal values of k and a may not be known, as noise strengths and aircraft speed may not be known exactly. For this reason,

Table 8-5. Variables of Path Following with Integral Control

| SYMBOL | VARIABLE | UNITS OR NOMINAL VALUE |
|---|---|---|
| $x_1$ | State variable of wind integrator | ft/sec |
| $x_2$ | State variable of crosstrack error | feet |
| $x_3$ | State variable of feedback integrator | feet-sec |
| $\tau$ | Time constant of wind integrator | 50 sec |
| v | Aircraft speed | 200 ft/sec (~120 kt) |
| a | Feedback control gain | (radians)/ft |
| k | Feedback control gain | 1/sec |

crosstrack standard deviations were calculated with k and a varying by a factor of 2. These results, shown in Table 8-6, show that the crosstrack standard deviation is remarkably insensitive to variations in k, and not too sensitive to variations in a. Thus, good performance can be expected in the face of varying conditions which are not explicitly modeled in the filter.

Table 8-6. Crosstrack Standard Deviations with Variations in Control Law Parameters

| NOMINAL VALUE TIMES | STANDARD DEVIATIONS WITH VARIATIONS IN | |
|---|---|---|
| | k (a OPTIMAL) | a (k OPTIMAL) |
| 0.5 | 1305.13 feet | 1579.82 feet |
| 0.67 | 1304.89 | 1394.84 |
| 0.8 | 1304.78 | 1332.14 |
| 0.9 | 1304.74 | 1310.73 |
| Unity | 1304.72 | 1304.72 |
| 1.1 | 1304.74 | 1309.46 |
| 1.2 | 1304.78 | 1321.27 |
| 1.5 | 1305.09 | 1385.00 |
| 2.0 | 1306.16 | 1529.46 |

## 8.5 Conclusions

Various analytical models have shown that Omega approaches can be flown with a standard deviation of less than 1500 feet in the presence of severe wind conditions with control laws which vary from the optimal. The optimal

system time constants were found to be on the order of 20 seconds, with the tradeoff being toward longer time constants to filter the Omega data more heavily when wind noise was low, and shorter time constants when the wind noise was high.

# CHAPTER IX

# OMEGA RECEIVER CONFIGURATIONS

## 9.1 Introduction

The primary measurements made in Omega receivers are phases of received Omega signals with respect to a local time source. These measurements are processed by circuitry to give a position estimate expressed in some coordinate frame. For aircraft navigation, the objectives of Omega navigation include providing position information of sufficient accuracy and quality to enable the pilot of the aircraft to maintain desired track within acceptable bounds; exclusion of misleading information (lane jumps) under essentially all circumstances; and preferably, some capability to determine position after loss of signals and/or receiver power.

## 9.2 Data Sources

In the various Omega receivers, various sources of data are utilized in different configurations, which are distinguished by what data measurements are made and how these data are processed.

Common to all Omega receivers are measurements of phase of the received Omega signals. Within this framework, however, many variations are noted. The simplest configuration measures phases at only one frequency, generally 10.2 kHz, for those stations defining the LOP's in use. Other phase measurements are either not made or are discarded. More complex receivers will add a second frequency (13.6 kHz), or a third frequency (11.33 kHz). With the increased number of phase measurements, all phase data may be utilized, with various weightings determined according to some scheme, or some phase measurements may be ignored, which is a weighting of zero.

Receivers may also measure how good the received Omega signal is, either in terms of S/N or some such similar measure, as for example, variance in successive phase measurements over 5 ms intervals (24). Because it is unacceptable for aircraft navigation systems to present position information based upon unusable signals, all receivers used for aircraft navigation will need some estimator of signal quality, even if this estimate is as simple as "good" versus "bad" signals.

Background noise information is also available on some receivers. By measuring noise between Omega station transmissions or during time slots when the transmitting Omega station is not receivable, background noise data is available for processing.

Air data is used on many more sophisticated Omega receivers. Usually, this consists of heading and true airspeed. These data are used for dead reckoning, rate aiding of the phase lock loops, and wind estimation routines. In addition, heading information is used to steer H-field antennae when these are installed. For rate aiding, airspeed data is not subject to the accuracy requirements that heading data is, as errors in airspeed show up as errors in wind estimates.

Differential Omega updates are also information sources. Generally, these updates are of phase errors, but as will be discussed later, other information is appropriate for uplink to the aircraft.

Visually derived position estimates are another source of information. Although this information is not available in flight during IFR conditions, this information is available with great accuracy when the aircraft is on the ground before takeoff.

Lastly, time and date information is available under most circumstances. These parameters are used in skywave correction routines, and minor errors in time are not critical to these routines. Time information for resetting atomic clocks is generally unavailable, however, as accuracies of 1 microsecond or better are desirable if clock offset is to be removed.

From the above set of data, each receiver has available a subset from which position estimates are made.

## 9.3 Receiver Configurations

Various receiver configurations will be discussed, including single frequency uncorrected Omega, difference frequency, composite, differential, and direct ranging.

By far the simplest receiver configuration is single frequency uncorrected Omega, as exemplified by the Dynell unit used in the flight evaluation. Front end requirements are minimal with only one frequency, and little processing is required. However, as discussed in Chapter XI, if system simplicity extends to definition of navigational coordinates in a coordinate frame based upon LOP differences from the last reset point, the system is prone to operator setting errors. Further disadvantages of single frequency uncorrected Omega include susceptibility to diurnal variations, PCAs and SIDs. The advantages of this configuration are simplicity, and errors which grow with time from zero. Augmenting this simple configuration with air data has been proposed (25).

Difference frequency Omega is a multiple frequency phase processing scheme for lane resolution. Fine scale navigation information is obtained from the 10.2 kHz Omega signals. Lytle and Bradshaw (26) have done some analysis on lane resolution with two frequencies, and these results indicate

unacceptable probabilities of erroneous lane resolution, which contraindicates this method for position determination after loss of position information. These results are displayed in Figure 9-1. With difference frequency Omega, skywave or differential Omega corrections are necessary for accuracy enhancement. Skywave correction programs have been implemented on several expensive Omega receivers, but these programs require extensive computation and memory on board, and susceptibility to unpredictable phase anomalies remains a problem.

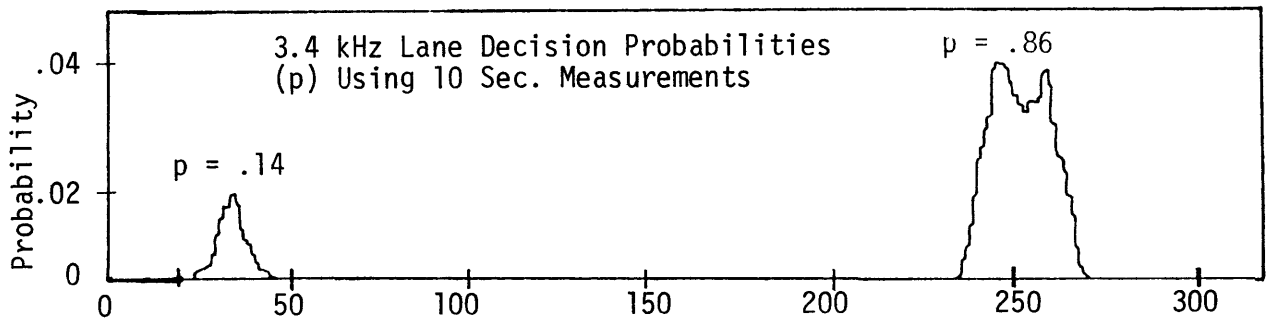


Figure 9-1. Chart Lane Decision Probability with Associated 10.2 kHz Phase Distributions for Norway - Trinidad Skywave Corrected LOP's at LRC (July 23-30, 1974) (26)

Composite Omega (27) uses the correlation between phase delay at 10.2 kHz and 13.6 kHz due to propagation anomalies and the observed difference in time delay of the two signals to enhance accuracy. This system provides significant accuracy enhancement, including reduction of unpredictable propagation variations with minimal processing. No complex skywave correction programs are required. Disadvantages include the need to receive two

frequencies to generate a correction, and lane resolution is not accomplished. Accuracies are reported (28) to be not as good as skywave corrected Omega in quiet atmospheric conditions.

Differential Omega involves uplinking phase correction information to local users for accuracy enhancement. With the phase correction at a ground station transmitted, phase errors due to diurnal effects as well as unpredictable phase anomalies can be corrected. However, relying entirely upon differential Omega for error correction reduces system accuracy to uncorrected Omega accuracies in the event of differential system failure. Differential Omega will be discussed further in Chapter XIII.

Any of the above schemes can operate in either hyperbolic or direct ranging mode. Hyperbolic navigation can be performed with a relatively inexpensive temperature compensated crystal oscillator, but this method generates lines of position from pairs of stations. To avoid having to use a noisy station for navigation, phase measurements can be made against an atomic time standard. Another advantage of direct ranging navigation is that only two stations are required, provided that the geometry is acceptable.

# CHAPTER X

## PRESENT REGULATIONS FOR OMEGA RECEIVERS

### 10.1 Introduction

FAA Handbook 7110.18, Air Traffic Control Services for Area Navigation Equipped Aircraft Operating in the National Airspace System, which includes Advisory Circular 90-45, describes the requirements for RNAV system installation and operation for use in the National Airspace System. The handbook is primarily concerned with VOR/DME RNAV, but also mentions inertial and Doppler radar sensors as examples of systems other than VOR/DME. Thus, the document is applicable to Omega navigation systems.

### 10.2 System Design Requirements

Requirements for RNAV system design are quoted below. Omega accuracy and response time have been discussed above. System error detection and performance checking will be discussed in Chapter XIV.

b. Area Navigation System Design

(1) General. The systems will normally use VOR/DME input sensor signals (or use combinations of VOR and DME for updating purposes) and indicate aircraft positions relative to the RNAV route and selected waypoint. It should give no operationally significant misleading indication.

Systems may be designed to utilize other sensor inputs if equivalent accuracy can be demonstrated.

(2) Checking of Input. If the system requires pilot input functions (such as the designations of waypoints), provisions should be made to enable the pilot to check the correctness of the inputs.

(3) Failure Warning. Provision should be made to alert the crew upon occurrence of any reasonably probable failure of major system functions or loss of inputs, including those that would affect aircraft position, heading, command course, or command heading indications.

(4) Performance Check. Provision should be made for checking the system's performance on the ground and in flight. This may be a built-in check, an auxiliary test system, or a procedural check.

(5) Response Time. The navigation display should indicate aircraft position, to the accuracy specified in Paragraph 2.a, assuming that navigation sensor outputs are available.

(a) During flight in any direction at the maximum ground speed declared by the equipment manufacturer; and

(b) Within five seconds after any normal maneuver, assuming sensor inputs are not lost during the maneuver.

(c) The time lag between selection of data and guidance derived from the display of the data should not be operationally significant.

Note: Terminal area speed limitations are taken into account in connection with this provision. Moving elements of the navigation display may be damped.

10.3 Area Navigation Equipment Installation

Requirements for RNAV equipment installation are quoted below. These requirements, although very general, provide guidelines for good operating practice in aircraft equipment installation.

c. Area Navigation Equipment Installation

(1) Location of the primary RNAV display. Where area navigation equipment with one or more display elements is to be installed, and a display element is to be used as a primary flight instrument in the guidance and control of the aircraft, it should be located where it is clearly visible to the pilot with the least practicable deviation from his normal position and from his line of vision when he is looking forward along the flight path.

(2) Failure protection. Any reasonably probable failure of the airborne navigation equipment should not affect the normal operation of required equipment connected to it, nor cause a flight hazard.

(3) Radio frequency interference. The area navigation equipment should not be the source of objectionable radio frequency interference, nor be adversely affected by radio frequency emissions from other equipment in the aircraft.

(4) Manufacturer's instructions. The area navigation equipment should be installed in accordance with instructions and limitations provided by the manufacturer.

# CHAPTER XI

## AREA NAVIGATION SYSTEM SETTING ERRORS

As quoted in Chapter X, Advisory Circular 90-45 states, "If the system requires pilot input functions (such as the designation of waypoints), provisions should be made to enable the pilot to check the correctness of the waypoints." As discussed in the literature (10) and as ascertained in flight tests, missettings of RNAV equipment are easily made.

On the Dynell receiver, waypoint designation is made by setting the LOP difference between the last reset point and the destination. Even after 60 hours of flight test experience, the Omega operator was prone to misset the Omega receiver occasionally, especially when settings had to be determined in flight. For example, when flying the approaches described in Chapter VI, taking off from an airport not specified in the original flight plan caused an error of several lanes to be made. The error was detected by visual observation of landmarks, not receiver indications. Similarly, conventional general aviation RNAV systems provide no feedback on correctness of system settings. For approach flying, this is a potentially dangerous situation.

Latitude/longitude provides the most useful coordinate system for area navigation settings, provided that sufficient computational capability is available. Latitude/longitude is applicable is applicable to all RNAV systems. In such a system, check digits can be generated from the receiver lat/lon settings and compared to check digits on a chart. For example, the sum of digits modulo ten will detect 90 percent of waypoint coordinate errors. An example is shown in Figure 11-1.

Millbury
N42 12.8/7
W071 48.1/1

Figure 11-1. Lat/Lon Definition of Waypoint with Check Digits

# CHAPTER XII

## TERMINAL PROCEDURES FOR OMEGA NAVIGATION

### 12.1 Introduction

Terminal procedures (29) are the guidelines by which proposed instrument approaches are evaluated for compliance with accepted standards. For instrument approaches using Omega navigation, changes to existing standards must be made to reflect the fact that crosstrack errors are not a function of radial distance from the facility. Existing criteria for minima, altimeter settings, missed approach procedures, etc., are easily carried over to Omega navigation systems.

### 12.2 Omega Navigation Terminal Procedures

Terminal procedures for differentially updated Omega receivers are discussed. As mentioned above, the possibility of misleading information being generated excludes from consideration Omega navigation schemes which do not employ differential updates.

Chapter 1.4 of the Terminal Procedures (TERPS) provides general criteria for the design of instrument approaches. These criteria are non-trivial, and each individual approach submitted to the FAA for approval is reviewed in light of these criteria. Thus, although Omega signal availability may theoretically allow approaches to any airport from any direction, safety and FAA regulations will not allow approach procedures to be improvised by the general aviation pilot.

General information is specified in the TERPS and are included here in a very condensed form. Distances are specified in nautical miles, headings and bearings in degrees from magnetic north, and altitudes in feet above mean

sea level. Aircraft are separated in categories based upon speed and weight, with the lightest and slowest aircraft being in Category A, and the fastest and heaviest being in Category E. Altimetry errors due to effects of wind on terrain and separation of the ground altimeter monitor from the airport at which the approach is being flown must be considered.

12.3 Example of TERPS for Differential Omega

Following is a sample of what a terminal procedure for Differential Omega might look like. References to chapters and sections are referenced in the actual TERPS, not cross references to this thesis.

> 00. GENERAL. These criteria apply to procedures based on Omega navigation with standard differential updates and standard demonstrated accuracies. A course deviation indicator and a readout of miles to the missed approach point are assumed.
>
> 01-00. RESERVED.
>
> 10. FEEDER ROUTES. Criteria for feeder routes are contained in paragraph 220 of the TERPS.
>
> 11. INITIAL APPROACH SEGMENT. The initial approach segment is that extension of the final approach path from the outer marker to the initial approach fix, as shown in Figure 12-1.
>
> 12. INTERMEDIATE APPROACH SEGMENT. This procedure has no intermediate approach segment.
>
> 13. FINAL APPROACH SEGMENT. The final approach segment begins at the outer marker and extends to cross the runway centerline within 5000' of the end of the runway.
>
> a. Alignment. The alignment of the final approach course with the runway centerline determines whether a straight in or circling approach may be established.
>
> 1. Straight In. The angle of convergence between the final approach course and the extended runway centerline shall not exceed 30 degrees.
>
> 2. Circling Approach. When the final approach course alignment does not meet the criteria for straight in landing, only a circling approach shall be authorized.

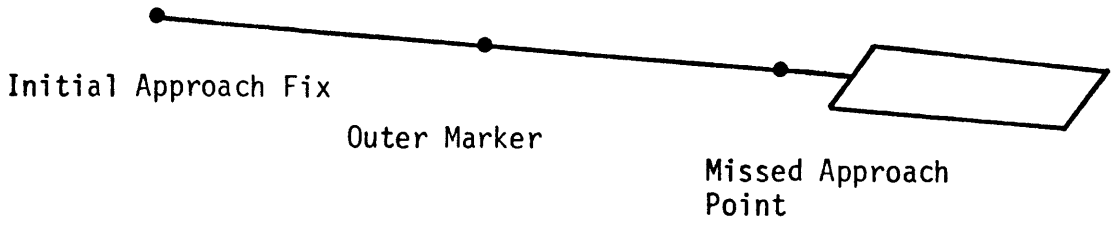


Figure 12-1. Designation of Fixes for Omega Approach

b. Area. Figure 12-2 illustrates the final approach primary and secondary areas. The primary area is longitudinally centered on the final approach course, and is at least ten, but no greater than 15 miles long. The primary area is one mile wide at the missed approach point and expands uniformly to a width of three miles at the initial approach fix. A secondary area is on each side of the primary area. It is one-half mile wide at the missed approach point and expands uniformly to one mile on each side of the primary area at ten miles from the missed approach point.

c. Obstacle Clearance.

1. Straight In. The minimum obstacle clearnace in the primary area is 300 feet. In the secondary area, 300 feet of obstacle clearance shall be provided at the inner edge, tapering uniformly to zero feet at the outer edge. The minimum required obstacle clearance at any given point in the secondary area is found in Appendix 2, Figure 126.

2. Circling Approach. In addition to the minimum requirements specified in Paragraph 413.c.(1), obstacle clearance in the circling area shall be as prescribed in Chapter 2, Section 6 of the TERPS.

d. Use of Stepdown Fix. Use of the stepdown fix (Paragraph 288.c.) is permitted, provided the distance from the stepdown fix to the missed approach point does not exceed four miles. Where the stepdown fix is used, the obstacle clearance (Paragraph 413.c.(1) may be reduced to 250 feet from the stepdown fix to the MAP. See Figure 12-3. See also Paragraph 251.

15. DIFFERENTIAL OMEGA UPDATE SIGNAL AVAILABILITY. The minimum descent altitude shall be 200 feet greater than that altitude at which differential Omega update signals cannot be detected due to terrain blocking.

16. OMEGA SIGNAL AVAILABILITY. No procedure shall be approved wherein local noise sources cause degradation of Omega S/N ratio to the extent that the Omega signal becomes unusable.

## 12.4 Considerations in Designation of TERPS

Using the above sample TERP as an example, various considerations peculiar to Omega operations are mentioned. These include crosstrack accuracy and availability of Omega and differential update signals. In addition, sufficient airspace must be included in the primary area to allow for the effects of wind shear.

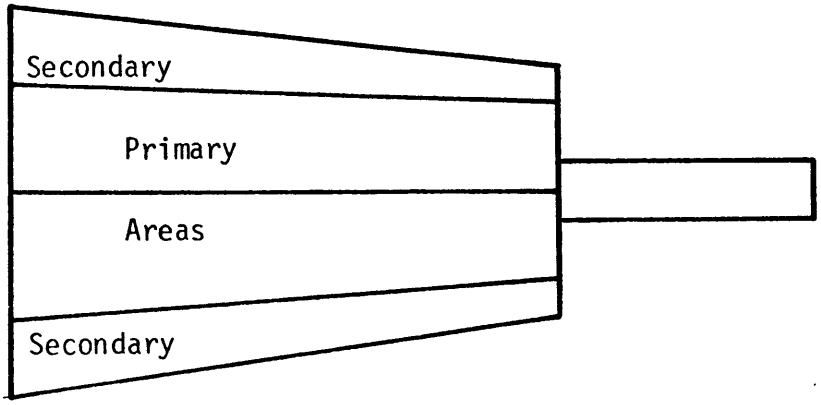


Figure 12-2. Final Approach Primary and Secondary Areas

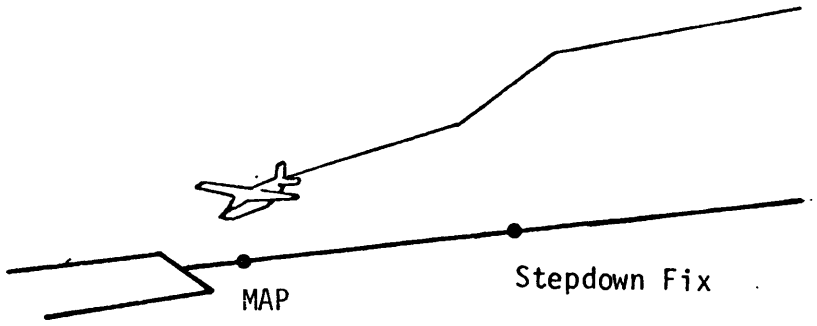


Figure 12-3. Use of Stepdown Fix

Variations in system accuracy are to be expected depending upon the amount of external data available. For example, the availability of high quality rate aiding devices, such as a low cost inertial unit, will increase the system accuracy. The width of the primary airspace is dependent upon the accuracy of the navigation sensor in the aircraft, so that the aircraft can stay within the protected airspace with 95 percent probability. Thus, with more accurate systems, less airspace is required in the primary area, whereas with a less accurate system, or a system degraded due to a partial failure, more airspace is required in the primary areas, which could dictate higher minima.

Omega signal availability is essentially independent of terrain effects, but the possibility of local noise sources which could seriously degrade weak signals must be remembered. No significant local noise sources were found in the flight tests of the Dynell receiver, but this result is inconclusive for definition of system standards. The presence of any local noise source could require higher minima to account for decrease in accuracy, or a change in the procedure to avoid the local noise source.

Depending upon the frequency, and hence the propagation characteristics chosen for differential Omega updates, signal availability of differential updates must be considered in designing approaches. In hilly terrain, line of sight constraints on signal availability could increase minimum descent altitudes for differential Omega approaches.

## 12.5 Conclusions

TERPS for Omega approaches will be substantially different from TERPS for other approaches due to the different characteristics of Omega naviga-

tion. Using the results of Chapter VIII, minimums for differential Omega approaches should be not as good as minimums for localizer approaches, but possibly lower than minimums for VOR approaches at a distance from the VOR.

# CHAPTER XIII

## DIFFERENTIAL OMEGA IMPLEMENTATION

This section will discuss the data to be broadcast by a differential Omega system and its formats. Differential Omega cost and location for VHF uplinks have been discussed by Dodge (30).

At the monitor site, the measurements made are phase of received Omega signals relative to a local oscillator or atomic standard. The errors are due to propagation anomalies and oscillator drift from what it "should" be. If sufficient calibration standards are available for airborne equipment and ground monitor atomic time standards, differential Omega can be provided to users operating in a direct ranging mode.

Miller (31) discusses differential Omega implementation using various uplink systems, as shown in Table 13-1. From this table, it may be concluded that differential Omega uplinks, if complete coverage is to be achieved, will be available at a data rate of 70 baud for VLF uplinks, and much higher data rates using UHF uplinks from a satellite.

As discussed in Chapter IX, composite Omega has certain inherent advantages. Pierce's formulation of composite Omega involves taking a linear combination of 10.2 and 13.6 kHz signals using a parameter m. Uplink of the desired parameter m instead of phase corrections could provide accuracy enhancement of the received Omega signals, and might be preferrable for low data rate differential Omega.

On the other hand, if sufficiently high data rates are available for differential Omega, phase correction information for all frequencies and

Table 13-1. Differential Omega Uplink Modes

| ALTERNATIVE | PROPAGATION | NO. OF STATIONS TO GIVE EQUIVALENT OMEGA COVERAGE | DATA RATE | COMMENTS |
|---|---|---|---|---|
| 1. Microwave | Line-of-Sight | 1000+ | Fast | |
| 2. UHF/VHF | Line-of-Sight | 1000+ | Fast | Comparable to Locations Transmitters at Existing VOR |
| 3. HF | Beyond Line-of-Sight | Not Assessed | Good | Poor Reliability Due to Signal Fading and Hoping |
| 4. DABS | Line-of-Sight | Projected DABS Structure (Still Not Complete Ground-Up CONUS Coverage) | Fast (Must Be Integrated Into DABS Format) | Navigation and Surveillance Systems Are Now Interdependent |
| 5. LF | Ground Wave | Six-Eight | Good | Cost of Transmitting Stations Would Be Substantial |
| 6. Existing LF/MF Beacons | Ground Wave | 1200 Existing (Still Not Complete Ground-Up Coverage) | Good | Maximum Range of 75 NMI |
| 7. Satellite | Equivalent Omega Coverage | One-Two Satellite Plus Ground Stations | Fast | Increased Avionics and Satellite Cost Unless Satellite Used For Other Functions |
| 8. Dedicated VLF Station | Equivalent Omega Coverage | One | 70 Baud | Must Obtain the Use of An Existing Station or a New Station |
| 9. Omega Dead-Time | Same as Navigation Signals | Existing Omega Ground Station | 70 Baud | Complete Ground-Up Navigation From the Existing Omega Station |

stations could be uplinked, providing service to all users, not just composite Omega system users.

With high data rate differential Omega, nine bits of phase correction per phase measurement update are suggested, as this allows corrections of $\pm 1$ lane to be made with resolution of eight bits, or $\frac{1}{256}$ lane. If transmissions of differential Omega are made in harmony with the Omega stations broadcase, no timing or identification bits would have to be included at moderate data rates. Instead of transmitting line of position correction information, individual station corrections, including ground system oscillator error, can be transmitted, and the ground system oscillator error, if any, can then be subtracted out in the air. This avoids the transmission of corrections for all possible pairs of stations (LOP's), or chained LOP corrections, such as A-B, B-C, C-D, D-F, F-H, which are susceptible to errors when corrections are sequentially added to form corrections for other LOP's, and an interior station measurement is for some reason bad.

An additional seven bits can be specified, bringing the total number of bits up to a standard 16 bits. Depending upon the frequency used for differential Omega updates and the propagation characteristics at this frequency, it may be desirable to have 16 "channels" of differential Omega update, each "channel" identifiable by a binary number of four bits in the differential Omega update word. Of the remaining three bits, one could specify whether the signal strength was sufficient for the ground monitor to successfully estimate the phase of the received signal, one could specify whether the ground oscillator was synchronized accurately enough to provide differential Omega service to $\rho$-$\rho$ Omega system users, and the last bit

could be a parity bit. An example of a differential correction word is shown in Figure 13-1.

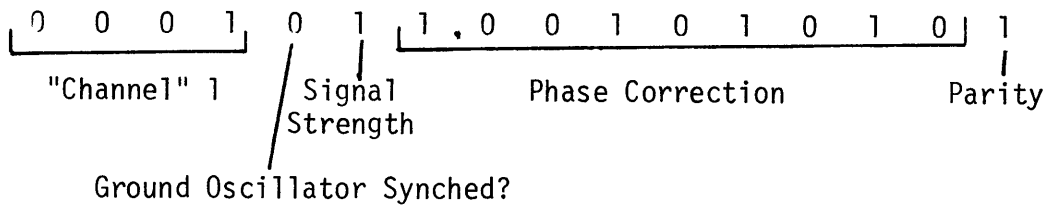


Figure 13-1. Differential Update Word

# CHAPTER XIV

## SYSTEM CHECKS AND REDUNDANCY

### 14.1 Introduction

General aviation Omega receivers may prove to be too expensive for dual installations. Thus, if Omega is the primary navigation aid, sufficient fail soft or fail safe modes must be supplied to provide navigational capability with system degradation. A receiver configuration supplying such redundancy is discussed.

### 14.2 Navigation System Failure in the National Airspace System

In the National Airspace System, sufficient redundancy is provided on the ground that a fail soft system is assured. In most light aircraft flown IFR, there is additional redundancy in on-board systems. Consequently, navigation system failure is not directly mentioned in Part 91 of the Federal Air Regulations.

Ground systems available for aircraft use include VOR, DME, ILS, LOC, SDF, NDB, MB, and various radar systems. In the event of a failure of one or more parts of the ground-based system, the pilot of the aircraft can still land his aircraft by flying to an operable facility, providing sufficient fuel is available and weather permits. On the east coast of the United States, the great number of navigational facilities of all sorts relegates individual ground system failure to the nuisance category only.

Airborne equipment failure is, in most instances, handled by equipment redundancy, and is easily detectable by system procedures. Common practice for light aircraft flown IFR is to equip the aircraft with dual VOR/LOC receivers, an ADF, and a marker beacon to provide redundancy of navigational

information. The known failure of any piece of equipment commands a change in the approach to be flown, and possibly higher minima. However, in an emergency, published minima can be bettered, although not necessarily safely. Thus, the safety of redundant equipment and the safety margins inherent in the determination of approach minima provide a reserve in the event of known navigation system failure.

System failures are relatively easy to detect in light aircraft radio installations. VOR/LOC receivers have "Off" flags which display low signal strength conditions. ADF receivers do not usually have low signal strength indications, but standard procedure when flying an approach utilizing an ADF is to aurally monitor the received signal. In addition, a "Test" button is provided which causes the indication of relative bearing to the station to rotate. The return of the needle to its previous position is a good indication of system performance.

Electrical system failure is a more serious situation than failure of a navigation radio. In the event of catastrophic electrical failure, the only options open to the pilot are flight into anticipated VFR conditions, or a controlled descent into the unknown. Partial electrical system failure, such as a generator failure, is less serious because a limited amount of electrical power is available for an immediate approach.

Although communications failure under IFR is thoroughly covered in FAR 91.127, navigation system failure is not specifically mentioned, perhaps an indication of its rarity. FAR 91.125c states, "The pilot in command of each aircraft operating under IFR in controlled airspace shall have a continuous watch maintained on the appropriate frequency and shall report by radio as soon as possible... (c) any other information relating to the safety of

flight." FAR 91.3 states, "In an emergency requiring immediate action, the pilot in command may deviate from any rule of this subpart or of subpart B to the extent required to meet that emergency."

## 14.3 Omega System Redundancy

Omega system redundancy requires consistently available signals, and a functioning receiver. Both requirements will be discussed.

Omega S/N ratio variations can be caused by either weak signal strength at the transmitter, propagation anomalies, or excessive noise. Lack of sufficient signal strength at the receiver is sufficient to cause system failure if there are not enough stations available for navigation. For example, in the mid-western states, when Station A is weak due to propagation anomalies, and Station D is unusable due to modal interference, Stations B, C, F, and H would be available for navigation. Station H was not observed to be a strong station during the flight evaluation, so the stations available for navigation would be B, C, and F, with relatively poor geometry. Difficulties with one of these stations during these conditions would make Omega unsuitable for aircraft navigation.

At the receiver, if sufficient signal strength is present, receiver functioning is necessary for navigation. Figure 14-1 shows a fail soft receiver configuration. Note that the failure of any block of the system is tolerable. Although the redundant processor seems superfluous, the state of microprocessor technology is presently such that a simple processor providing minimal information could be included for little additional cost. Most expenses for small processors are incurred in memory, interfacing, and peripherals, all of which would be of negligible cost. An example of a minimal redundant processor is shown in Figure 14-2. It is anticipated that a

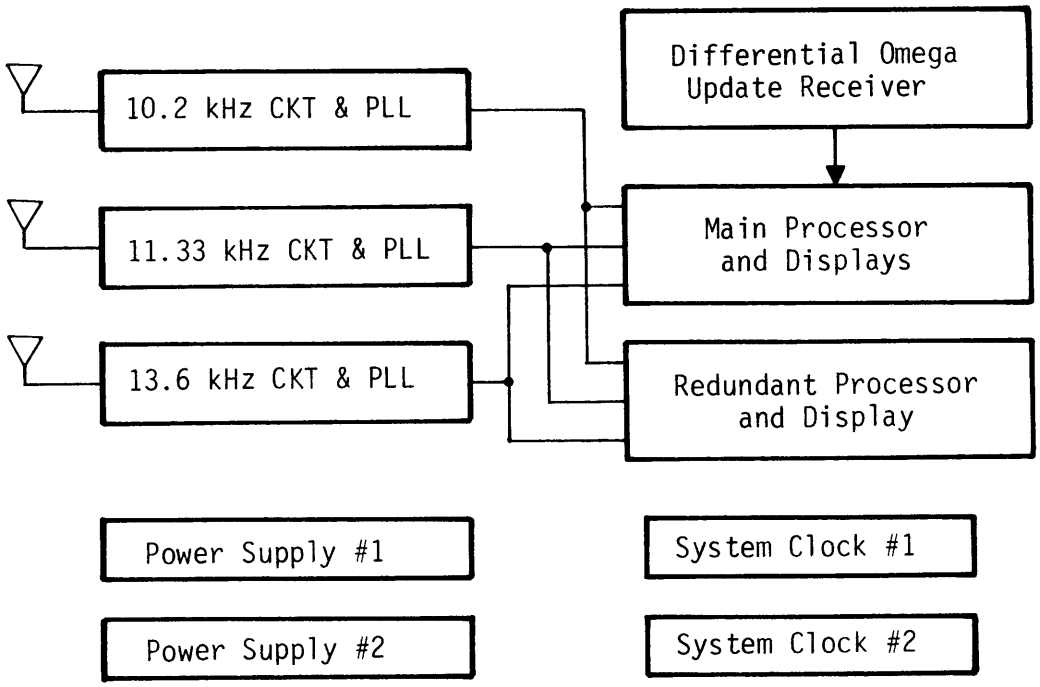


Figure 14-1. Fail Soft Omega Receiver Configuration.

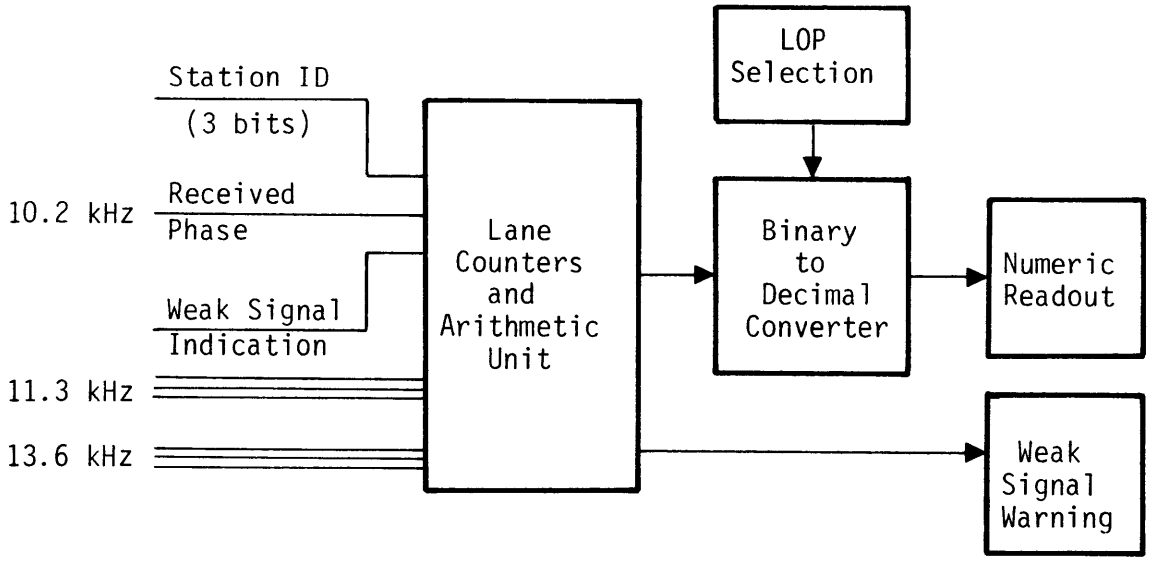


Figure 14-2. Minimal Configuration for Redundant Processor.

decimal readout of line of position would suffice for flights along an LOP. If sufficient stations are available for navigation, this would provide several directions for flying approaches in an emergency. With some additional complexity, lat/lon readouts could be provided, but these would be less useful during propagation anomalies.

## 14.4 Ground Testing of Omega Receivers

Proper functioning of the Omega receiver is, of course, necessary for safe flight. Verification of receiver operation on the ground is desirable, but perhaps not easily attainable.

Conventional radio aids used for light aircraft navigation include VOR, DME, localizers and SDF, glide slope receivers, and ADFs. Of these, only VOR is required to be checked before instrument flight, despite the fact that aircraft navigation may be entrusted to another sensor. VOR alone, however, provides enough information for both enroute and approach flying.

Ground testing of Omega sets is more complex than testing of VOR receivers, due to the greater complexity of Omega receiver. However, technology for incorporating self test features into electronic systems can be incorporated into Omega receivers to provide assurance of receiver performance.

# CHAPTER XV

## OMEGA SIGNAL AVAILABILITY AND GEOMETRY CONSIDERATIONS

### 15.1 Introduction

For navigation using Omega, signals of sufficient strength must be received in a usable station geometry. Based upon predicted -20 dB (through 100 Hz) S/N contours, in the New Jersey area signal strengths will not be well above this contour for many stations at various times during the day. Subjective experience shows that -20 dB through 100 Hz is about 5 dB optimistic for good receiver performance. Station geometry is as important as signal strength, for it relates how the Omega phase measurements may be used for navigation. Using available signals, after Station B is moved to Liberia, it is shown that geometries in the New Jersey area are acceptable for aircraft navigation, but are not especially good.

### 15.2 Omega Signal Strength

Bortz, et al. (32) have plotted predicted -20 dB S/N (through 100 Hz) contours of Omega signals from various stations along with modal interference regions for the world. Based upon these plots, signal strengths in the New Jersey area at local noon and midnight are presented in Table 15-1. Based upon these plots, at noon Stations B, C and D should be available, and Station A available, but weak. At midnight, Stations C and F should be available.

Subjective experience in the evaluation of Omega using the Dynell receiver shows that -20 dB S/N through 100 Hz is optimistic for good receiver performance, and that -15 dB is a more conservative estiamte of required S/N. Exact S/N determination was not possible due to the jitter of approximately

Table 15-1. Bearings to Omega Stations from New Jersey and Predicted Signal Availability

| STATION | BEARING (TIME) | LOCAL NOON | LOCAL MIDNIGHT |
|---|---|---|---|
| A | 33° | Weak( $\sim$-20 dB) | Weak |
| B | 103° | Avail.(> -20 dB) | No (< -20 dB) |
| C | 282° | Available | Available |
| D | 293° | Available | No |
| F | 173° | No | Available |
| G (Australia) | 271° | No | Weak |
| H | 340° | No | Weak |

$\pm$6 dB in the S/N measurements. Furthermore, with the limited position measurements available, it was not possible to record degradation of receiver accuracy with decreasing S/N ratios. As mentioned in Chapter VI, statistical analysis of observed accuracies at waypoints did not correlate with observed S/N ratios, but this result is not conclusive due to the low quality of position measurements made. What was noted was that with S/N averaging -20 dB, the weak signal light, indicative of insufficient signal strength, was flickering consistently, meaning that a portion of the phase measurements were measurements of noise, not Omega signals.

15.3 Omega Geomtries

For hyperbolic navigation, the spacing between LOPs is given by

$$d = \frac{\lambda}{[2-2\cos\Theta]^{\frac{1}{2}}} \qquad (15.1)$$

where $\Theta$ is the angle between the great circles from the receiver to the transmitters defining the LOPs. This function is plotted in Figure 15-1. A rule of thumb for acceptable angles is that if the minimum included angle is $90^{o}$ or greater, LOP spacings are acceptable (11 nm or less).

Table 15-2 and Figure 15-2 show LOP spacings and directions in the New Jersey area. From Tables 15-1 and 15-2, it is apparent that daytime navigation requires Station A availability, and both daytime and nighttime navigation will rely upon at least one weak station. Howschinsky (17) has demonstrated that in flights along various LOPs, most of the noise observable by the pilot in Omega position readouts is attributable to Station A. As mentioned in Chapter VI, however, because the power output of Station A is not available, no firm conclusion as to signal characteristics of Station A can be assumed.

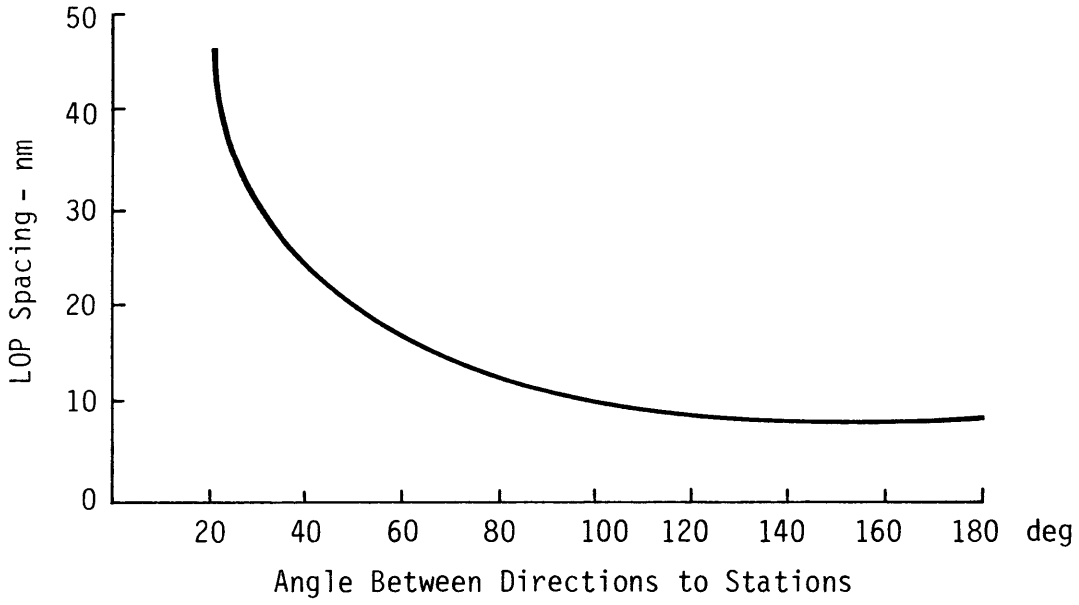


Figure 15-1. LOP Separation vs. Included Angle Between Great Circle Routes to Stations

Table 15-2. LOP Spacing (nm) and Directions (True) in New Jersey

| STATION / STATION | | H | F | D | C | B |
|---|---|---|---|---|---|---|
| Norway | A | 18.1/97° | 8.5/103° | 10.4/163° | 9.71/158° | 14.0/68° |
| Liberia | B | 9.1/132° | 10.6/154° | 8.0/18° | 8.0/13° | --- |
| Hawaii | C | 16.4/41° | 9.8/48° | 83.5/103° | --- | --- |
| North Dakota | D | 49.9/47° | 9.2/53° | --- | --- | --- |
| Argentina | F | 8.1/167° | --- | --- | --- | --- |

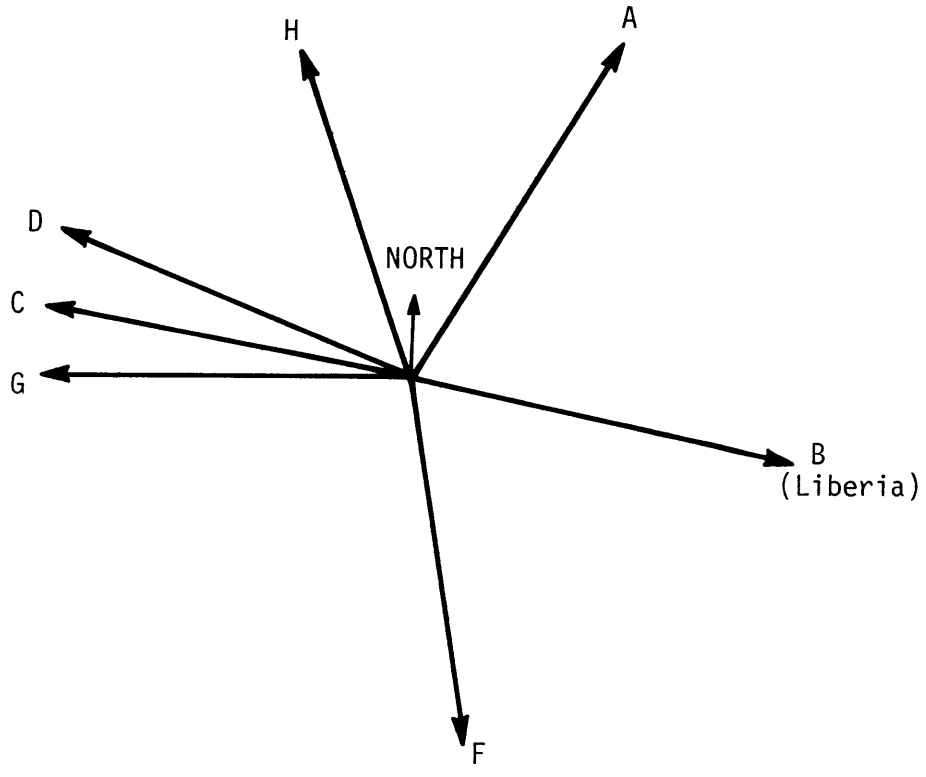


Figure 15-2. Directions to Omega Stations from New Jersey.

## 15.4 Conclusions

On the basis of the above discussion, it can be concluded that Omega geometries and availabilities are not good in New Jersey. Other well-known anomalies affecting Omega reception in the Continental United States include modal interference on Station D, and the Greenland shadow on Station A (32).

# CHAPTER XVI

# AVIATION CHARTS FOR OMEGA NAVIGATION

## 16.1 Introduction

Current aviation charts are available from either the U.S. Government or Jeppesen and Co. for instrument flying. These charts include enroute charts, local area charts, approach plates and Standard Terminal Arrivals (STARS) and Standard Instrument Departures (SIDS). Modifications of these charts for use with Omega navigation is shown to be fairly straightforward. The approach plates actually used for flying the Omega approaches are discussed, as are suggested sample approach plates based upon the experience of flying the Omega approaches. Copyright information on these charts is included as an appendix.

## 16.2 Modification of Existing Charts for Use with Omega

Modifications of existing IFR charts for use with Omega reduces to inclusion of latitude and longitude information on all waypoints and navigational fixes. On some charts, this is in fact already done. Figure 16-1 shows the Millbury Three departure from Hanscom Field, Bedford, MA. Note that all waypoints are specified in terms of latitude and longitude in addition to their specification in relation to VOR stations. Thus, this chart is acceptable for Omega navigation as is. However, there is no error detection capability, as would be provided with the check digits discussed in Chapter XI. Use of latitude and longitude assumes that the Omega receiver on board interfaces with the pilot in terms of latitude and longitude, even in fail soft modes.

SID

**BEDFORD, MASS.**
HANSCOM

10-3 JUN 22-73

Jeppesen

*Standard Instrument Departure (SID)*

MEETS FAA REQUIREMENTS FOR AERONAUTICAL CHARTS

## MILLBURY THREE DEPARTURE (7MB3-7MB)

NOT TO SCALE

**TAKE-OFF**
**Rwys 5-29**: Climb to 800' then turn LEFT to a heading of 230° to intercept Boston 285 R Thence
**Rwy 11**. Climb to 1200' then turn as vectored by ATC to intercept Boston 285 R Thence
**Rwy 23**. Climb to 800' on runway heading to intercept Boston 285 R Thence

**DEPARTURE**
Via Boston 285 R to intercept Hartford 057 R to Millbury Int. Intercept Hartford 057 R as assigned by ATC Thence via (transition) or (assigned route)

**TRANSITION (LOW ALTITUDE)**
**Hampton** (7MB3-HTO): Via Putnam 022 R to Putnam VORTAC, thence V-308 to Hampton VORTAC Cross Putnam VORTAC as assigned by ATC

**TRANSITION (HIGH ALTITUDE)**
**Kennedy** (7MB3-JFK) Via Hartford 057 R to Hartford VORTAC, thence J-48 to Kennedy VORTAC Cross Hartford VORTAC as assigned by ATC

ILLUSTRATION ONLY - NOT TO BE USED FOR NAVIGATIONAL PURPOSES.

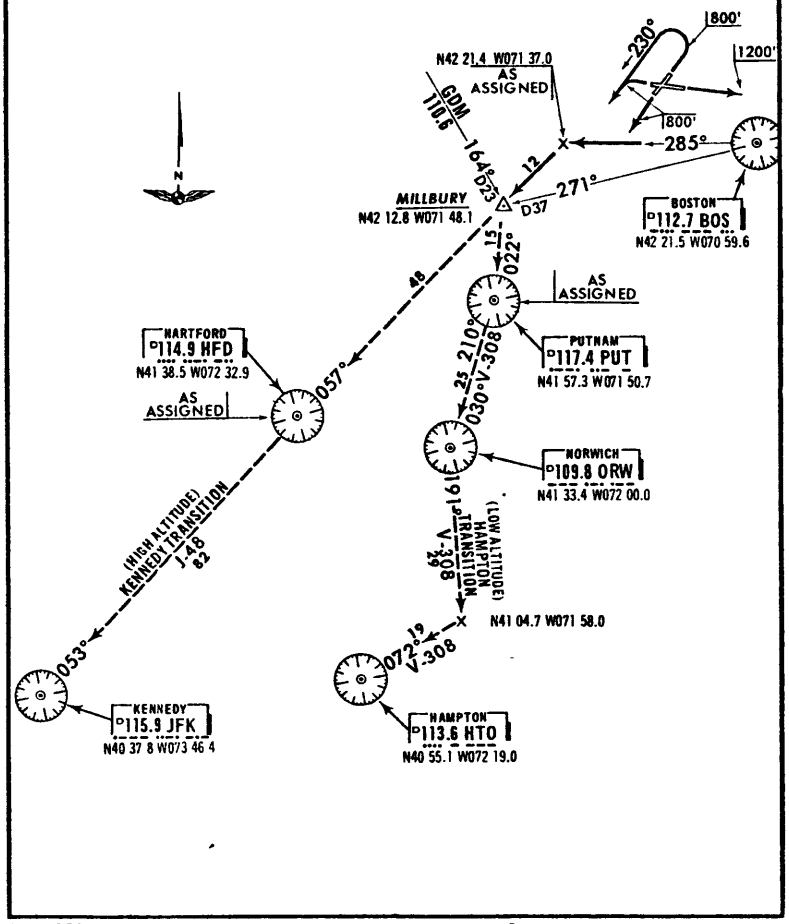


CHANGES. Kennedy (High Altitude) Transition



Figure 16-1. Millbury Three Departure

The inclusion of latitude and longitude on all waypoints and fixes is a fairly simple task. Inclusion of station acceptability on charts seems superfluous, as measurements of signal quality are required for safety. Thus, existing charts can easily be modified to include data acceptable for Omega navigation, as well as conventional VHF radio navigation.

16.3 Modification of Approach Plates

Figure 16-2 shows an approach plate modified for Omega navigation. The modifications are addition of an initial approach fix (Manjo intersection), addition of latitude, longitude and check digit information and modification of the initial approach legs to reflect approaches made from Manjo, not starting at the Bedford LOM. Starting the approach at Manjo reflects the area navigation capability of Omega providing guidance to Manjo directly, rather than requiring flight to the outer marker and a procedure turn as would be required with another type of approach. Note that latitudes and longitudes are specified to 0.01 minutes (60') rather than 0.1 minutes (600') as was done on the Millbury Three departures.

Specification of waypoints in degrees, minutes and tenths of minutes is already standard practice, as is shown on the Millbury Three departure. Further increased accuracy for approaches is available by adding an extra digit to give hundredths of a minute, whereas specifying position in degrees, minutes, and seconds would not give this flexibility because in one case the last digit would be between 0 and 5 and in the other case, between 0 and 9. Thus, it seems appropriate to specify waypoints in degrees, minutes and tenths of minutes.

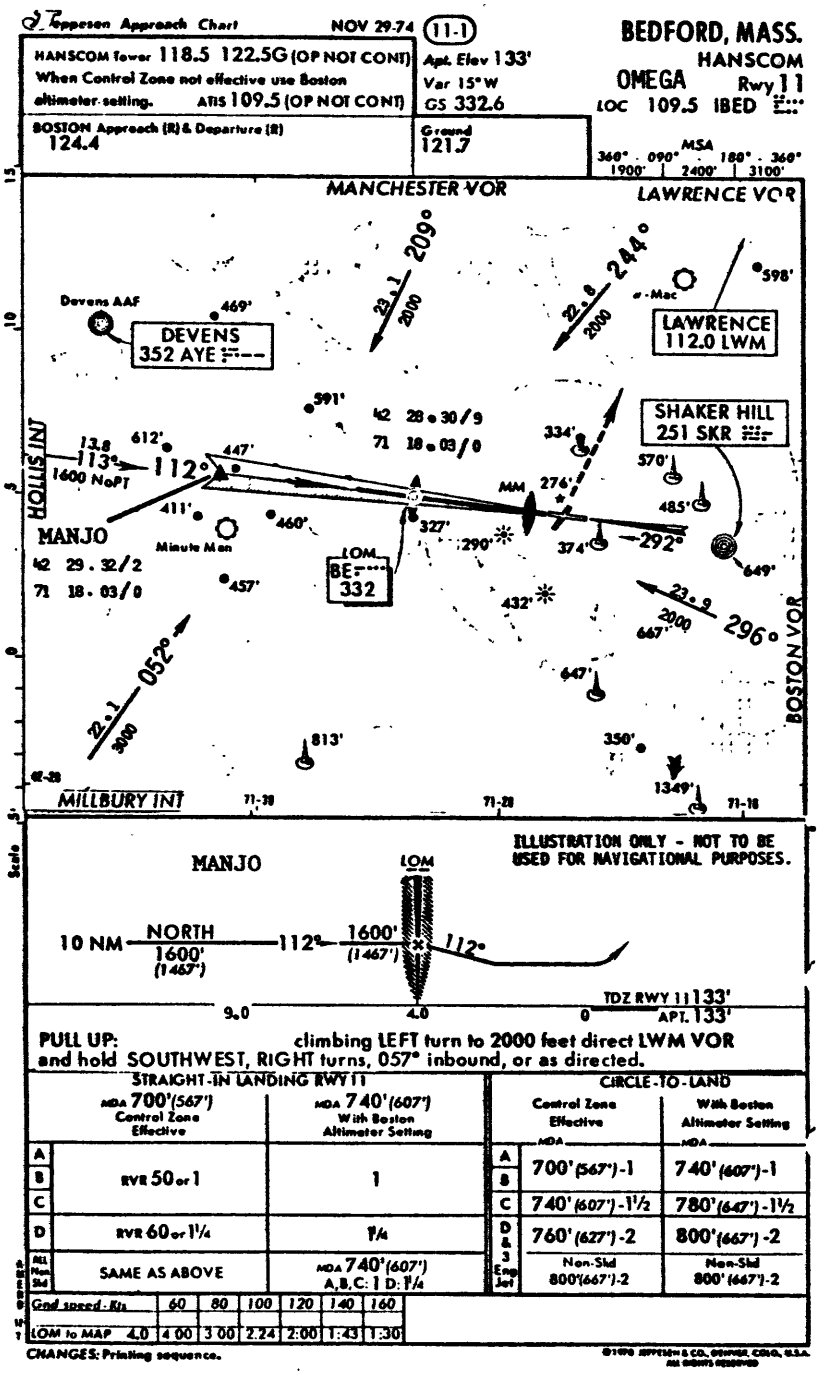


Figure 16-2. Omega Approach Plate with Latitude and Longitude

Observe that a specification of a waypoint to hundredths of a minute in an accuracy specification of 0.066 μsec, or roughly 9 bits of phase precision at 10.2 kHz. Thus, map parameters should introduce negligible error into the overall system.

## 16.4 Approach Plates Used on Flight Evaluation

Figures 16-3 and 16-4 show the modified approach plates drafted for the Omega approaches. In fact, only the approach depicted by Figure 16-3 was actually flown.

This approach plate is a modification of the NDB approach to Runway 11, shown in Figure 16-5. Observe that Manjo intersection has been added, as have been LOP differences between Manjo and the airport, and the point marked "Tower" and the airport. In addition, course numbers for the Dynell receiver are included so that the desired path to the airport can be followed. The path from the tower to Manjo was included to provide an easy transition onto the final approach course. In practice, this was found not to be necessary.

Observe that no LOP specifications are present on this chart. The actual LOPs specified are A-B and B-D, which was implicit for this chart. However, specification of all LOP combinations for an approach would submerge the plate in a confusing amount of clutter.

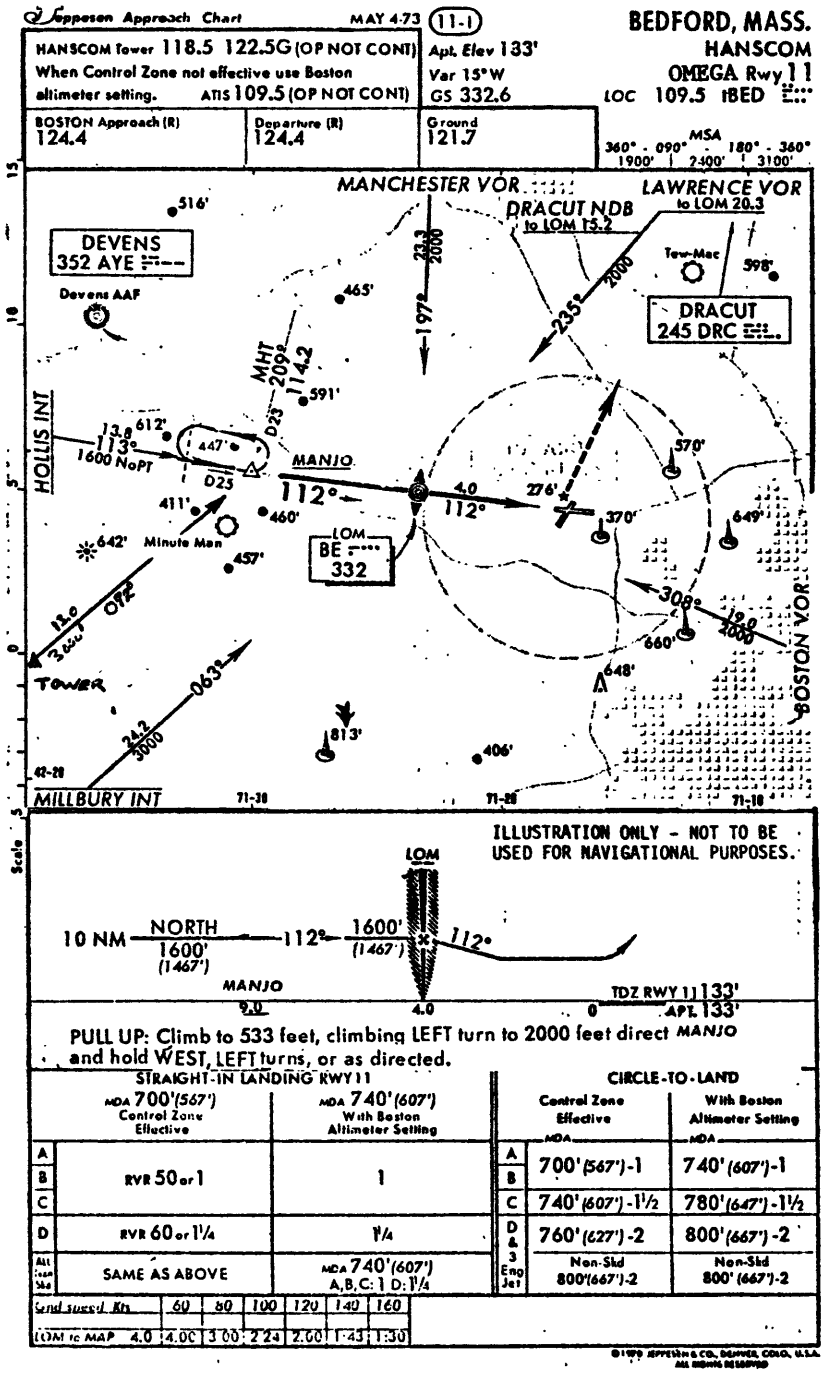


Figure 16-3. Omega Approach to Runway 11, Hanscom Field

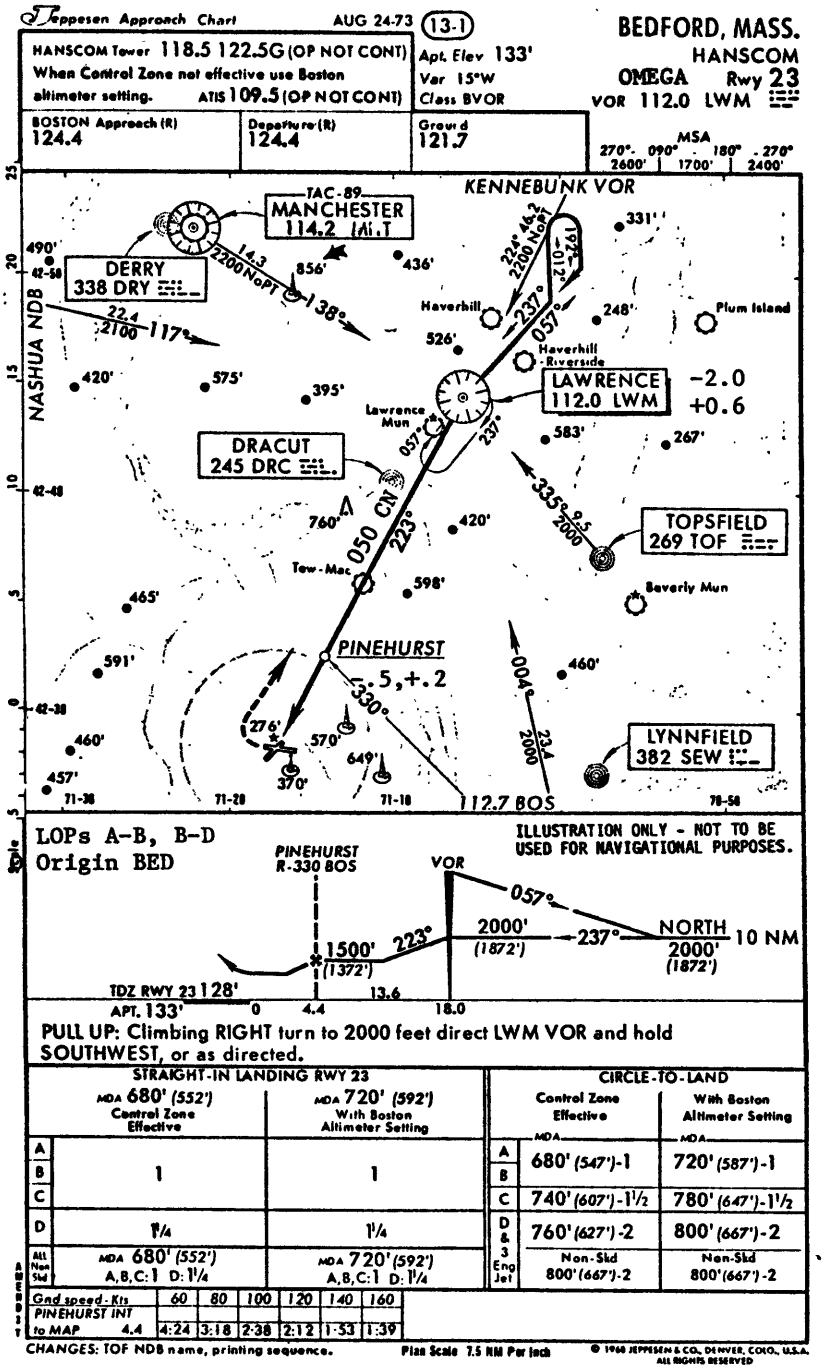


Figure 16-4. Omega Approach to Runway 23, Hanscom Field

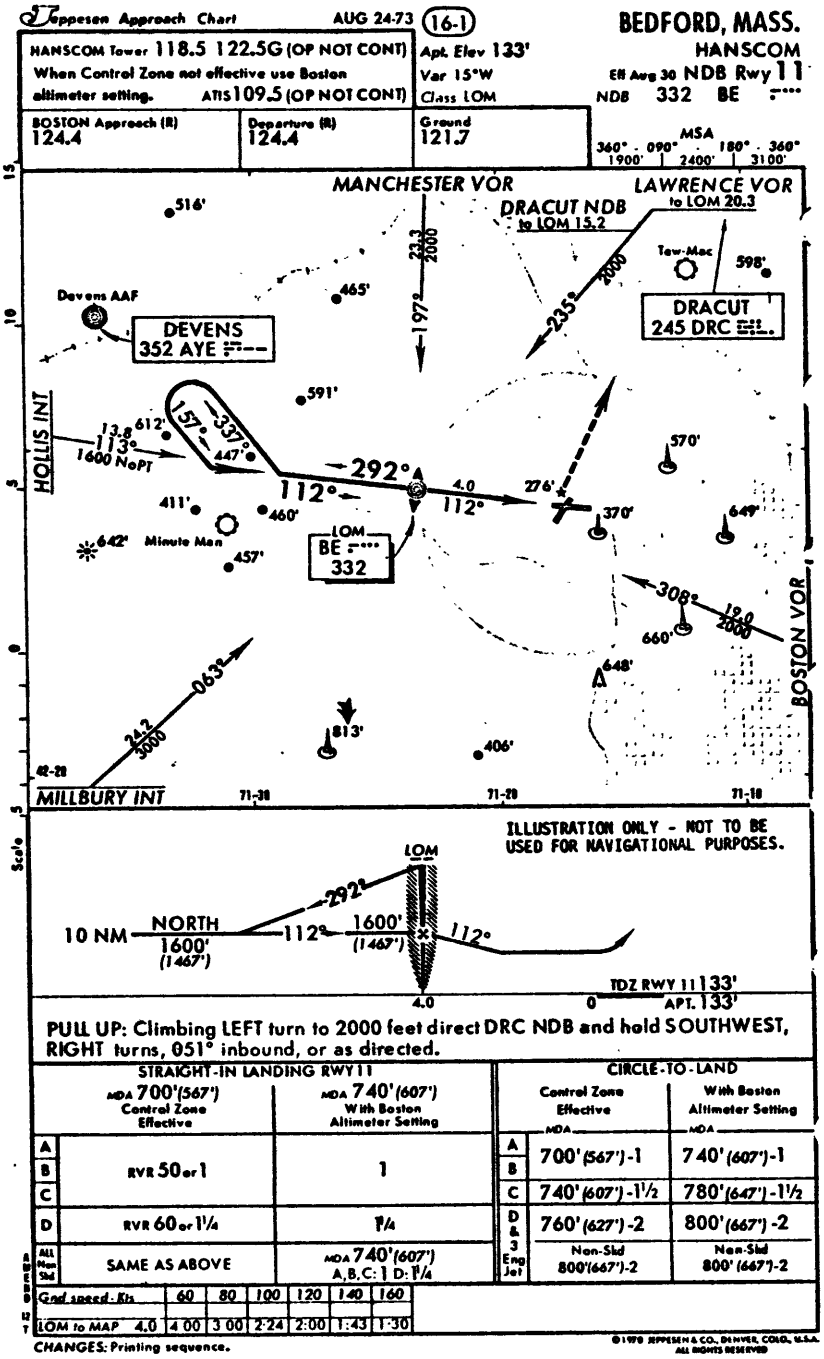


Figure 16-5. (Unmodified) NDB Approach to Runway 11, Hanscom Field

# CHAPTER XVII

# CONCLUSIONS AND RECOMMENDATIONS FOR FURTHER STUDY

## 17.1 Conclusions

(1) Various Omega propagation anomalies were discussed, including Polar Cap Absorption and Sudden Ionospheric Disturbances. These unpredictable disturbances were found to be potentially so great that all Omega systems used in the National Airspace System must be able to reduce the effect of these anomalies to prevent serious undetectable navigational errors in the presence of these phenomena. The cost for not having this correction capability as a system requirement could be epidemic aircraft accidents due to navigation systems supplying erroneous information.

(2) The Weibull distribution was investigated as a model for radial errors of Omega systems, and not found to be satisfactory. The Weibull distribution does not describe radial errors for multivariate Gaussian errors except those which have circular contours of equal probability and zero mean.

(3) Short term Omega noise was defined as the variation between successive phase measurements. This noise is important for aircraft navigation, as it is within the bandwidth of the pilot/aircraft system. A ground test set up showed that a reasonable model for this short term Omega noise is Gaussian noise, uncorrelated between samples, with a standard deviation of 4 cec.

(4) Data analysis of some 70 hours of flight test data showed various operational factors:

- Some receivers are prone to have a random bias introduced when reset.
- VHF power supply noise can result in S/N degradation of 10-15 dB (through 100 Hz).
- Precipitation static sufficient to make Omega signals unreceivable with simple E field antennas can be expected whenever the aircraft is flying in precipitation near the freezing level.
- Station power variations, although not reported, occurred during the flight test program.
- Station A S/N ratios were observed to be higher after local noon by approximately 10 dB, and these results are statistically significant.
- Linear fits of S/N ratio to observed position accuracy were attempted, but no meaningful conclusions could be drawn.
- Radial errors over the entire flight test program showed a mean and standard deviation of about three-quarters of a mile, but the quality of the radial error data was poor.

(5) Four approaches were flown to Hanscom Field, Bedford, MA, using the Omega set as the only guidance system. With the exception of the reset bias mentioned above, on two approaches accuracies were experimentally observed on various approaches comparable to those achievable on VOR or ADF approach at five mile distance from the facility. However, pilot workload was excessive.

(6) Mathematical models of differential Omega showed that with receiver phase lock loop time constants varying by a factor of 10 in the airborne and ground monitor receivers, unacceptably large errors could occur during phase anomalies even with real time differential Omega updates.

(7) For matched receiver time constants, one minutes is a reasonable upper bound for differential Omega update intervals, with accuracy enhanced by real time differential Omega updates.

(8) Various analytical models have shown that differential Omega approaches can be flown with a standard deviation of less than 1500 feet in the

presence of severe wind conditions with control laws which vary from the optimal. The optimal system time constants were found to be on the order of 20 seconds, with the tradeoff being toward longer time constants to filter the Omega data more heavily when the wind noise was low, and shorter time constants when the wind noise was high.

(9) Current regulations for area navigation systems require checking of pilot inputs to the system so that waypoint definitions are correct. In the flight test program, it was found that the non-orthogonal coordinate frame of Omega lines of position was confusing to the pilot, and numerous errors were made in setting the Omega receiver because no feedback was provided to the pilot as to correctness of setting. From these two points, the best coordinate frame to use for Omega waypoint definition and position settings is latitude and longitude, an orthogonal coordinate frame familiar to all pilots, and one in which error detection/correction digits can be appended to waypoint definitions on charts to provide error detection/correction capability.

(10) Terminal procedures for Omega approaches must take into consideration the special characteristics of Omega and differential Omega signal propagation characteristics. Although few local interference areas or anomalies were found in the flight test program, the presence of any such phenomena on an approach might have to be reflected in higher minima. Similarly, the characteristics of the differential Omega signal, such as distance and direction from the monitor station to the approach course (which would dictate system accuracy and signal availability) would have to be considered in specification of minima for approaches.

Safety considerations preclude pilots "improvising" approaches using Omega.

(11) Many schemes are available for differential Omega update, using various auxiliary radio uplinks. One form of differential Omega providing a reduction in the amount of data to be incorporated into the uplink is differential/composite Omega, in which the parameters uplinked are not the phase corrections of each individual signal, but rather the composite Omega parameter "m", which has a nominal value of 3.3.

(12) Conventional aviation charts can be used for Omega by simple addition of latitude and longitude information, just as is currently done on Standard Instrument Departure Charts.

(13) Safety requirements dictate that navigation signals displayed be meaningful, and that system redundancy or fail soft capability be provided. For light aircraft Omega systems, these requirements suggest self-test circuitry and failure detection circuitry.

17.2 Recommendations for Further Study

(1) The greatest requirement for Omega implementation in the National Airspace System is that much greater experience with Omega navigation systems be achieved so that meaningful decisions can be made on operational system characteristics.

(2) Composite Omega has shown great theoretical promise in correction of both predictable and unpredictable phase anomalies. Confirmation of these characteristics in noisy solar conditions would be a worthwhile exercise.

(3) Composite Omega uses only the 10.2 and 13.6 kHz Omega frequencies because composite use of the 11.33 kHz frequency requires phase measurements to great accuracy for use in composite form. However, the 10.2 and 11.33 kHz signals could be used to perform some lane resolution in composite Omega systems, with primary navigation information derived from the 10.2 and 13.6 kHz Omega signals. The expected errors and implementation difficulties of this system should be investigated.

(4) Short-term noise has been shown to be important for approach flying. However, distance correlation of Omega errors has not been performed with an eye towards short-term noise, and distance correlation effects should be studied. Similarly, factors affecting short-term noise and short-term noise statistics should be measured in detail.

(5) Omega signal strength and station geometry were not found to be particularly good in the New Jersey area. Analysis of signal availability and station geometry should be performed for the continental United States to determine whether a different station configuration would be worth the costs of a separate Omega-like system.

# APPENDIX A

## RESULTS OF FLYING APPROACHES WITH AN OMEGA RECEIVER

### A.1 Introduction

This section consists mainly of graphical data. Various receiver parameters were recorded during the flights which included the approaches and some ferry flying. The various approaches themselves are plotted in squares of the same size and scale as the Jeppesen approach plates with various filtering schemes simulated.

### A.2 Receiver Parameter Plots

As was done previously (16), S/N ratios for stations A, B, C, and D were plotted versus time. Discontinuities in these plots indicate that garbled data was collected, the result of transmissions on a portable VHF transceiver garbling the FSK data recorded on a cassette recorder. The horizontal axis is marked with both time hacks every five minutes and changes in discrete operator code, which provides better identification of data points.

Other plots include readout of miles to go and needle deflection, with to/from flag, weak signal light, reset and autozero activations also plotted. These last four are abbreviated on the plots by T, F, W, R, and A.

Six plots of both sets of receiver parameters are included, containing data as shown in Table A-1.

### A.3 Map Plots

Each of the approaches was plotted in several different ways. The raw data was plotted first, resulting in a rather noisy plot. Other filters used included an ad hoc filter with a time constant of about 20 seconds,

Table A-1. Route of Flight for Various Plots

| PLOTS | ROUTE | INCLUDES APPROACHES |
|---|---|---|
| A2, A3 | Haverill, Mass. to Bedford, then SW | --- |
| A4, A5 | To Bedford, then to Manjo Intersection | ILS 1 |
| A6, A7 | To Bedford, then to Manjo Intersection | ILS 2 and 3 |
| A8, A9 | To Bedford, then to Norwood | ILS 4 |
| A10, A11 | Norwood to Haverill | --- |
| A12, A13 | Haverill to Bedford | --- |

shown in Figure A-1, straight averagers over 100 and 200 seconds, and exponential lags with time constants of 100 and 200 seconds. Not all of the 24 map plots of the four approaches are included, but those with significant value are included. Table A-2 lists map plots and filters used to generate them.

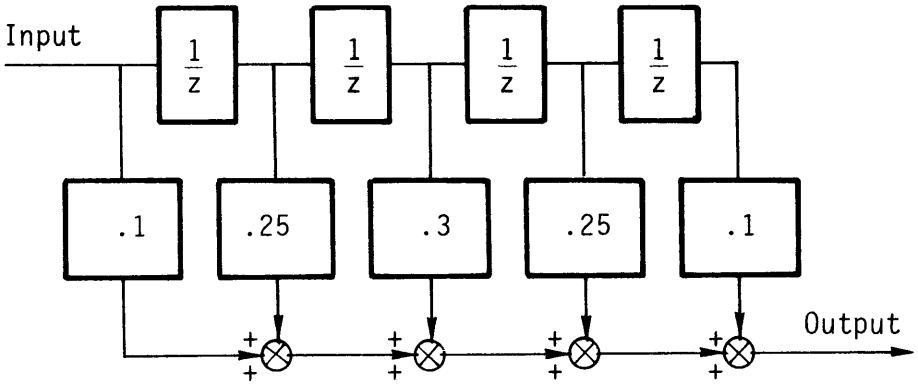


Figure A-1. "Map" Filter.

Table A-2. Plots of Approaches Flown with Various Filters on Data

| APPROACH | FILTER | FIGURE |
|---|---|---|
| 1 | none | A-14 |
| 2 | none | A-15 |
| 2 | map | A-16 |
| 2 | 100 sec. avg. | A-17 |
| 2 | 100 sec. exp. | A-18 |
| 2 | 200 sec. avg. | A-19 |
| 2 | 200 sec. exp. | A-20 |
| 3 | none | A-21 |
| 3 | map | A-22 |
| 3 | 100 sec. avg. | A-23 |
| 3 | 100 sec. exp. | A-24 |
| 3 | 200 sec. avg. | A-25 |
| 3 | 200 sec. exp. | A-26 |
| 4 | none | A-27 |
| 4 | 100 sec. avg. | A-28 |
| 4 | 100 sec. exp. | A-29 |
| 4 | 200 sec. avg. | A-30 |
| 4 | 200 sec. exp. | A-31 |

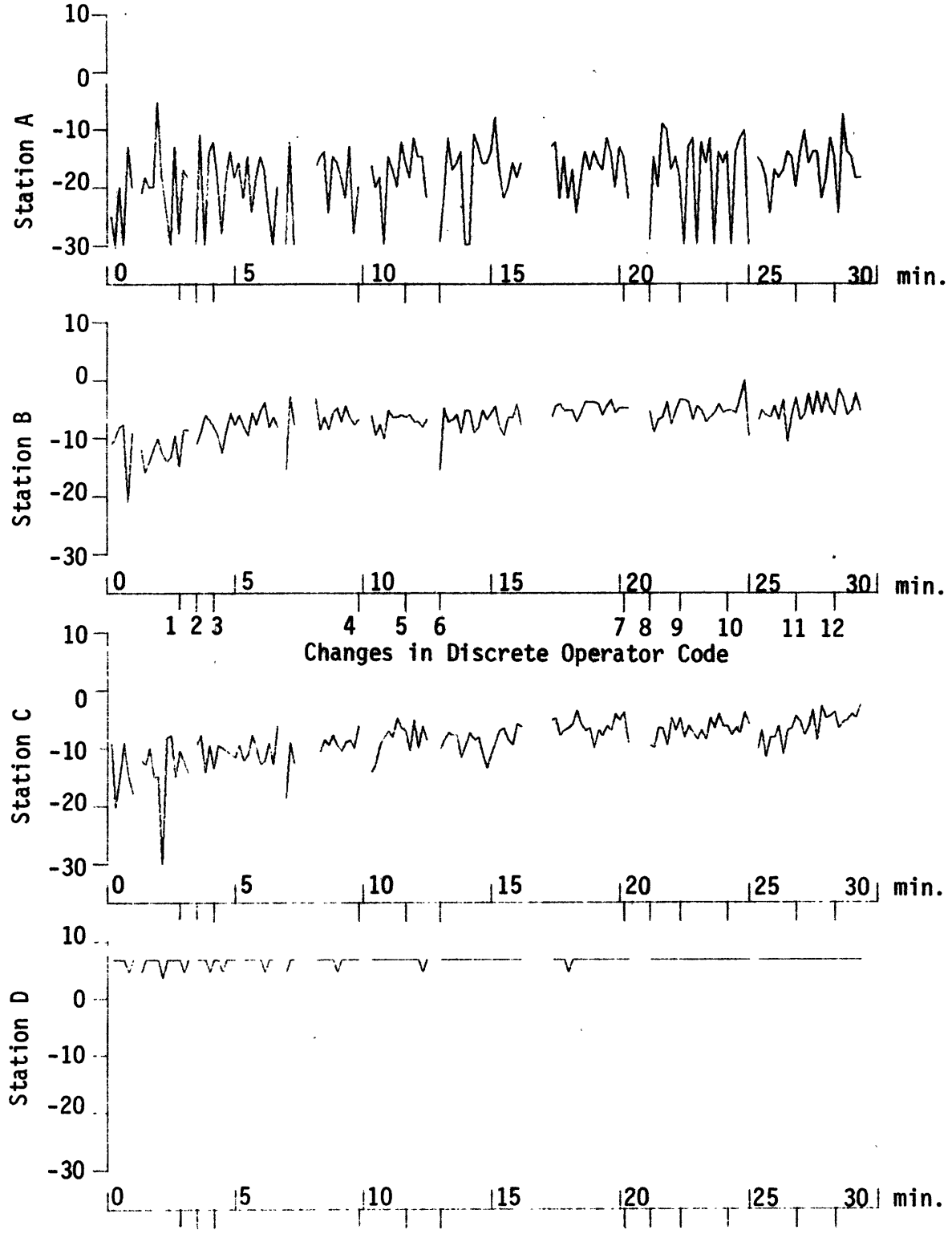


Figure A-2. S/N Ratios for Stations A, B, C, and D - First Leg (dB through 100 Hz)

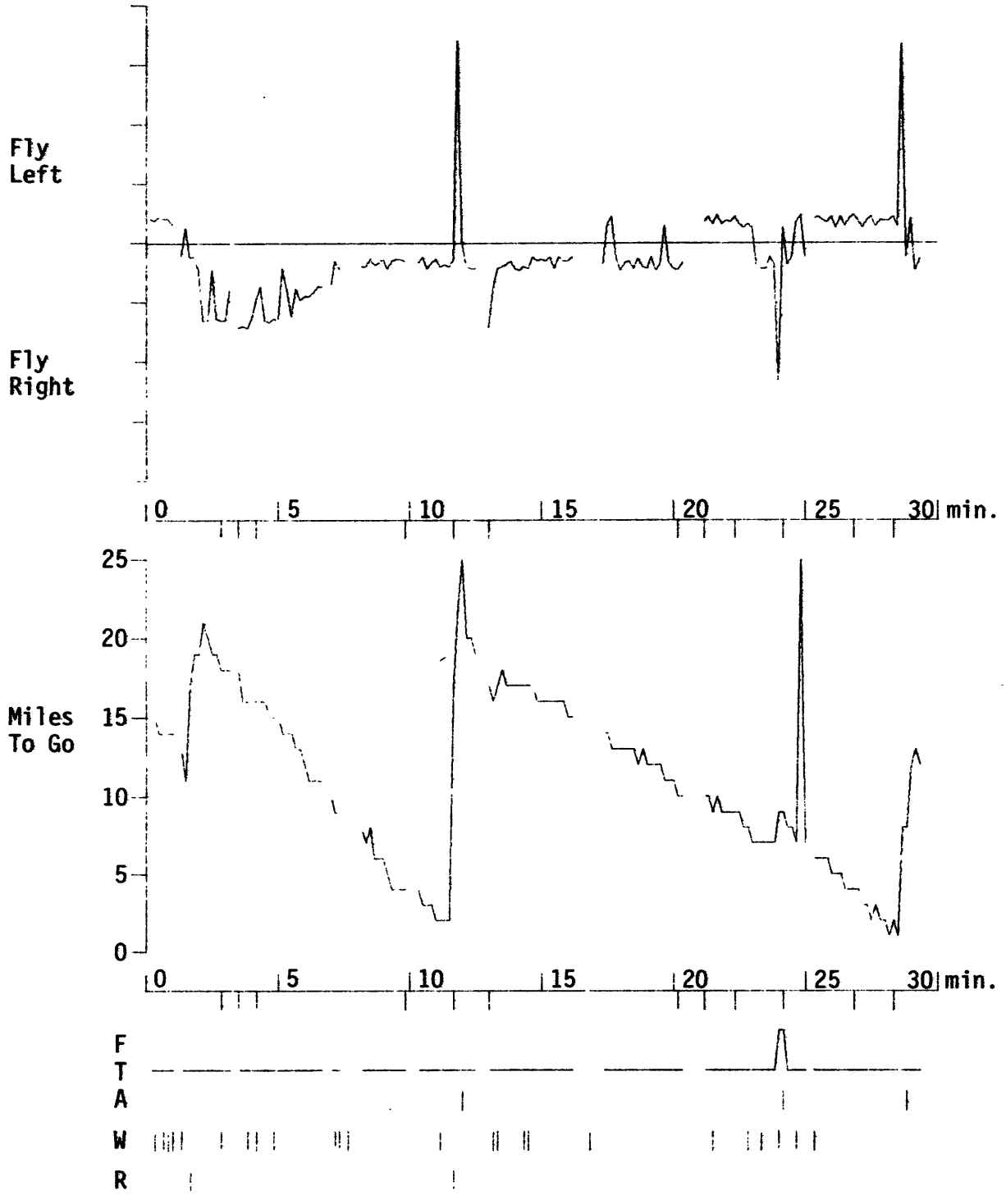


Figure A-3. Needle Deflection, Flags, and Miles to Go - First Leg

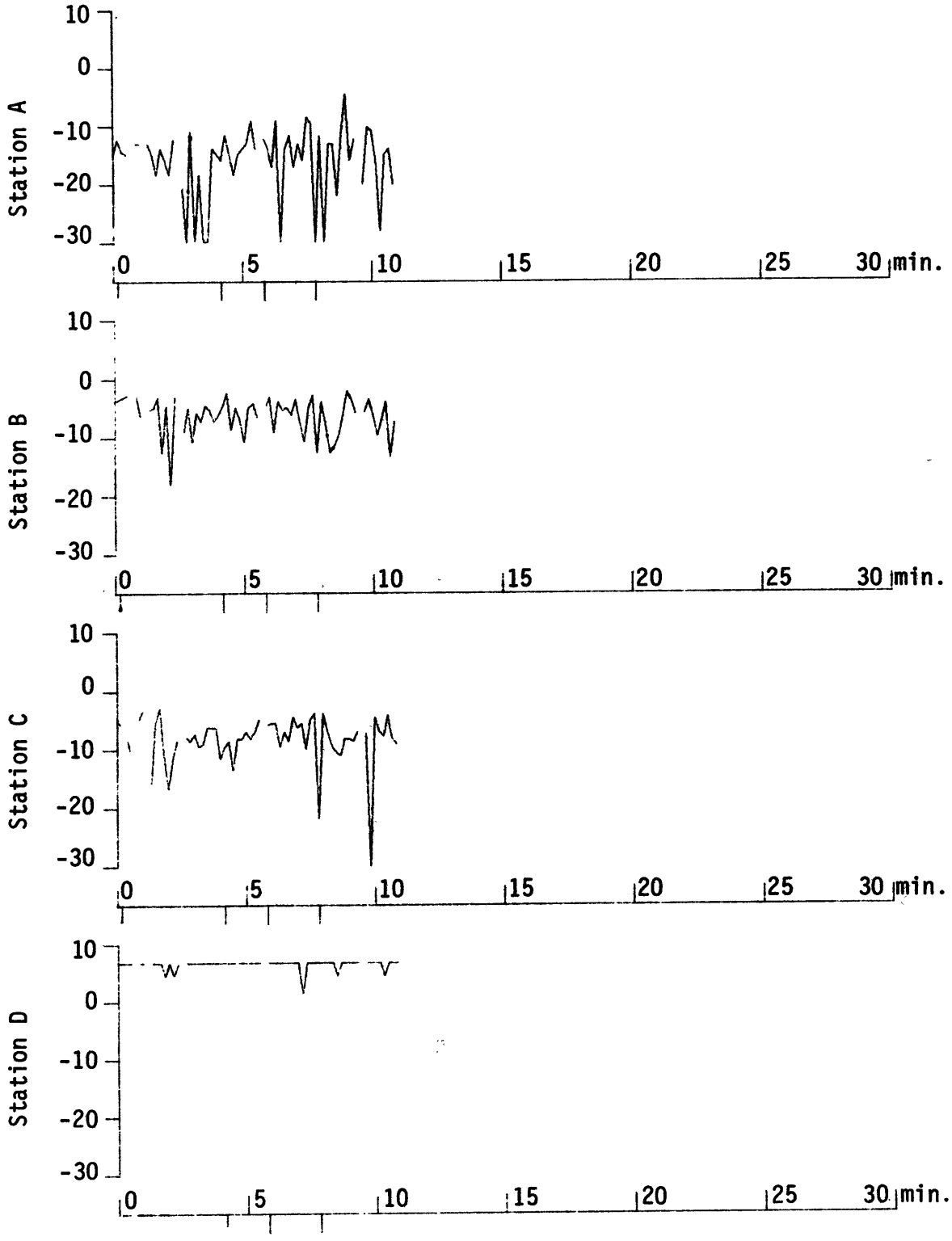


Figure A-4. S/N Ratios for Stations A, B, C, and D - Second Leg (dB through 100 Hz)

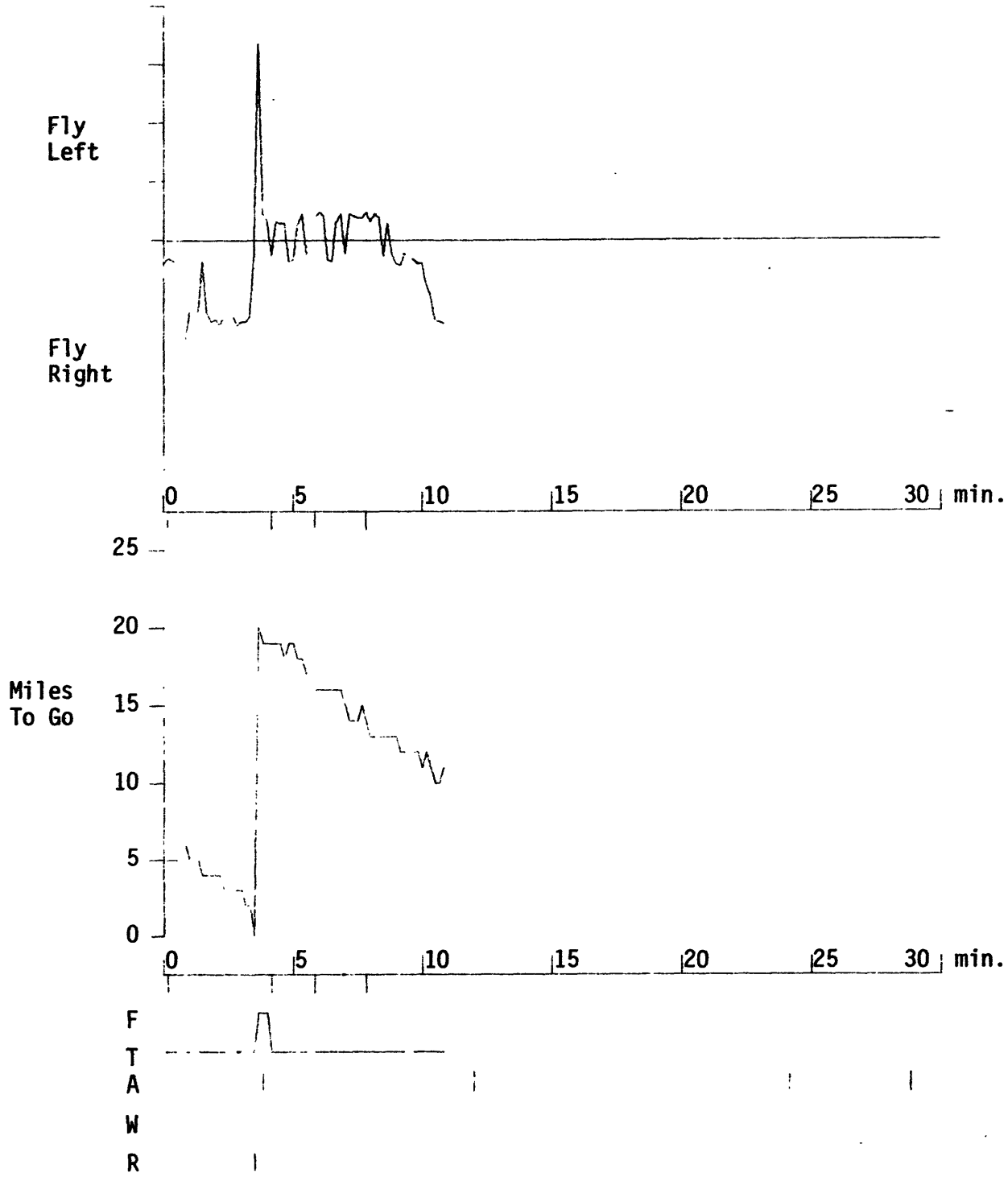


Figure A-5. Needle Deflection, Flags, and Miles to Go, Second Leg

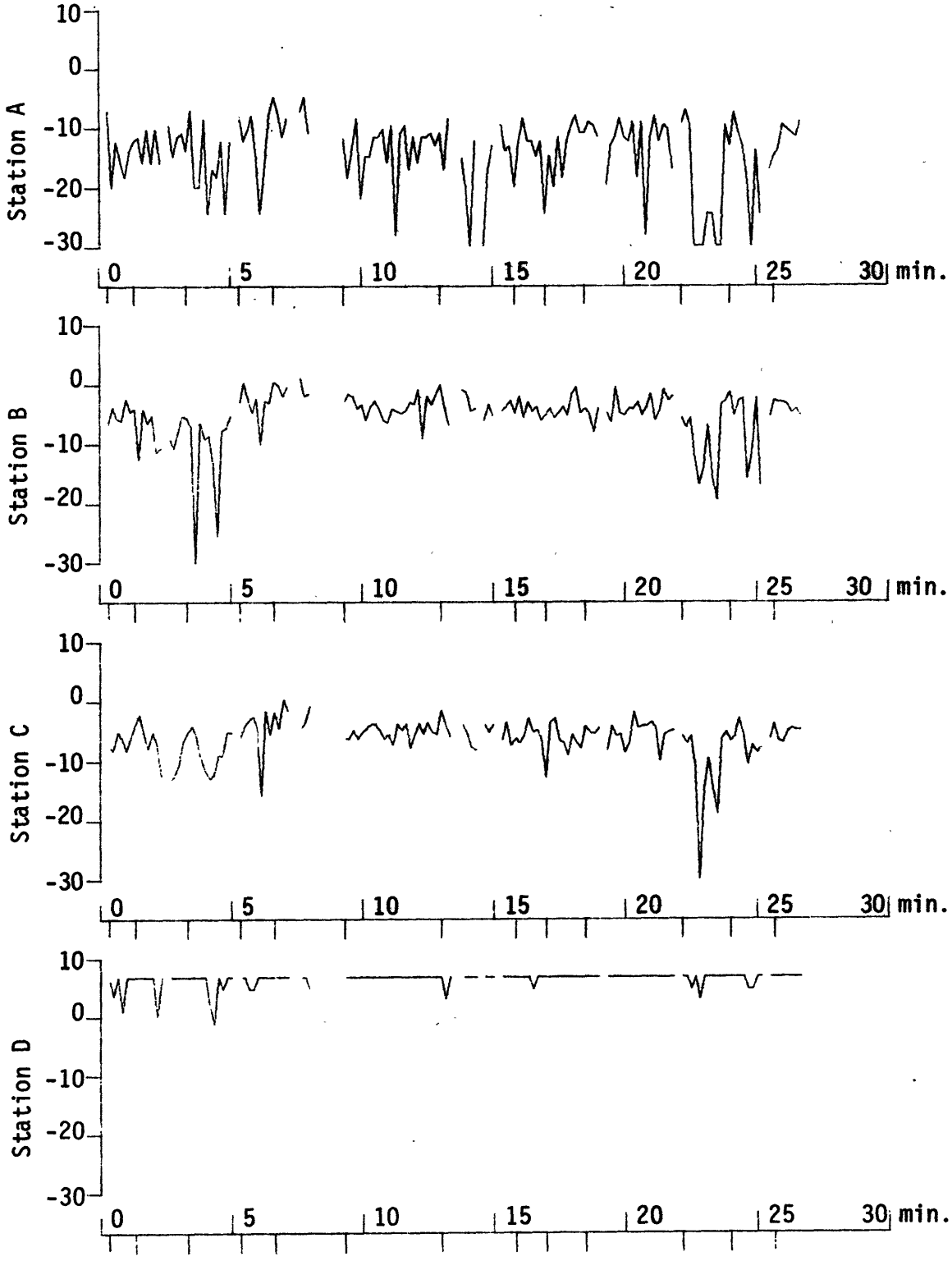


Figure A-6. S/N Ratios for Stations A, B, C, and D - Third Leg
(dB through 100 Hz)

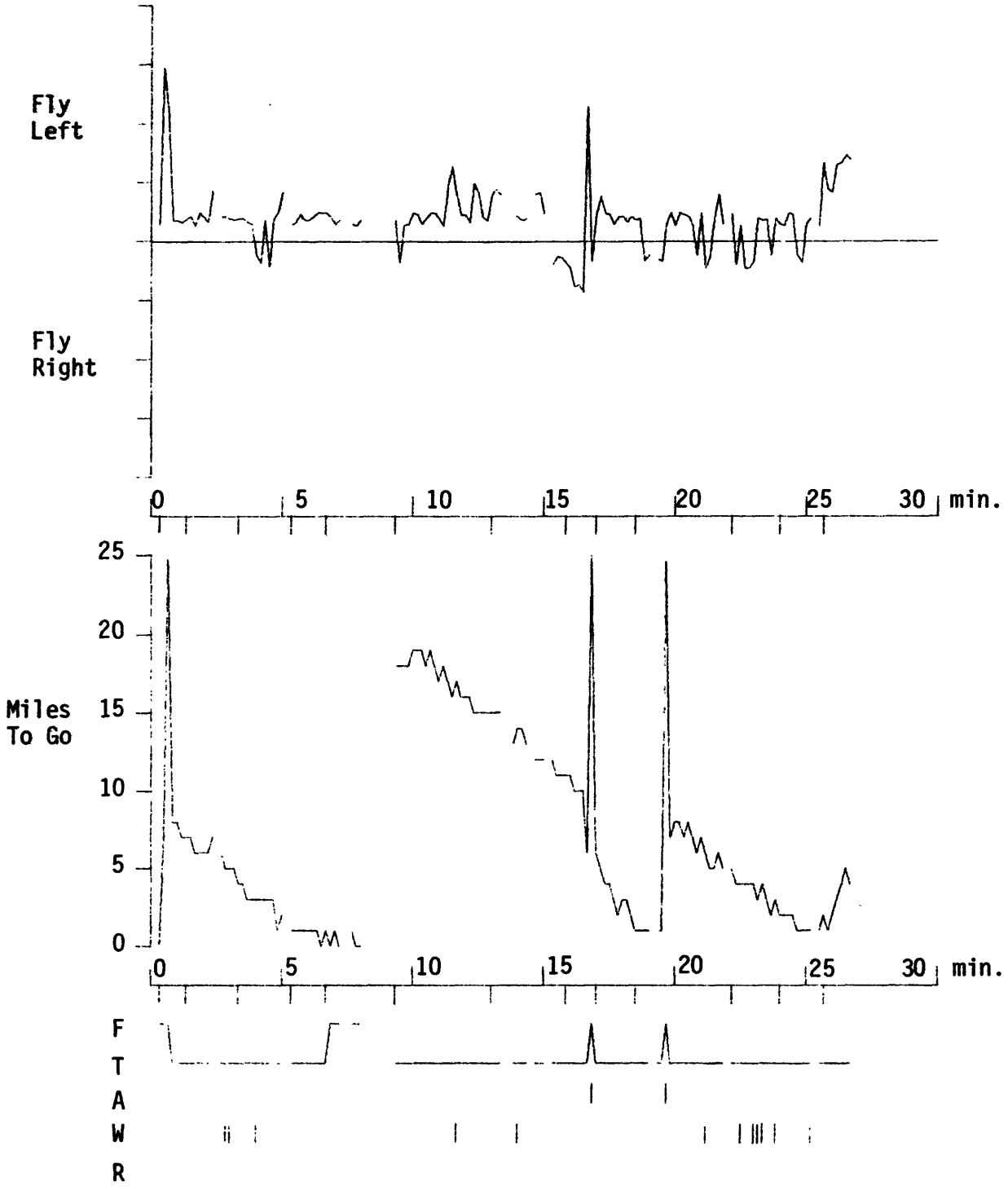


Figure A-7. Needle Deflections, Flags, and Miles to Go - Third Leg

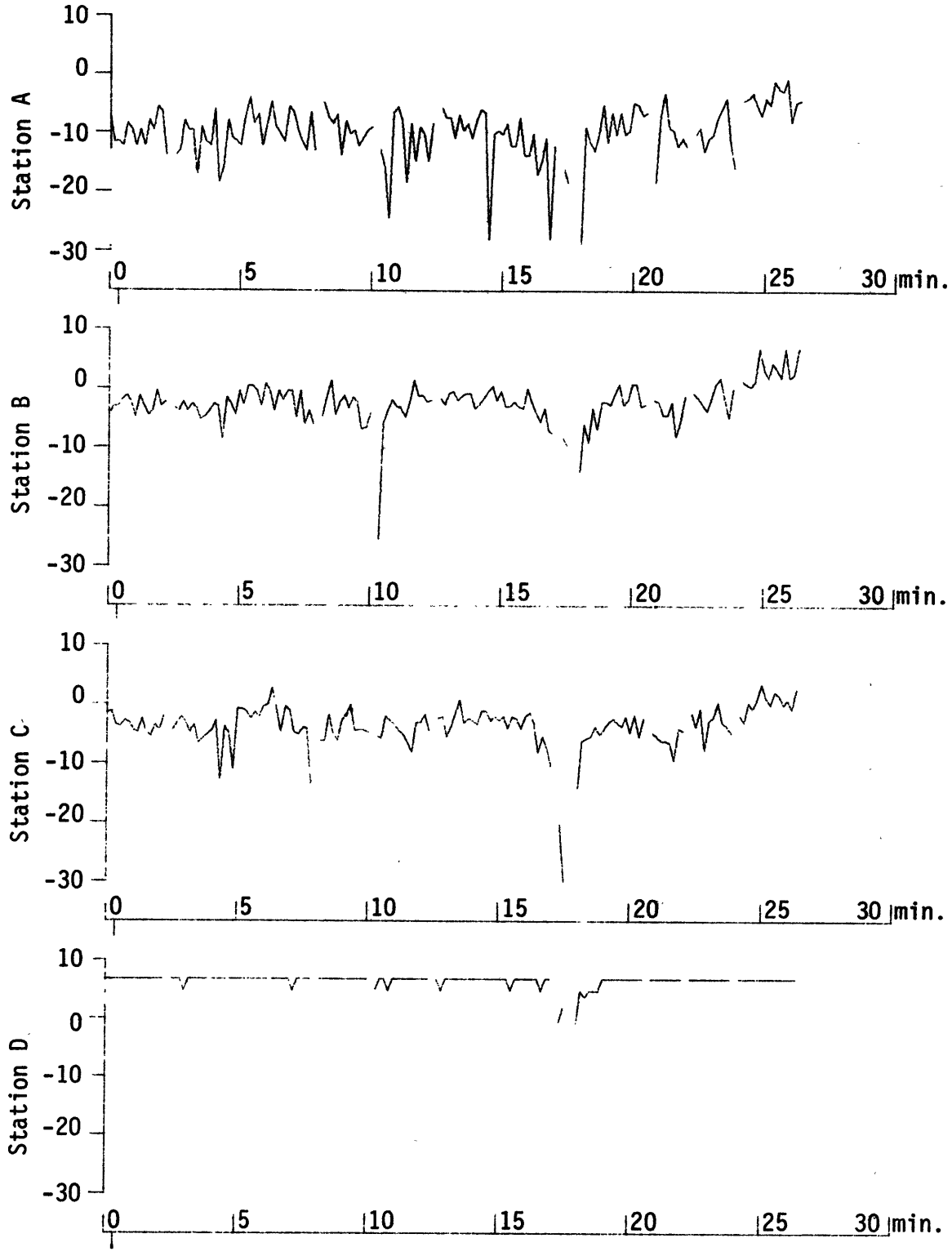


Figure A-8. S/N Ratios for Stations A, B, C, and D - Fourth Leg (dB through 100 Hz)

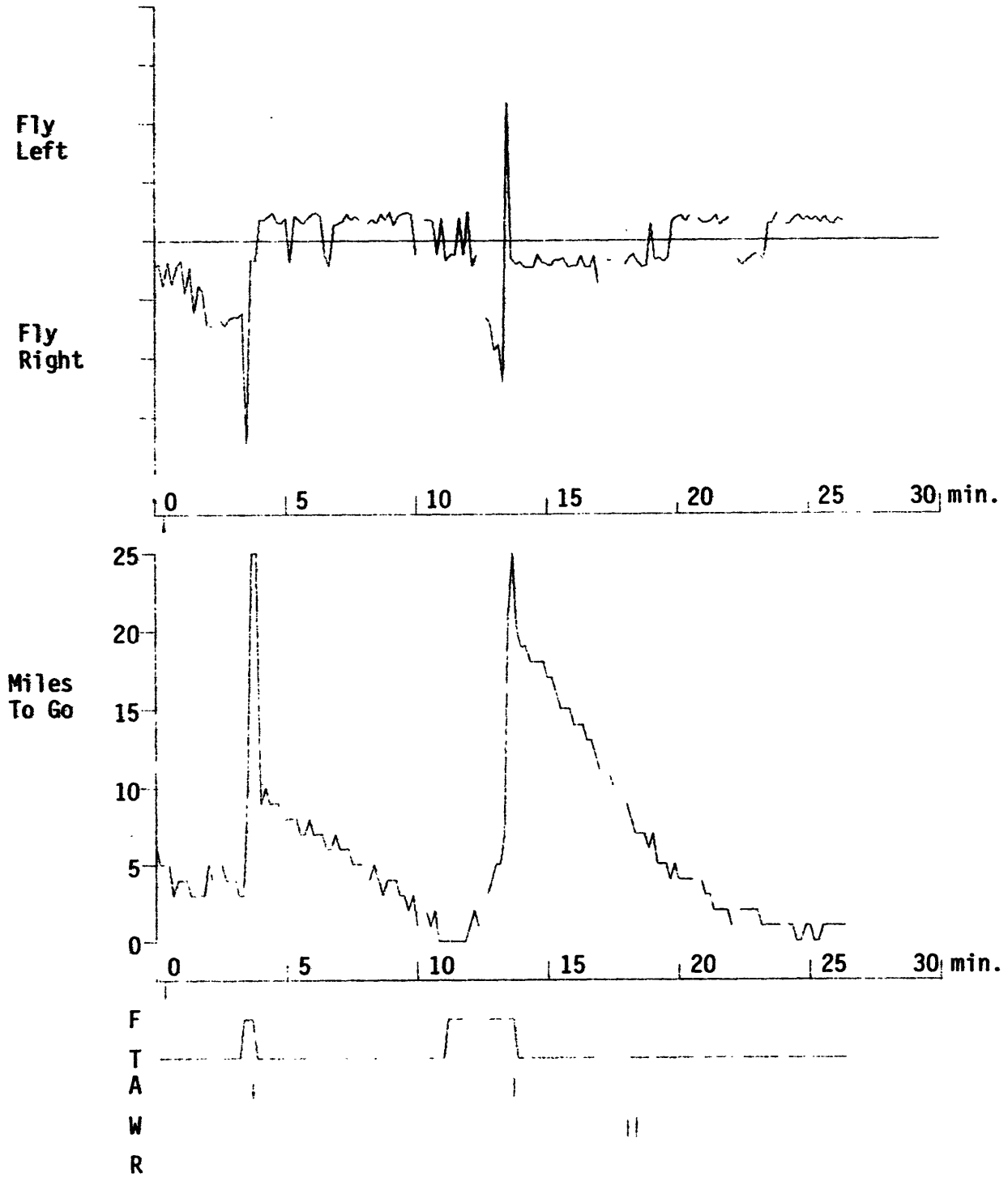


Figure A-9. Needle Deflections, Flags and Miles to Go - Fourth Leg

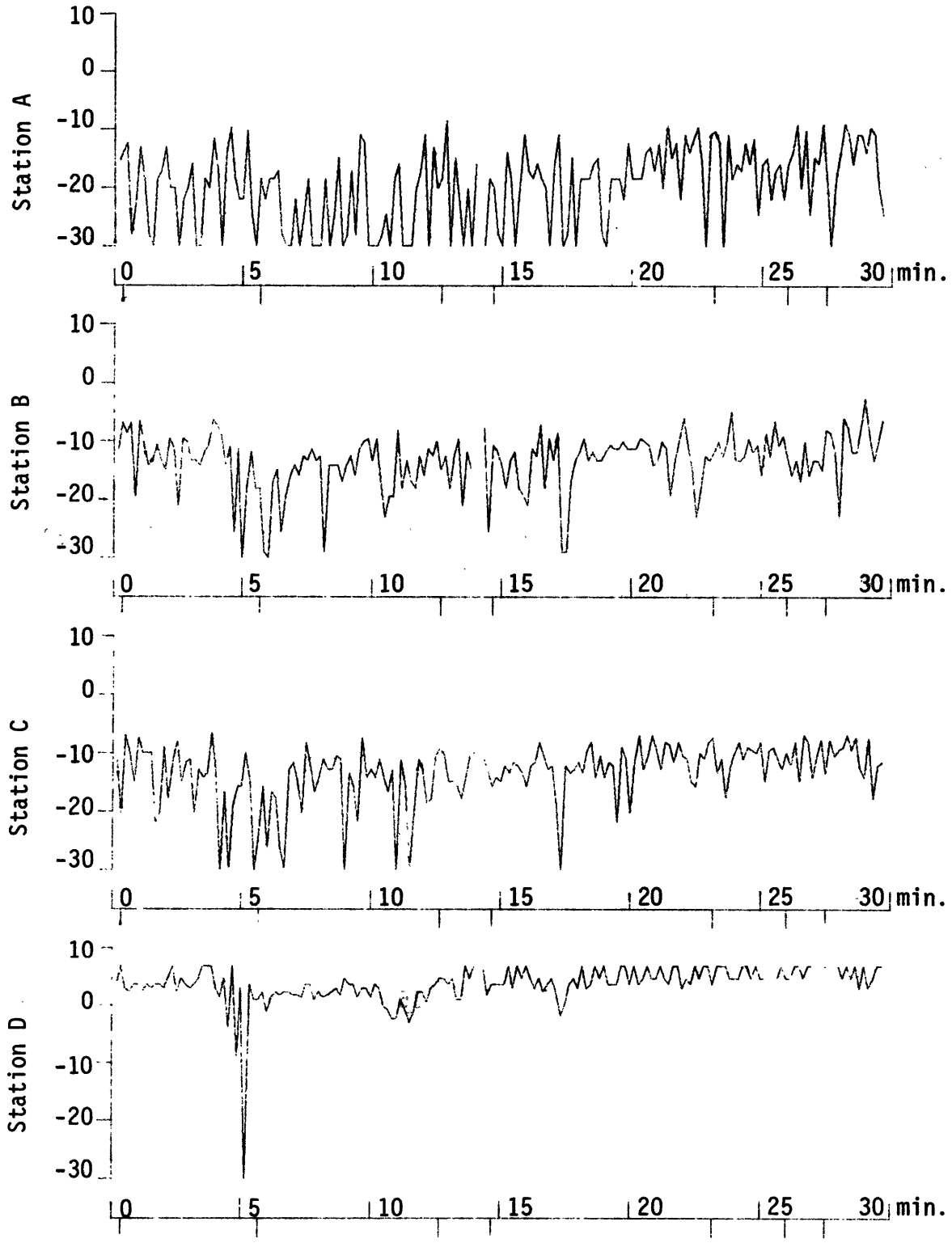


Figure A-10. S/N Ratios for Stations A, B, C, and D - Fifth Leg (dB through 100 Hz)

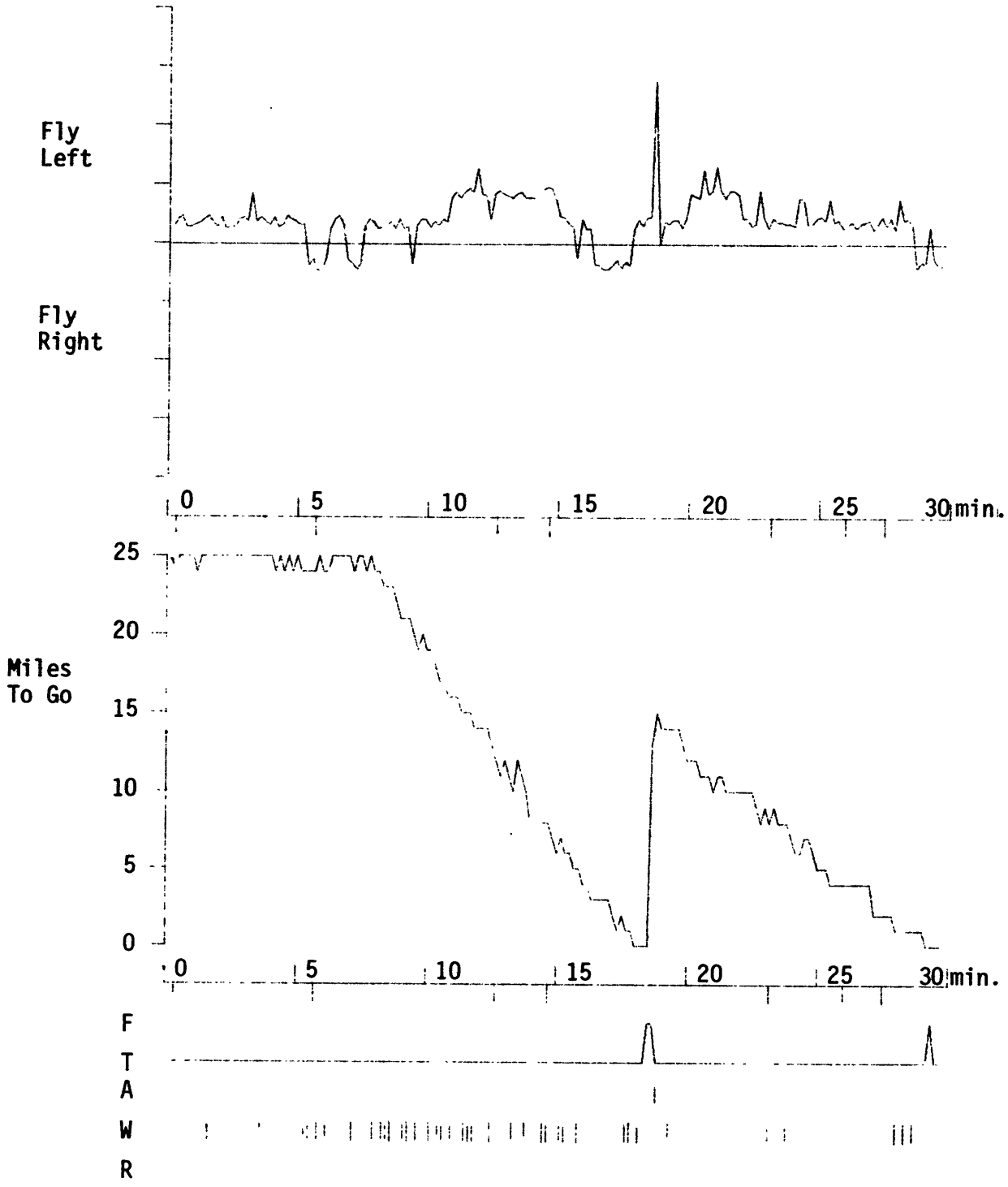


Figure A-11. Needle Deflections, Flags and Miles to Go - Fifth Leg

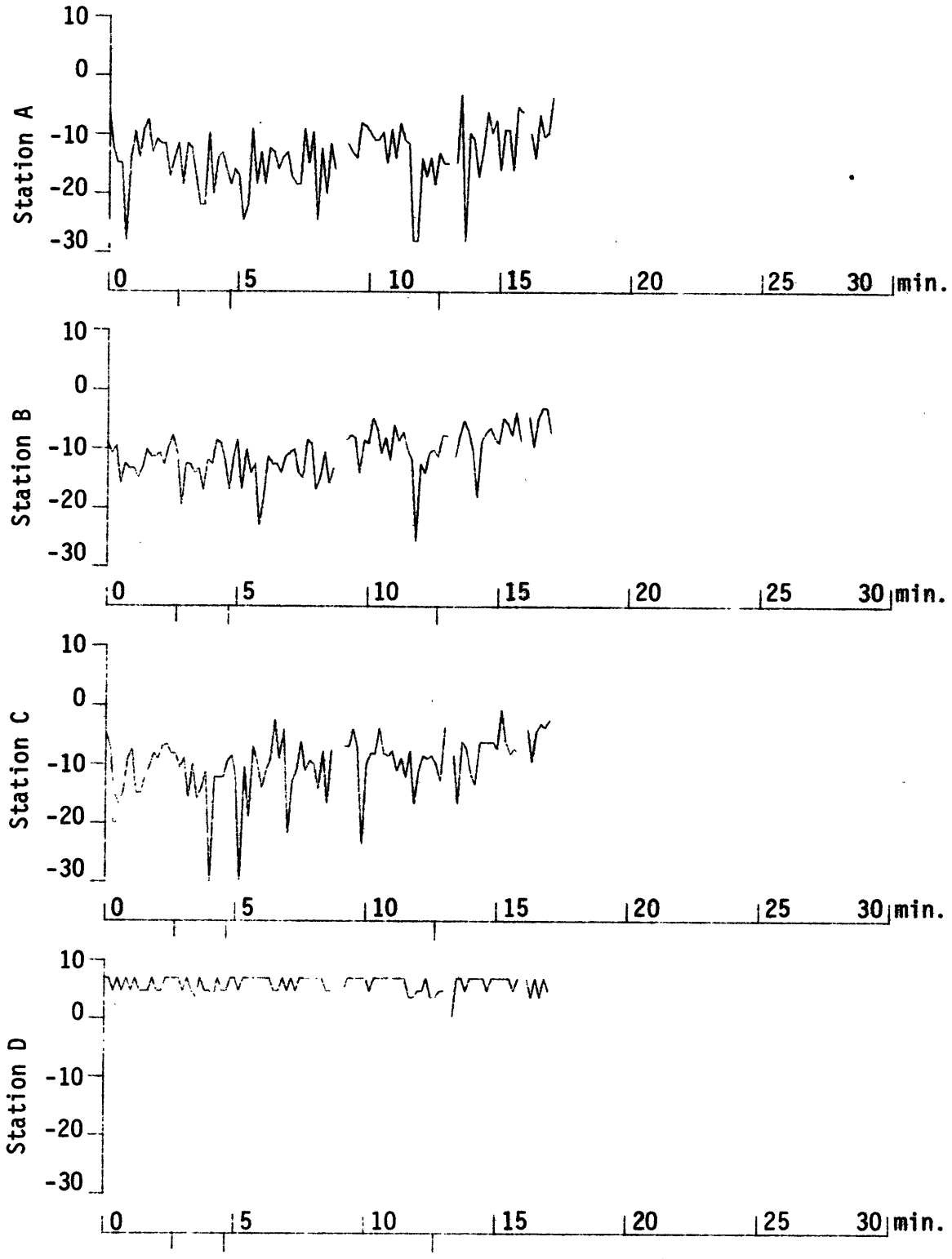


Figure A-12. S/N Ratios for Stations A, B, C, and D - Sixth Leg (dB through 100 Hz)

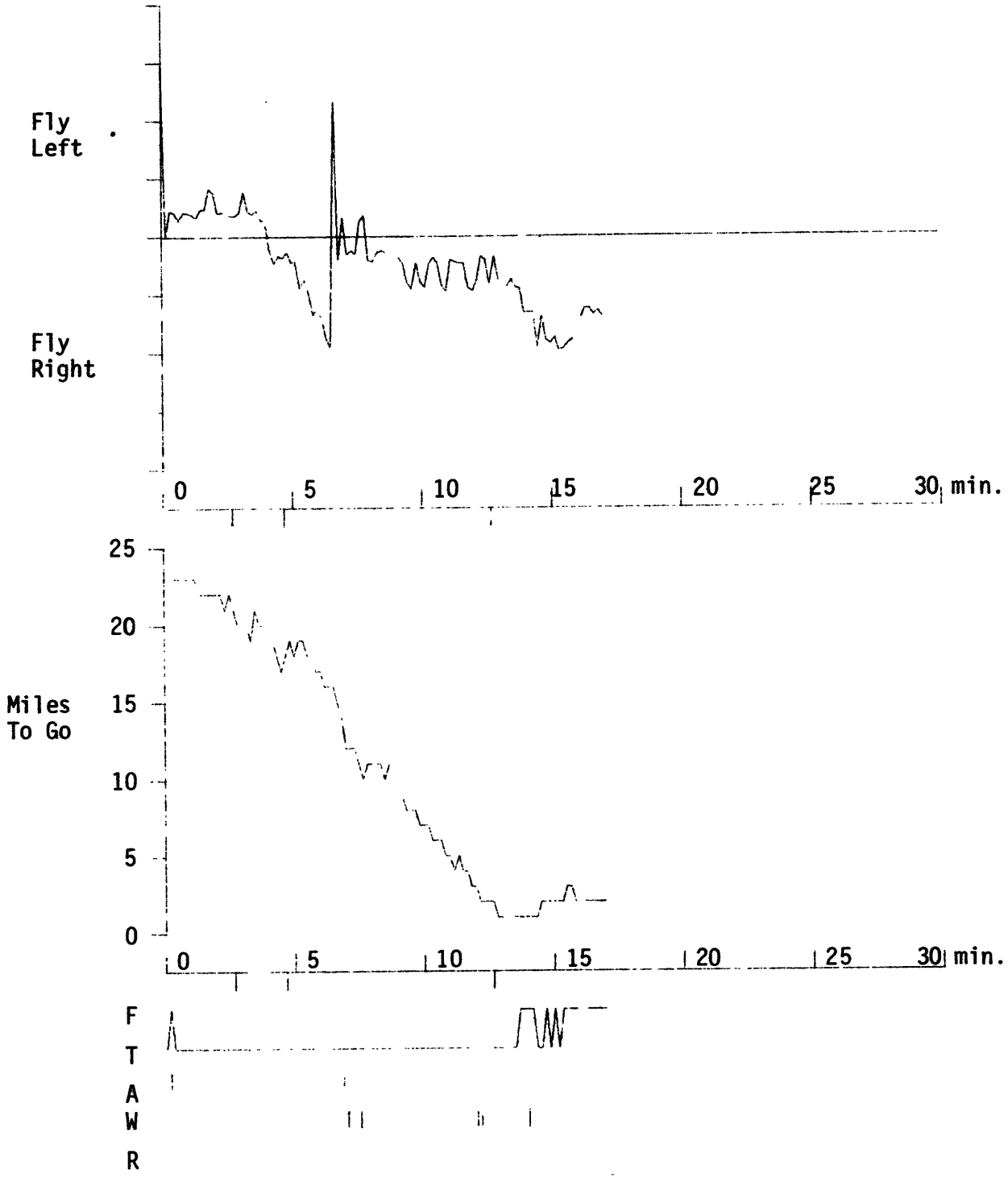


Figure A-13. Needle Deflections, Flags and Miles to Go - Sixth Leg

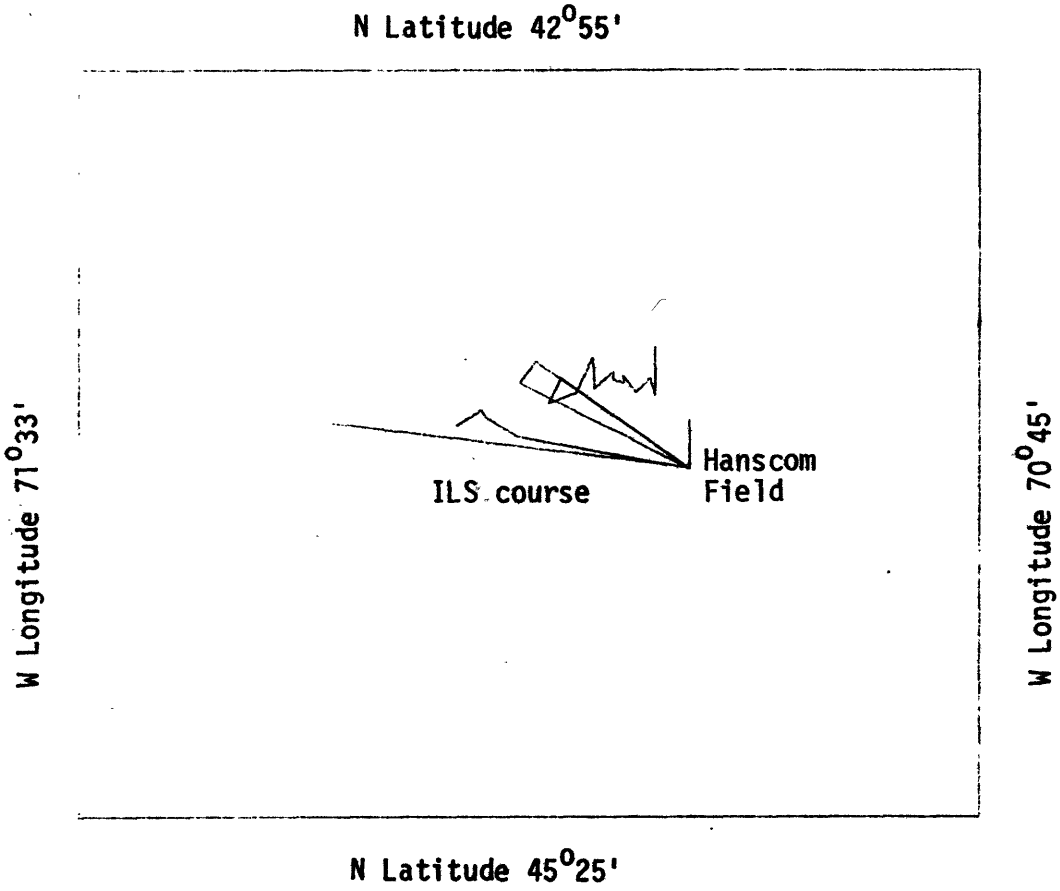


Figure A-14. Approach 1 - No Filter (Vertical tics on approach are spaced two minutes apart)

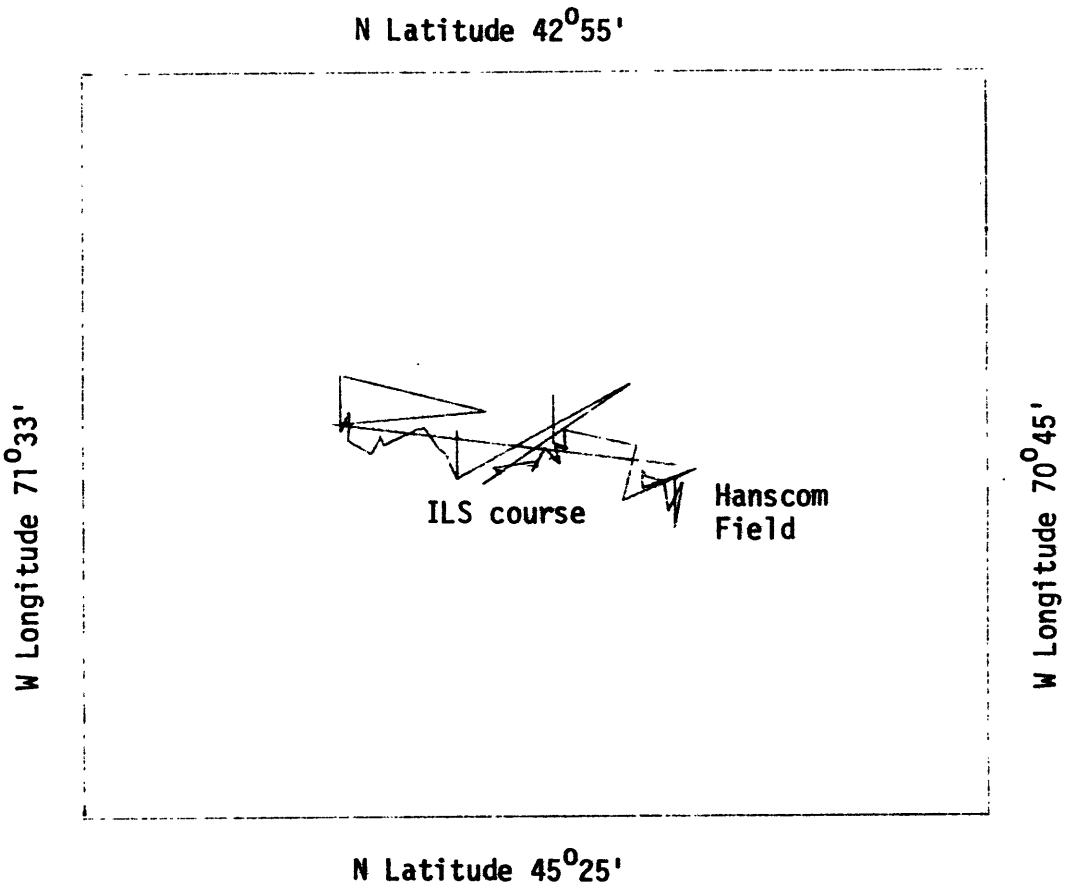


Figure A-15. Approach 2 - No Filter

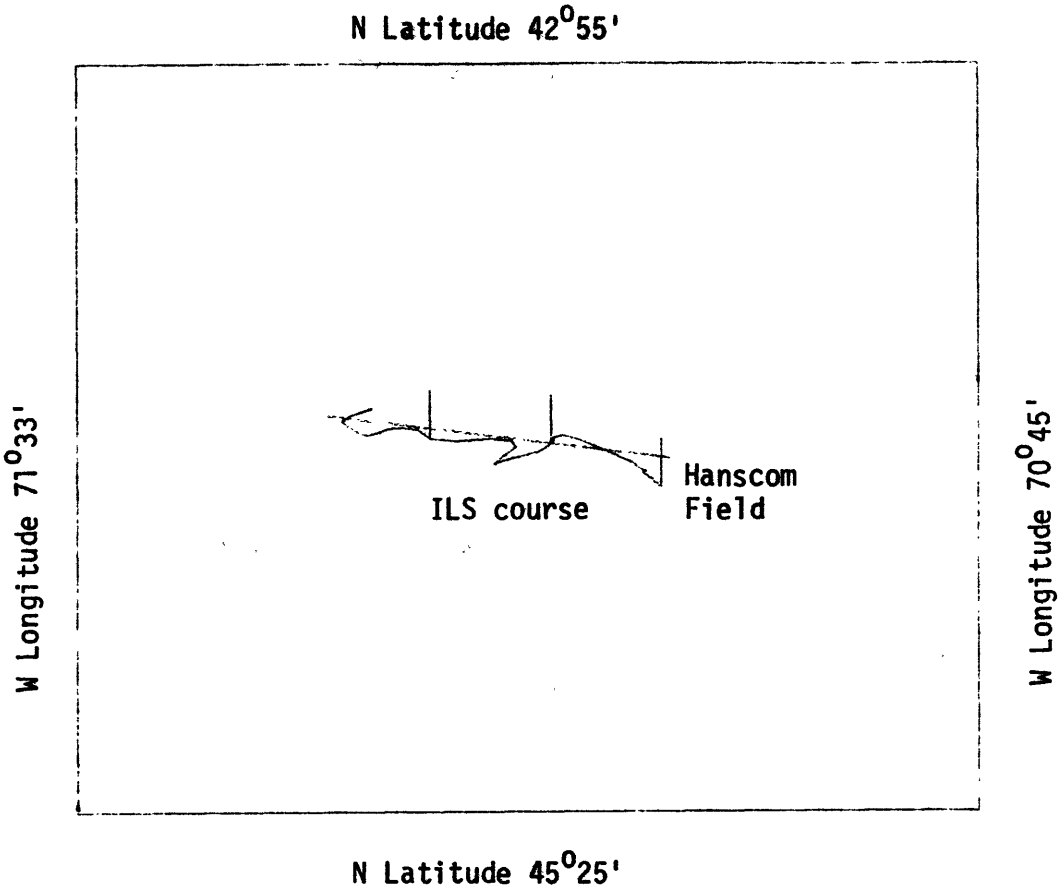


Figure A-16. Approach 2 - Map Filter

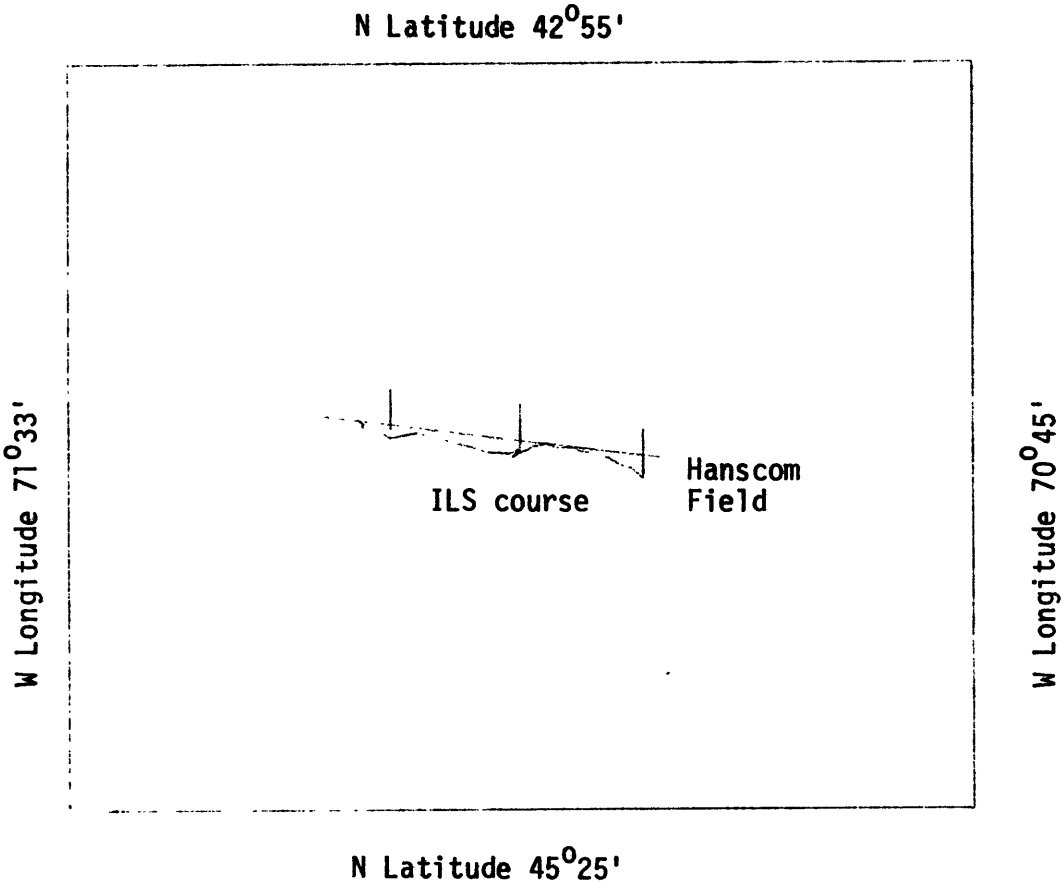


Figure A-17. Approach 2 - 100 Sec. Avg. Filter

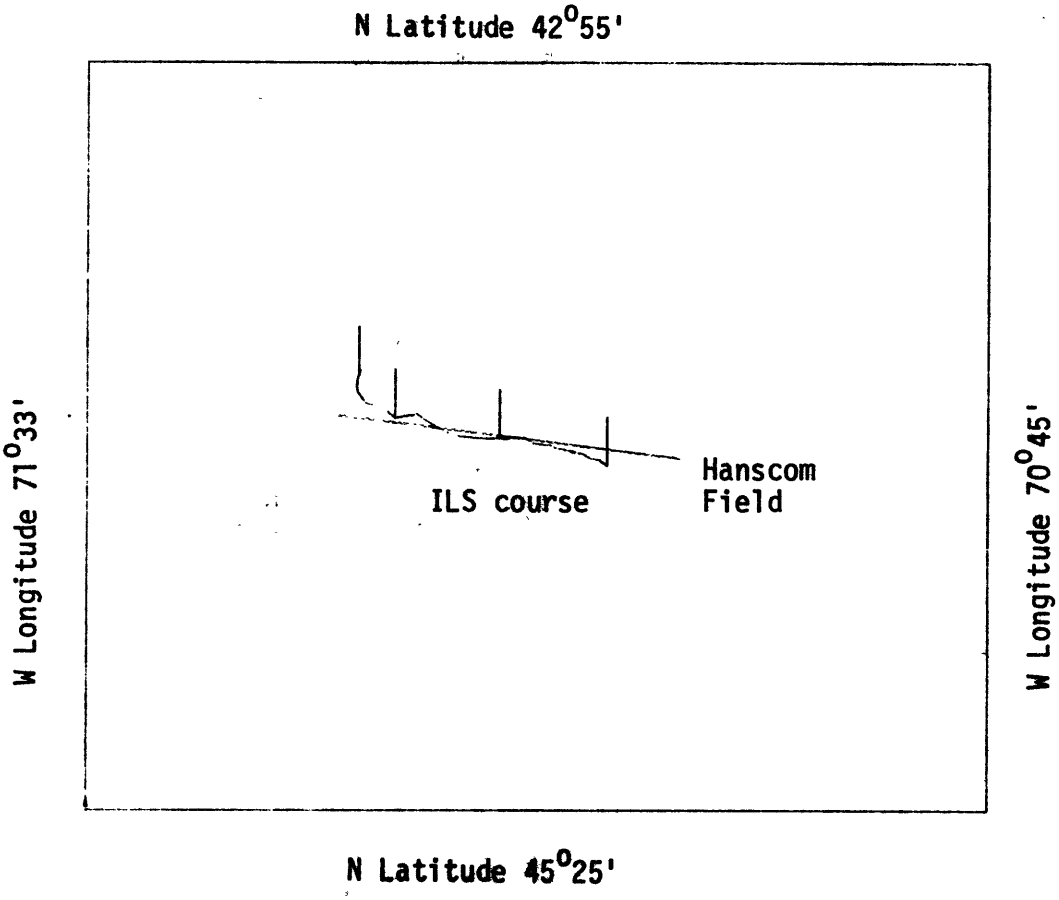


Figure A-18. Approach 2 - 100 Sec. Exp. Filter

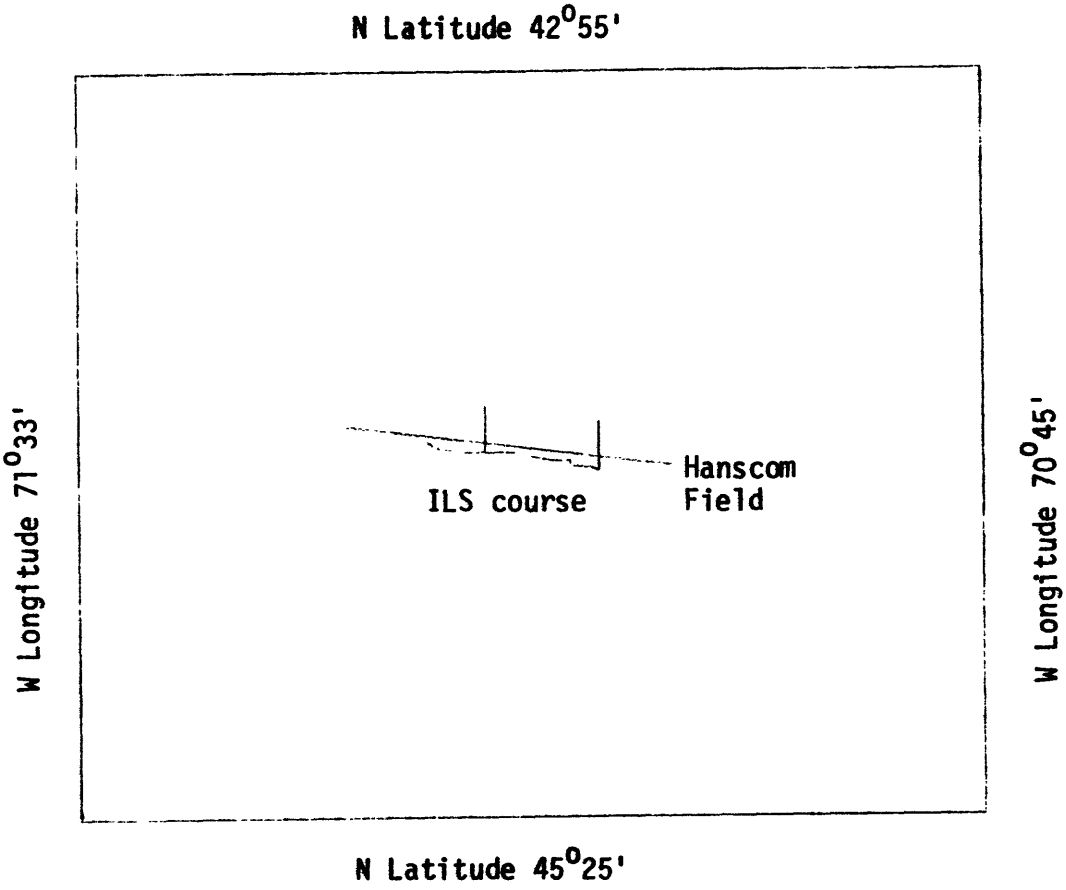


Figure A-19. Approach 2 - 200 Sec. Avg. Filter

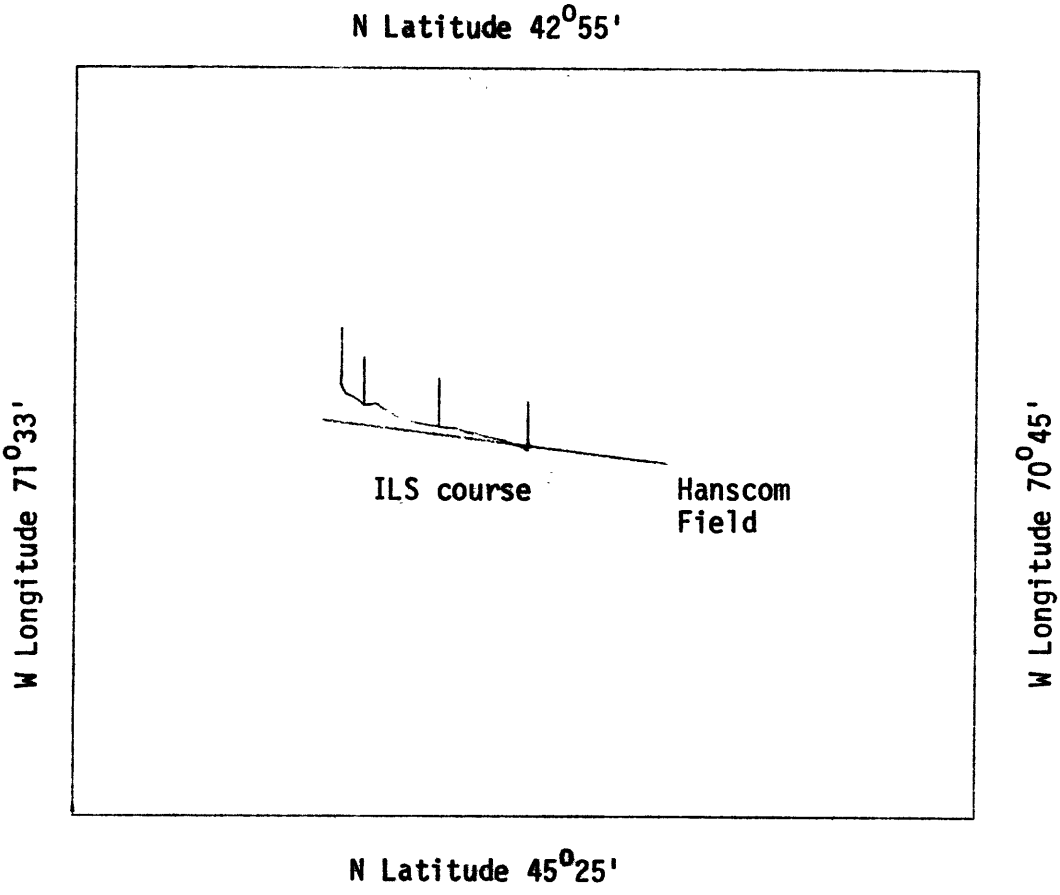


Figure A-20. Approach 2 - 200 Sec. Exp. Filter

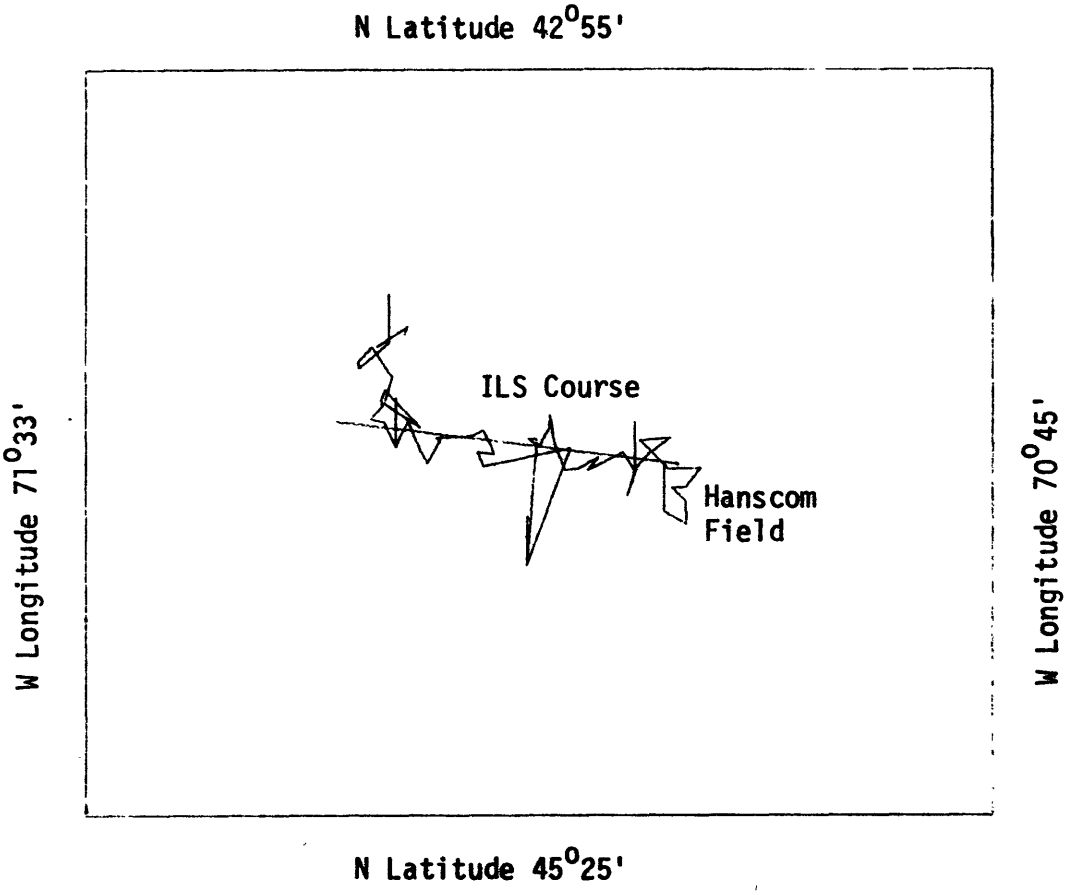


Figure A-21. Approach 3 - No Filter

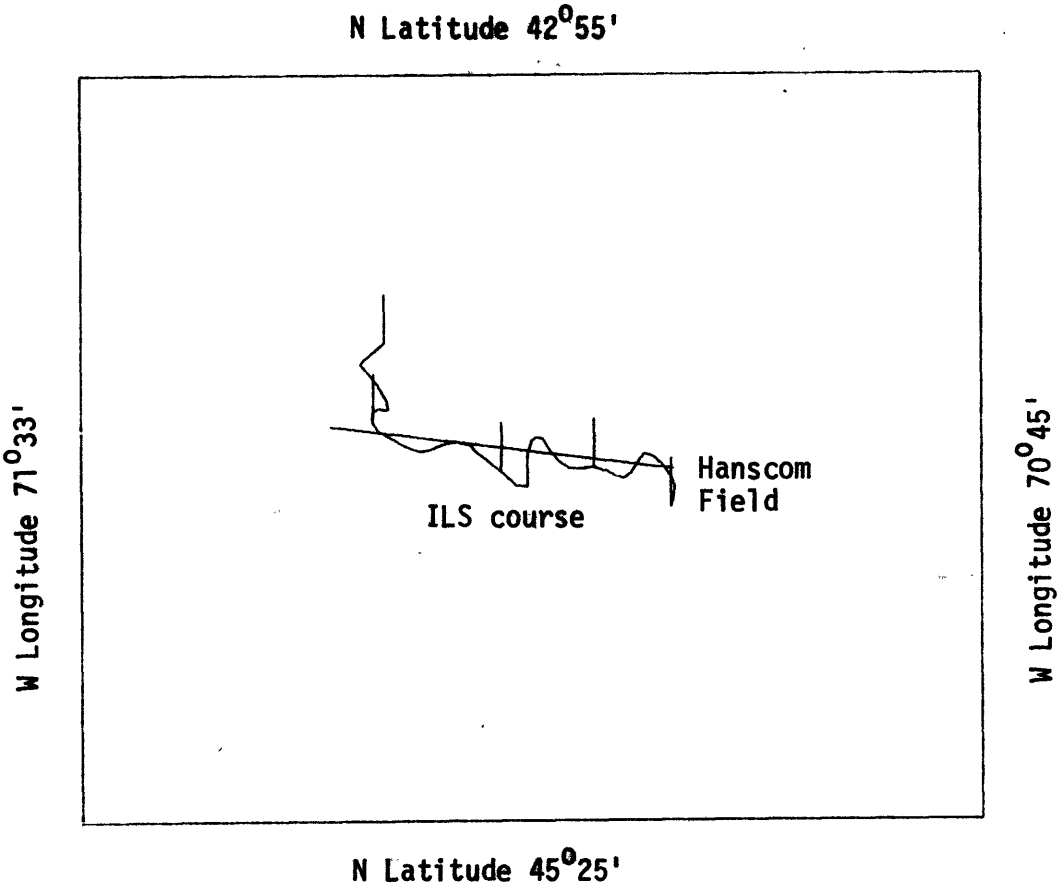


Figure A-22. Approach 3 - Map Filter

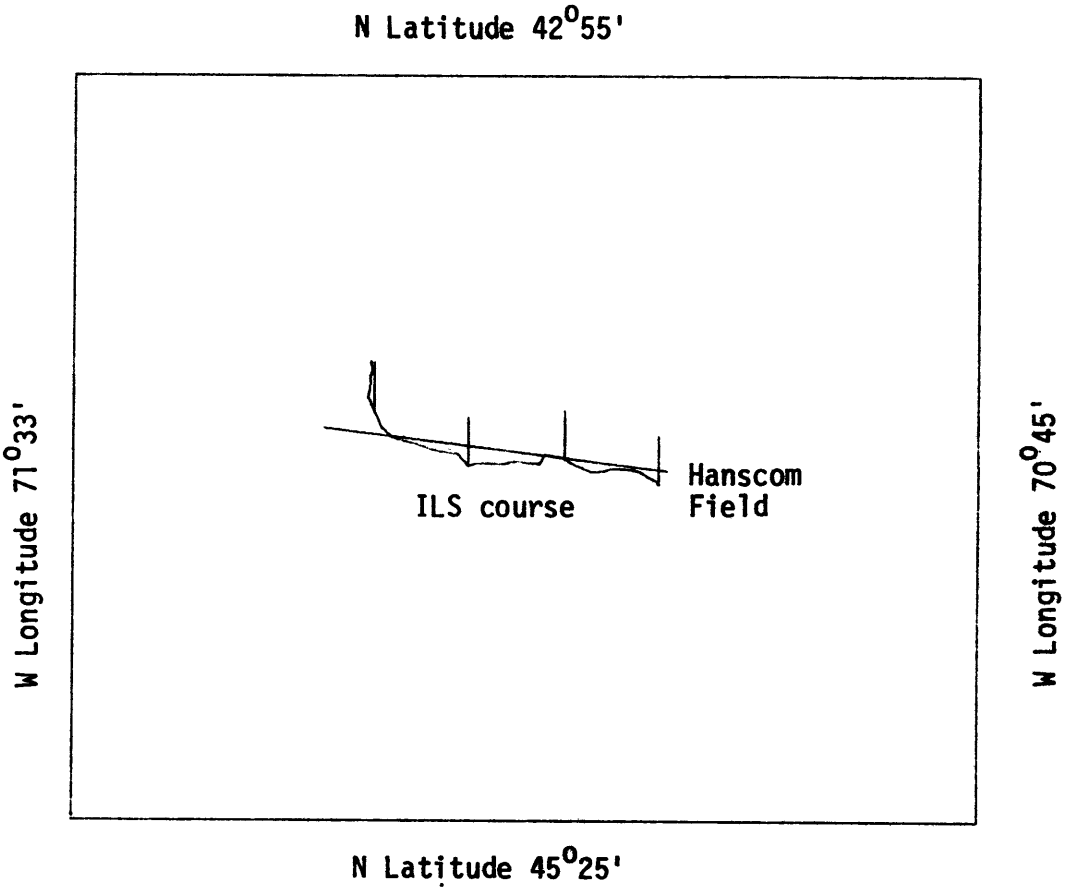


Figure A-23. Approach 3 - 100 Sec. Avg. Filter

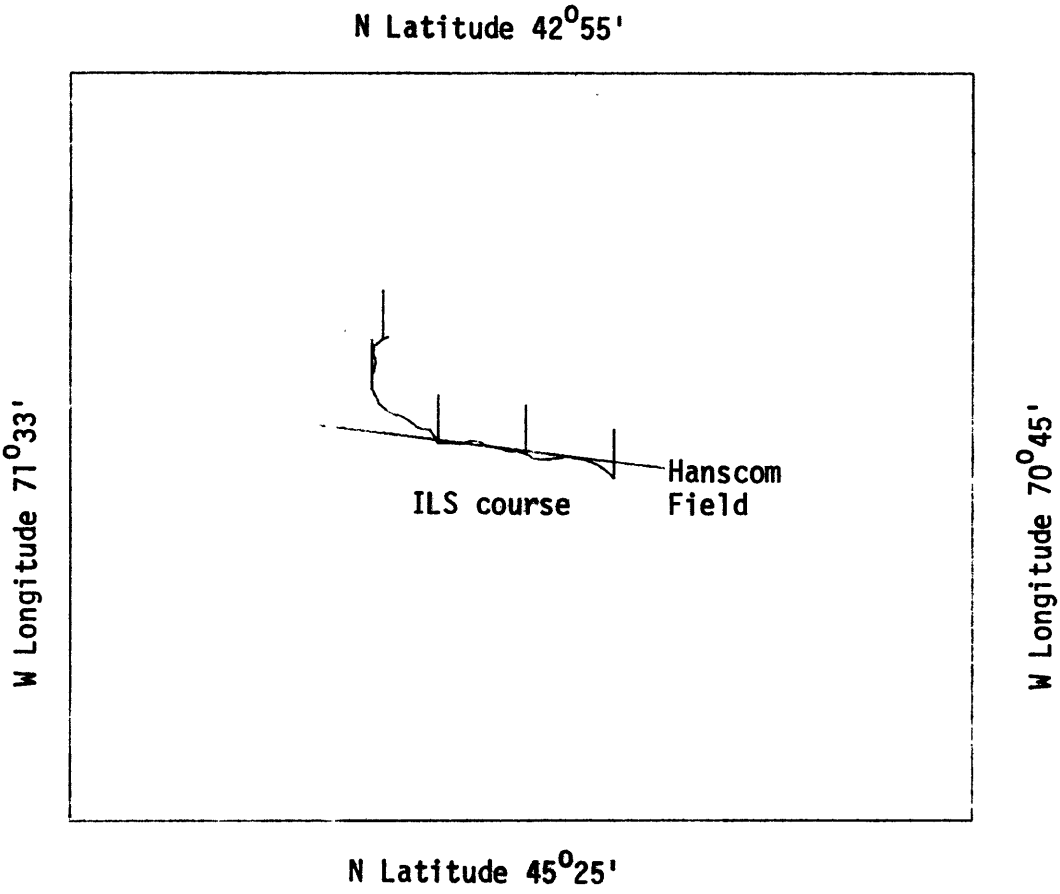


Figure A-24. Approach 3 - 100 Sec. Exp. Filter

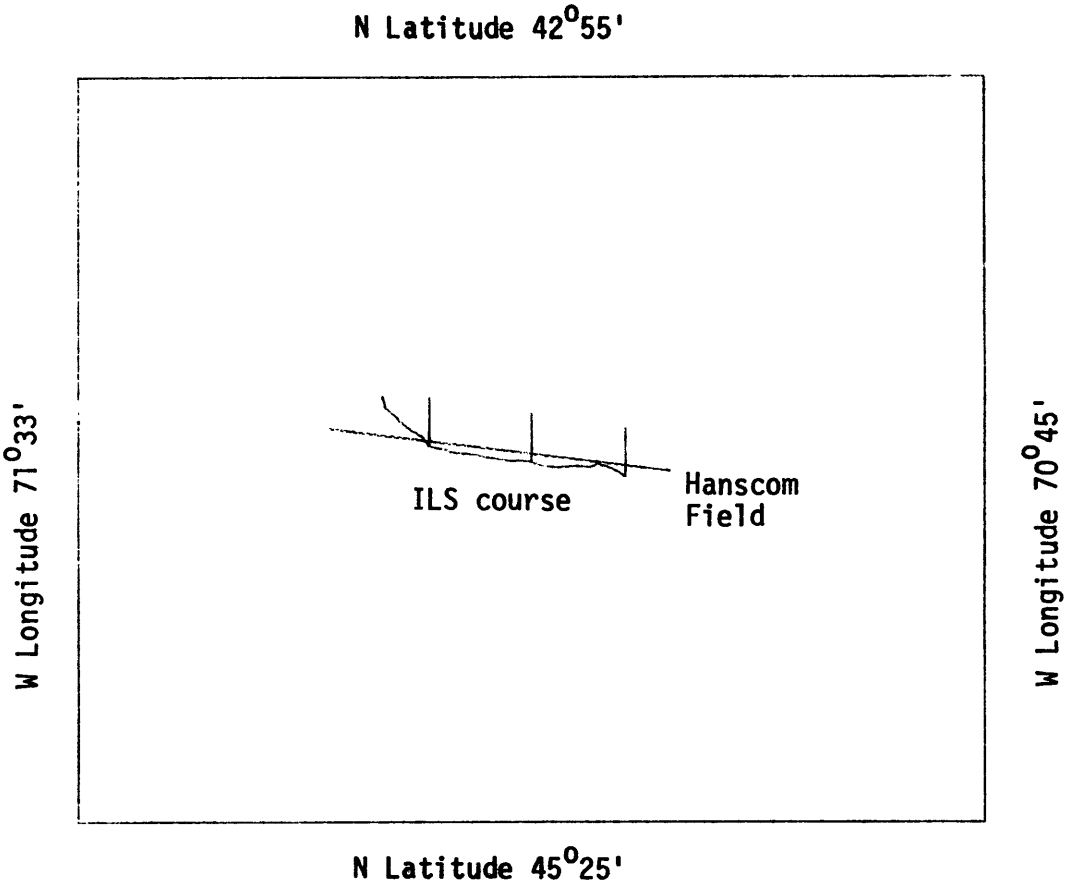


Figure A-25. Approach 3 - 200 Sec. Avg. Filter

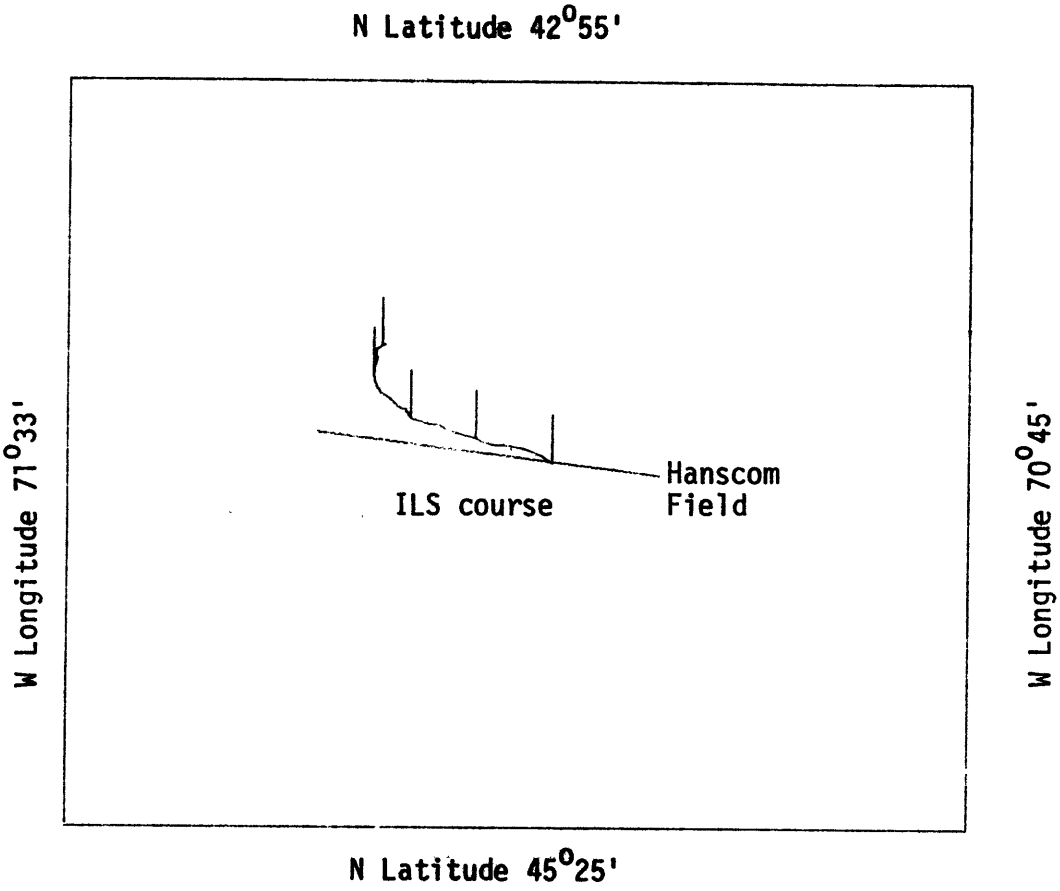


Figure A-26. Approach 3 - 200 Sec. Exp. Filter

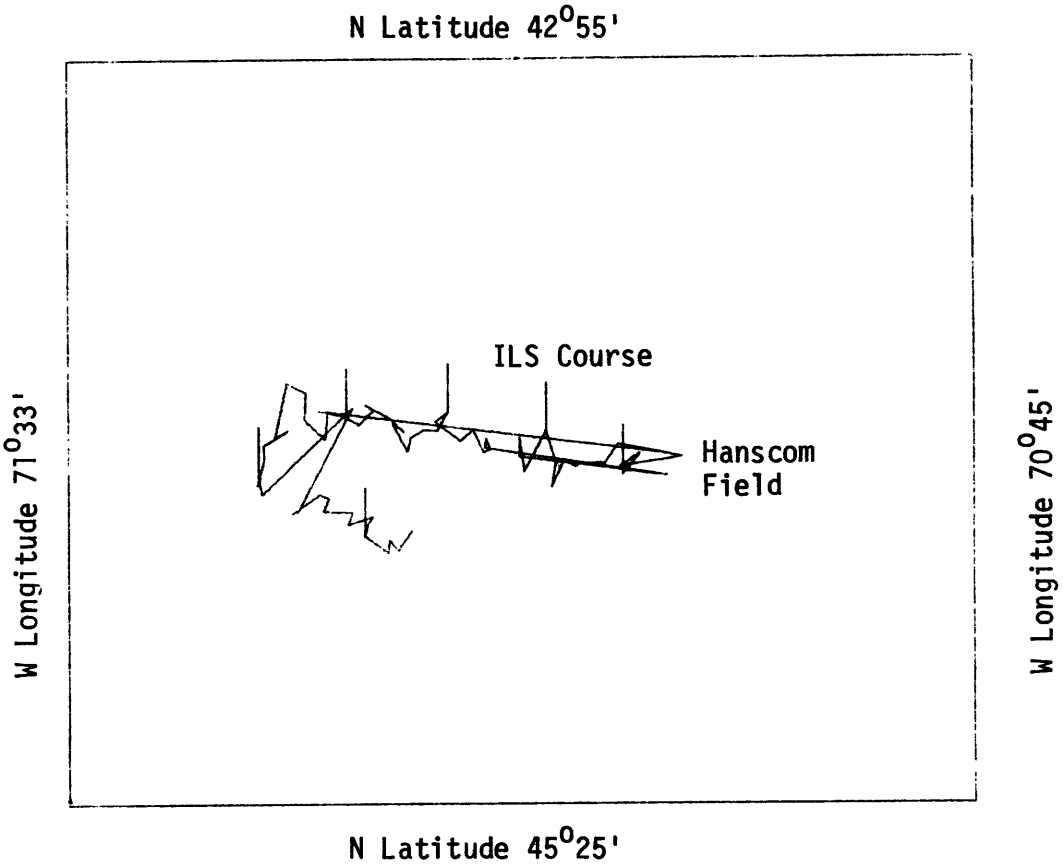


Figure A-27. Approach 4 - No Filter

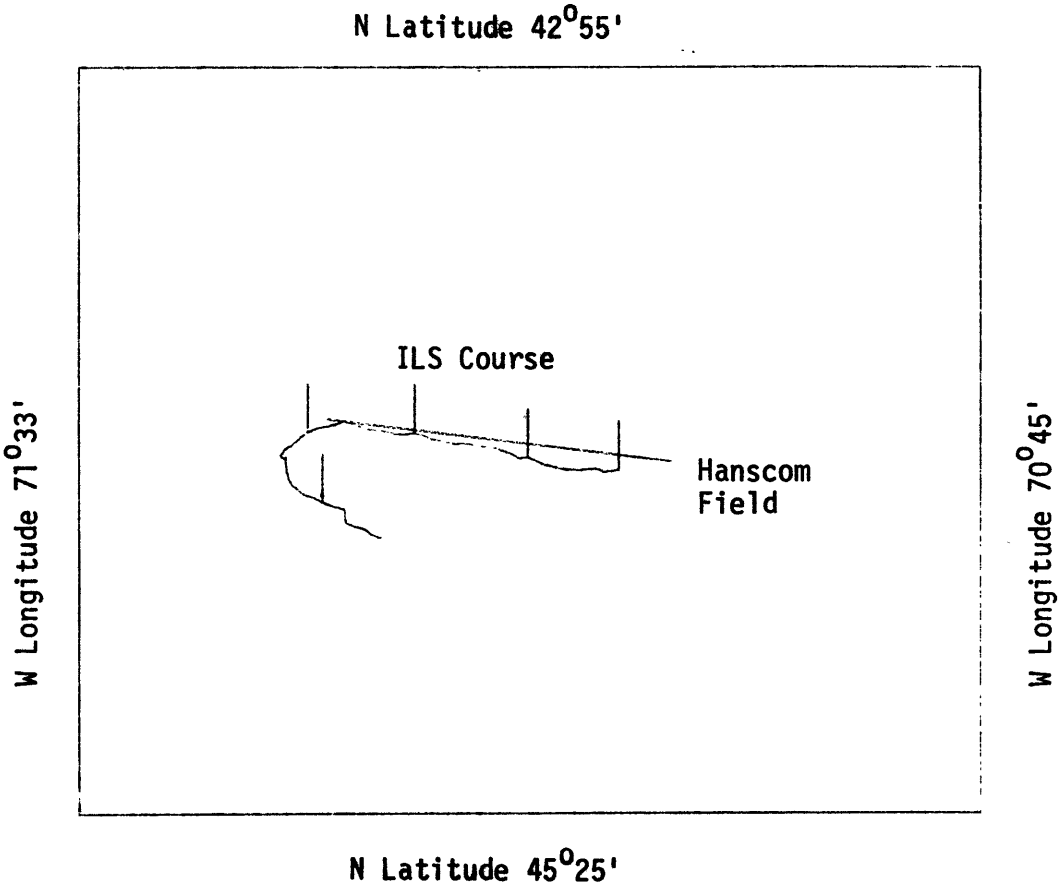


Figure A-28. Approach 4 - 100 Sec. Avg. Filter

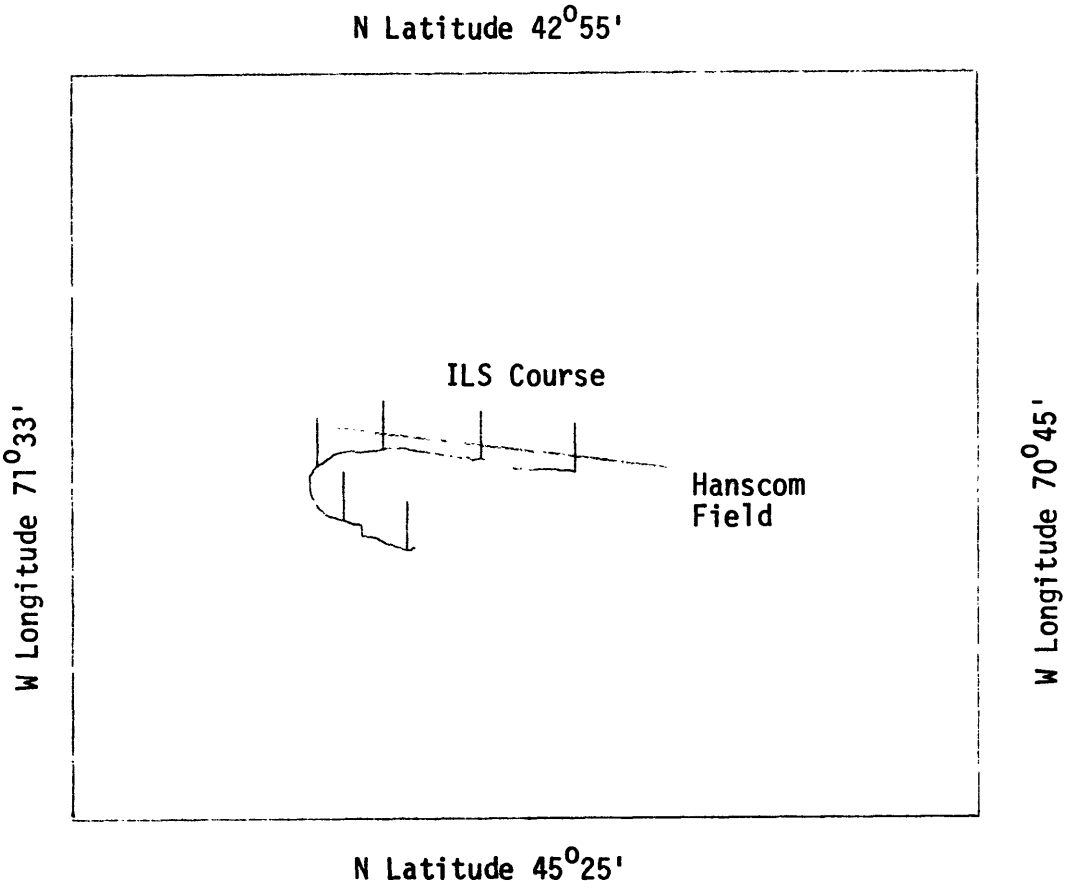


Figure A-29. Approach 4 - 100 Sec. Exp. Filter

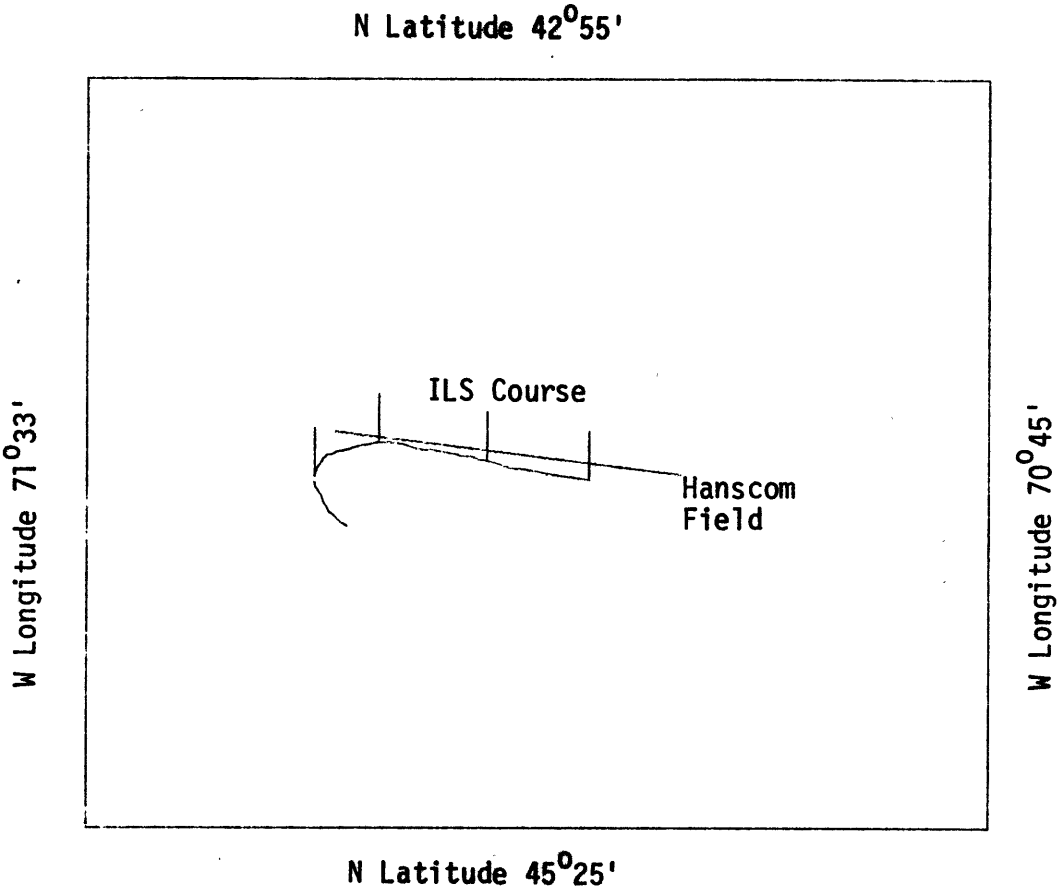


Figure A-30. Approach 4 - 200 Sec. Avg. Filter

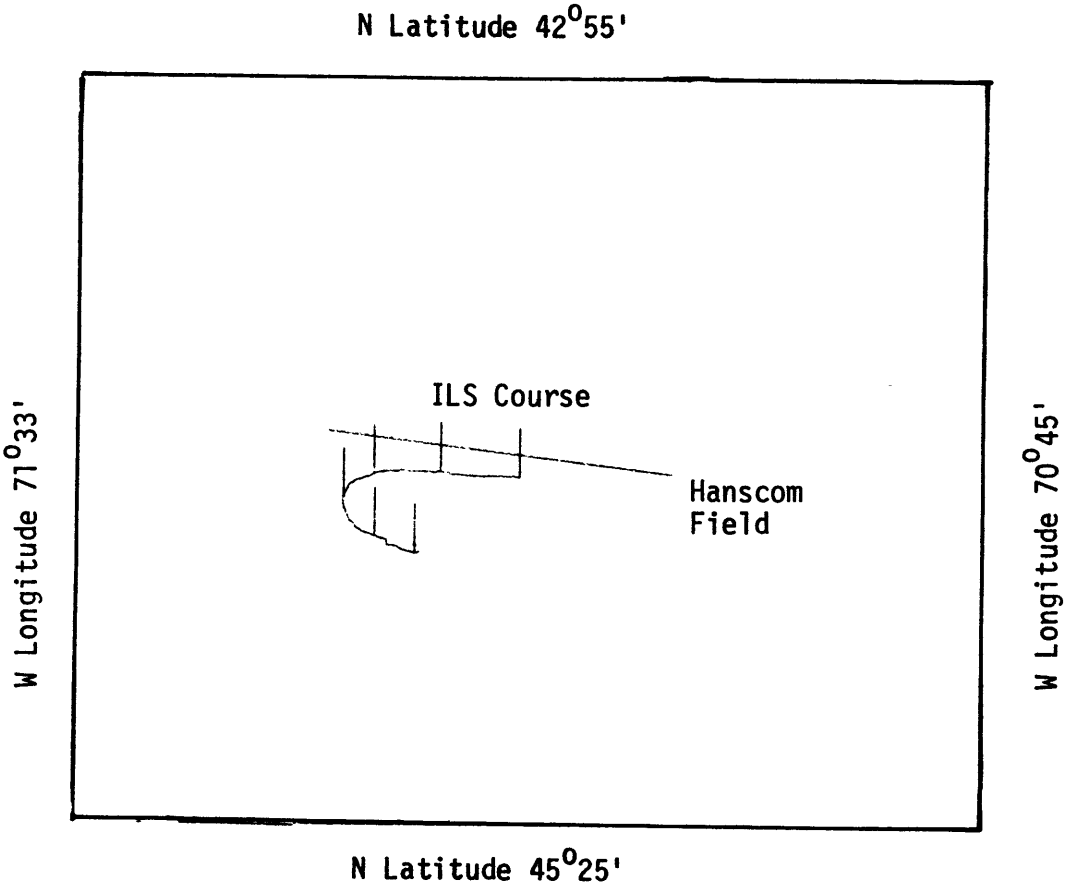


Figure A-31. Approach 4 - 200 Sec. Exp. Filter

# APPENDIX B

## ASI PROGRAM OBJECTIVES AND SCOPE

### B.1 Program Objectives and Scope

The Omega navigation system flight evaluation program consisted of two major parts: Part One, conducted in the Wallops area, and Part Two, conducted in the Northeast Corridor (Boston-New York-Washington). The objectives of each part were slightly different, corresponding to the ultimate application of the information obtained in each of the two geographic areas. The overall objectives for each part were:

- Part One--Wallops Flight Program. Obtain Omega signal and phase data in the Wallops area to provide preliminary technical information and experience in the same geographic area where NASA plans to evaluate the performance of a differential Omega system.
- Part Two--Northeast Corridor Flight Program. Examine Omega operational suitability and performance on the VTOL RNAV routes developed by ASI (10) for city-center to city-center VTOL commercial operations in the Boston-New York-Washington corridor.

The scope of the flight program conducted in each part was consistent with the preliminary nature of the overall effort and with the low-cost emphasis placed upon the project.

#### B.1.1 Part One: Wallops Flight Program Scope

A 30-hour flight program was conducted to obtain preliminary Omega signal and phase data in the Wallops vicinity. The tests provided both quantitative and qualitative Omega technical information and flight experience to be used in preparation of a more comprehensive joint NASA/FAA flight test program to evaluate the performance of a differential Omega system. Factors investigated in Part One were:

- Phase Anomalies Along Coastlines
- Altitude Effects
- Various Station Pair Combinations
- Performance in Flights Parallel and Perpendicular to LOP's
- Diurnal Effects
- Precipitation Effects
- Interference (60 Hz, RFI) Effects
- Influence of Maneuvers (Steep Turns, Spirals, etc.)
- Accuracy (With Radar Tracking)

The routes flown were designed to test Omega performance under the conditions listed above. Several short flights were conducted in the Boston area prior to deployment to the Wallops area to verify operation of the avionics system and recording devices and to review flight duties and procedures. Portions of the Part One flight paths were monitored by the Wallops tracking radar to provide an indication of position accuracies.

B.1.2 Part Two: Northeast Corridor Flight Program Scope

Part Two was a 30-hour flight program designed to examine Omega performance on the low-altitude VTOL RNAV routes developed by ASI in Ref. 10 for the Boston-New York-Washington corridor. The Omega equipment was used to repeat the same Zulu routes that were previously flown with the VOR/DME RNAV equipment. This provided a means for comparison of Omega performance with the previous VOR/DME RNAV results in order to give preliminary operational indications on the suitability of Omega navigation for city-center to city-center commercial VTOL operations. Primary emphasis was placed upon determining suitability and accuracy, but evaluation of signal and phase

information as in Part One was continued. Other factors investigated were:

- Performance at Various Altitudes Over and Near Cities
- Terrain Effects
- Performance During Operational Maneuvers
- Ground Versus Airborne Performance

Because a range instrumentation system was not available over the proposed VTOL test routes, it was not possible to measure the absolute position accuracy of the Omega system. Consequently, accuracy was checked by comparing Omega indications of position with those obtained by visual sightings of known landmarks and/or VOR/DME waypoints.

## B.2 Flight Program Equipment and Facilities

The equipment and facilities used to conduct the Flight Evaluation of Omega navigation included the following:

- Mark III Dynell Navigation System
- Custom Interface Unit (CIU) and Data Recorder
- Voice Recorder
- Wallops Island C-Band Tracking Radar
- Piper Cherokee 180 Aircraft

Each of the above items is described in this section.

### B.2.1 Omega Mark III Navigation System

The Omega avionics system used in the program was the Omega Mark III Navigation System manufactured by the Dynell Electronics Corporation in Melville, NY. This avionics system described in Ref. 11 transforms Omega phase data into crosstrack deviation and miles-to-go displays familiar to

pilots. The system consists of the two units shown in Figure B-1, plus an antenna coupler. The DR-30 Receiver houses the majority of the electronics, and the front panel contains the switches to set the circuits for navigation. The DI-30 indicator provides the readouts used during flight, as well as switches for setting miles-to-go (MTG) and course number (a parameter describing flight course in terms of lines of position). Power requirement is 1 amp at 12 V D.C. An antenna coupler is provided so that the standard ADF sense antenna may be used without affecting other equipment. A functional block diagram for the Mark III set (Receiver and Indicator) is shown in Figure B-2. The basic system specifications are shown in Table B-1.

The range of the navigator in excess of 1,000 miles for a single flight leg, but is unlimited if multiple waypoints are used. Basic system accuracy is independent of length of the flight. Should a course deviation be encountered, simply re-zeroing the CDI will provide the pilot with a new direct course to the original destination. Flight plan changes may be made at any time by inserting the new destination and re-zeroing the CDI. The Mark III System is provided with a standard autopilot output which can be used in the same manner as that from a VOR system.

The receiver unit contains three subsystems. Thse are clock generation and synchronization, phase tracking, and phase data processing to compute crosstrack errors and distance-to-go. These three subsystems are briefly discussed below.

- Clock Generation and Synchronization

  The clock generation subsystem includes a stable oscillator from which the reference signal is derived for the phase tracking

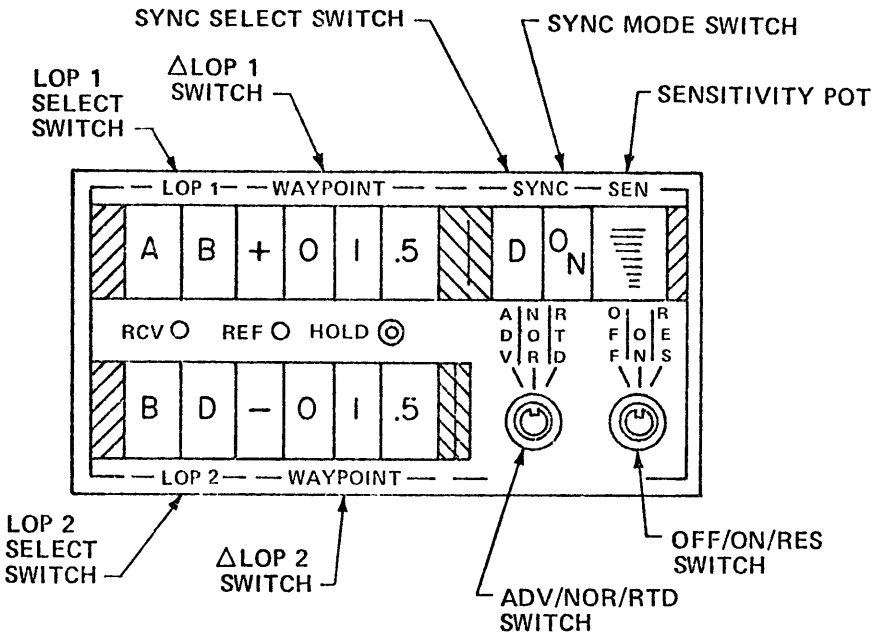


DR-30 RECEIVER UNIT

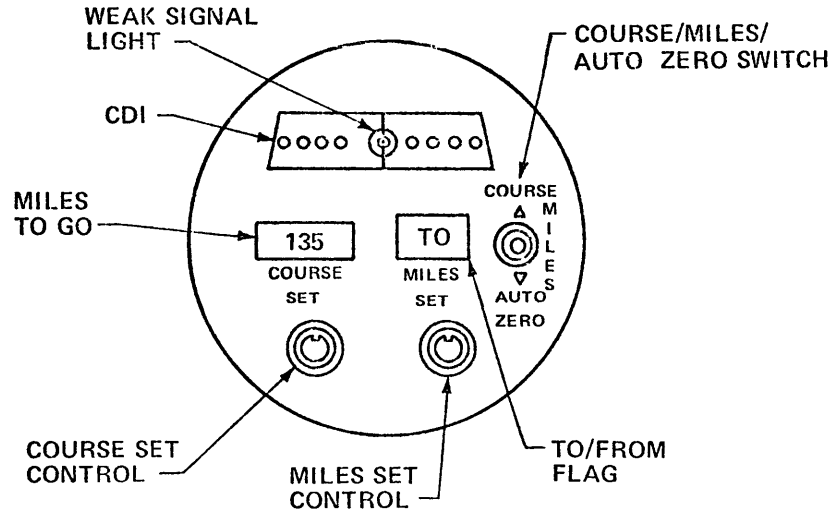


DI-30 INDICATOR UNIT

Figure B-1. Omega Mark III Navigation System Components

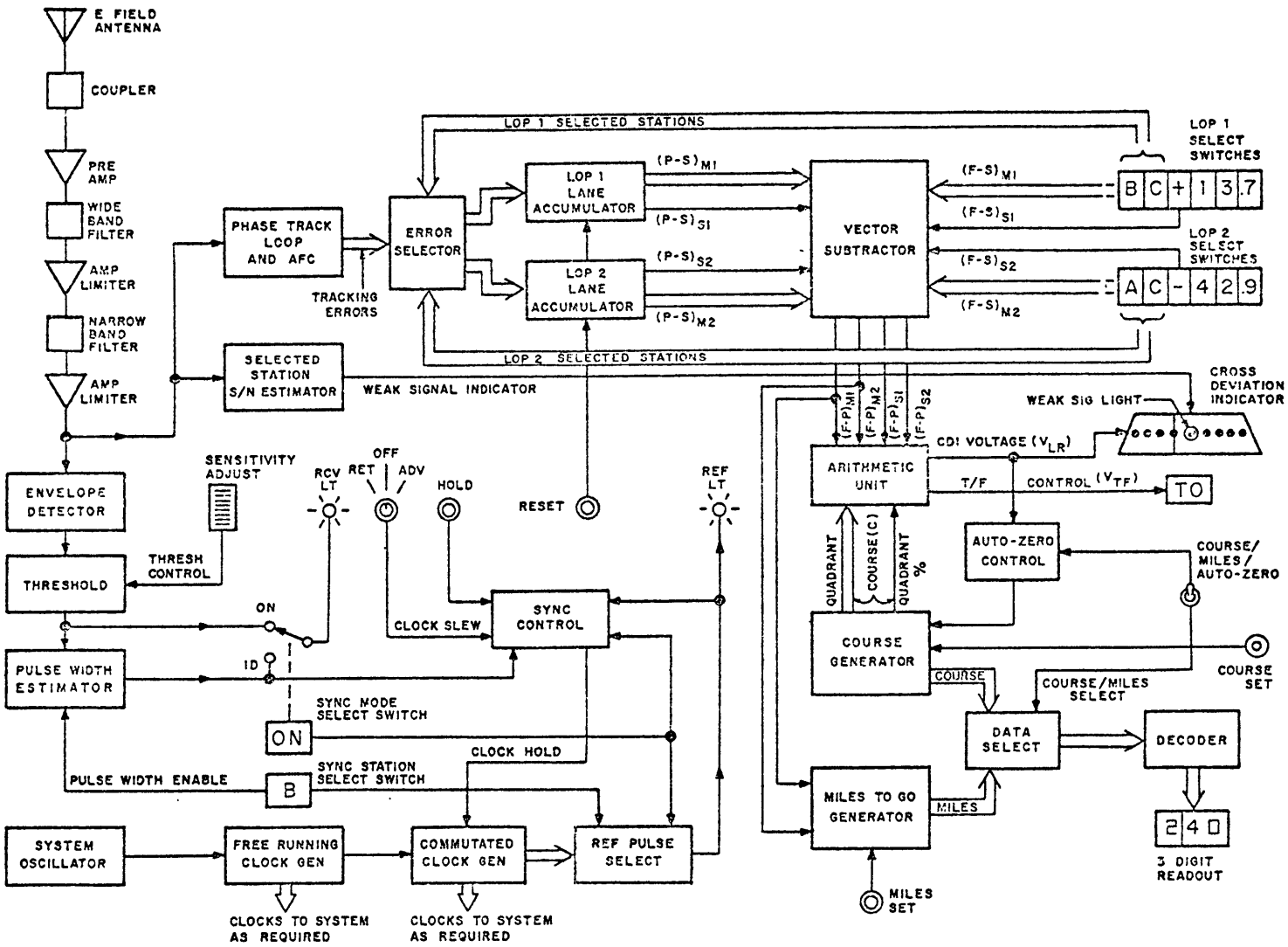


Figure B-2. Mark III Omega Navigation System, Functional Block Diagram

Table B-1. Omega Mark III Navigation System Specifications.

| | |
|---|---|
| Dimensions: | |
| Receiver Unit (DR-30): | 6" W x 3" H x 13" D |
| Indicator Unit (DI-30): | 3.5" Dia. x 5" D |
| Weight: | |
| Receiver Unit: | 4.5 lbs |
| Indicator Unit: | 1.5 lbs |
| Power Requirement: | 12 V DC, 1A |
| Operating Temperature: | -20°C to +60°C |
| Maximum Aircraft Speed: | Approximately 400 knots |
| Navigation Range: | |
| Single Leg Flight: | Approximately 1,000 miles |
| Multi-Waypoint Flight: | Unlimited |
| Navigation Readouts: | |
| CDI: | Sensitivity nominally $\pm$4 miles full-scale |
| Miles-to-Go: | 3-digit display to 999 miles |
| To/From Flag: | Indicates destination arrival |
| On Ground Setup Time: | Approximately 2 minutes with destination number predetermined |

loop and a commutator clock which matches the Omega transmission sequence. Synchronization of the receiver involves the aligning of this commutator clock with the received Omega signals which operate the RCV light on the receiver front panel. The SENSE GAIN pententiometer adjusts the threshold for this light. The REF light is

illuminated by the internal clock gate while the RCV light responds to signals from Omega stations. Manual synchronization is accomplished by depressing the HOLD button on the front panel when the REF light comes on and releasing it when the desired station illuminates the RCV light. The alignment of the two lights can be refined by use of the ADV/RTD (advance/retard) control on the receiver panel. Synchronization is complete when the REF and RCV lights are illuminated simultaneously.

- Phase Tracking

  Once the receiver is synchronized, phase tracking of the 10.2 kHz transmissions from the Omega stations begins automatically. A single tracking loop is time multiplexed between stations used. By the use of this single loop, differential instrumentation errors between stations are eliminated and the tracking system error is reduced. Auxiliary features include an AFC loop to correct small errors in the system master oscillator and an S/N (signal-to-noise) ratio estimator. The S/N ratio estimator is thresholded to drive a warning light if the S/N ratio of a station selected for navigation is insufficient.

- Position Calculation

  The position calculator circuitry is essentially a special-purpose computer which calculates various parameters based upon position vectors in the Omega coordinate system whose origin is the position of the receiver when last reset (usually at the start of the flight). The present position of the aircraft is computed from

the outputs of the phase tracking loops and is stored as a vector from the origin to the aircraft position. The position of the desired waypoint is supplied to the computer as a vector from the origin to that waypoint. The crosstrack component of this vector is displayed on the CDI, and the length of this vector is scaled and displayed on the miles-to-go readout. By flying to keep the CDI centered, a great circle path from the present position to the desired waypoint is achieved.

The particular Omega Mark III Navigation set used in this flight evaluation was originally procured by MIT in 1974 under a NASA-sponored research grant to investigate Omega for general aviation aircraft. For the ASI program the Omega receiver was hard mounted in the test aircraft to facilitate operation of the unit and to decrease the number of separate test items in the aircraft. It was fixed under the instrument panel on the right side of the aircraft, easily accessible to the co-pilot/Omega operator. The indicator was installed in a spare opening in the instrument panel among the flight instruments directly in front of the pilot.

The antenna coupler was mounted behind the instrument panel near the ADF. The lead from the existing ADF sense antenna was connected to the coupler, which supplied signals to both the ADF and the Omega receiver, but kept the two electrically isolated. Proper grounding of the sense antenna was necessary for good performance of the Omega receiver. Power for the Omega receiver was supplied by the aircraft 12-volt electrical system.

Operation of the Mark III was straightforward in that two pairs of Omega stations were chosen and selected on the front panel thumbwheels. The

differences between the first waypoint (or destination) and the starting point in terms of changes in "lanes" (LOP's) generated by the selected station pairs were acquired from a table and entered using the other thumbwheels. The receiver was synchronized, the CDI (Course Deviation Indicator) zeroed, and the miles-to-go counter set to the known distance from the starting point to the first waypoint. The receiver then displayed cross-track deviation and miles-to-go during the flight, along with a to/from flag and a weak signal light which warned of excessively low signal-to-noise (S/N) ratios.

B.2.2 Custom Unit (CIU) and Data Recorder

The custom interface unit (CIU) was fabricated by Dynell Electronics to assist data recording and reduction. The unit was portable to facilitate its use in two separate functions: in the air, for converting (digital) parameters from the receiver to frequency-shift-keyed (FSK) signals for recording on a standard cassette tape recorder; and on the ground, for demodulating the FSK signal to standard teletype format (R232C) for post flight computer processing of data. A functional diagram of the airborne equipment used in the flight program is shown in Figure B-3. The CIU received power from the Omega receiver, and it supplied power to the data recorder.

The CIU is housed in an aluminum box approximately 3.25" x 14" x 10". On the front of the box are switches for power on/off, circuit enable/disable, and operator discrete code select. In addition, there are three fuses on the front panel. On the back panel are two input plugs, wired in parallel, and four BNC plugs: to tape recorder, from tape recorder, 6V power output, and teletype output. Internally, the circuitry consists of

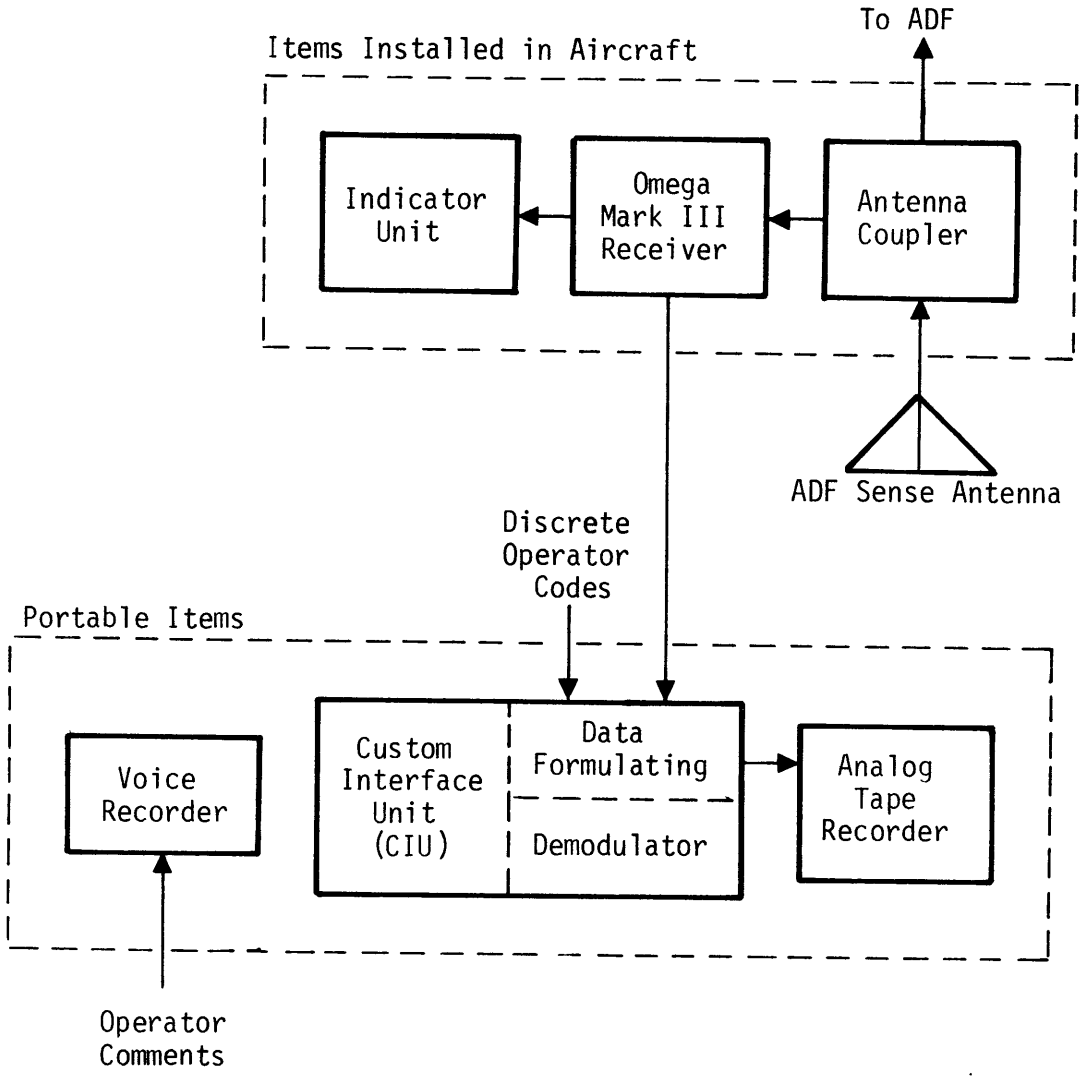


Figure B-3. Airborne Equipment Functional Diagram.

CMOS integrated circuits on a wire wrap board, with power supply components mounted separately.

The Mark III Omega receiver was modified to supply the following parameters to the CIU after each 10-second Omega cycle:

- LOP 1: Present position relative to origin
- LOP 2: Present position relative to origin

- Crosstrack deviation
- Miles-to-go readout
- Signal-to-noise ratio of each station (8)
- Weak signal indicator
- Auto-zero activation
- Reset indication
- To-from flag indication
- Operator discrete code selection.

These parameters are all present inside the Mark III in digital form, and no A/D conversion is required. (The analog CDI is driven by a D/A converter.)

The various parameters, timing signals, and DC power are fed to the CIU by a cable connected to the Mark III. The timing signals select which parameter or part of a parameter is put onto an internal data bus which feeds the FSK converter. The CIU output is routed to the microphone input of a portable cassette recorder.

Unlike the Omega receiver itself, the CIU was not hard-mounted in the aircraft. Instead, it usually was placed on the back seat or on the floor of the aircraft. When data was to be recorded, the unit was turned on and the enable/disable switch was placed in the "disable" position. This caused a high frequency tone to be written on the cassette tape as a "header." After approximately 30 second, the switch was placed in the "enable" position, allowing data to be written on the tape.

One difficulty encountered with the CIU was the failure of the chip supplying the four most significant bits of the fractional part of the LOP 1 lane accumulator. This failure was detected after the first set of flights

at Wallops. Since the chip was temporarily unavailable locally, it was replaced by the chip supplying the least significant four bits of the fractional part of LOP 1, leaving an empty socket on the board. This caused the least significant LOP byte to be duplicated in the data string as the preceding signal-to-noise ratio byte. This known error was not judged significant as the maximum error this could induce was less than 0.0625 lanes, much smaller than the observed noise in the LOP counters.

B.2.3 Voice Recorder

A portable battery powered cassette recorder was used for recording inflight notes. The recorder had several attributes making it extremely useful for this purpose: small size, no external power requirements, and easy control. The small size of the recorder allowed it to be placed under the co-pilot/Omega operator's seat. Because no external power was required, there were no superfluous wires to be attached and checked before flight. With the primary recorder controls preset, the recorder was started and stopped using a remote switch on the microphone. The tape recorder was activated only when recording was desired so voice records were sequential on the tapes with no intervening dead time. This provided tape economy and freed the operator from inflight tape changing requirements on this recorder.

B.2.4 Wallops FPS-16 Tracking Radar and Transponder

Four of the first set of flights at Wallops (Flights 1-1, 1-3, 1-8, 1-9), were tracked by the Wallops FPS-16 tracking radar. For this purpose, a C-band transponder was installed in the test aircraft. The transponder was supplied by NASA and consisted of a battery pack, an antenna, and the

transponder itself. The battery pack was carried in the luggage compartment of the test aircraft and supplied power to the transponder. The transponder antenna was hard-mounted on the underside of the aft fuselage of the test aircraft. Due to short battery life, the transponder was normally used only for radar identification of the test aircraft. After the aircraft was identified, tracking was accomplished by skin traking.

The tracking provided real time plot board tracks of each flight and reduced digital readouts. These data were to be processed with the Omega receiver estimates of position in order to generate comprehensive statistics on Omega accuracy. However, with the above mentioned failure of a CIU chip, the Omega position readouts were not available (see Section B.2.2).

B.2.5 Piper Cherokee 180 Aircraft

The 60-hour ASI flight evaluation program was conducted in a leased Piper Chrokee 180 aircraft based at Hanscom Field, Bedford, Massachusetts. This is the same aircraft used previously by MIT to conduct the NASA-sponsored research program to investigate Omega navigation for general aviation. The Cherokee is a four-place general aviation aircraft powered by a 180 HP Lycoming engine. The electrical system includes a 60-amp alternator and a 12-volt, 25-amp battery. The aircraft has a standard instrument panel and avionics including dual VHF transceivers, automatic direction finder, glideslope receiver, transponder, single-axis autopilot and the Omega Mark III Navigation System used in the flight evaluation. The aircraft specifications and performance details are presented in Table B-2.

B.3 Flight Program Procedures

This section describes the planning and procedures used in the Omega flight evaluation program. The importance of safety in flight operations

Table B-2. Piper Cherokee Dimensions and Performance Characteristics

| | |
|---|---|
| Dimensions, External: | |
| Wing span | 30 ft 0 in |
| Length overall | 23 ft 6 in |
| Height overall | 7 ft 3½ in |
| Weights and Loadings: | |
| Weight empty | 1,330 lb |
| Max gross weight | 2,400 lb |
| Performance: | |
| Max level speed at S/L: | 132 knots |
| Max cruising speed (75% power) at 7,000 ft (2,130 m): | 124 knots |
| Stalling speed, flaps down: | 50 knots |
| Rate of climb at S/L: | 750 ft/min |
| Service ceiling: | 13,000 ft |
| Range (75% power at 7,000 ft): | 629 nm |

was stressed throughout the program, and all operations were conducted in accordance with the ASI Flight Safety and Procedures Handbook. Flight objectives were secondary to considerations of flight safety. The following subsections include brief discussions of flight planning and check lists, data recording procedures, and navigational techniques employed.

B.3.1 Flight Planning and Check Lists

Extensive flight planning was conducted throughout the program to take maximum advantage of each flight hour. This planning ranged from the broader aspects that included standardization of documentation, formats, proced-

ures and check lists for the flight program to the detailed aspects that involved determination of specific flight paths, airspeeds, altitudes, etc., for each flight.

B.3.1.1 Flight Planning Documents

For each flight, a standardized information packet was made for each flight crew member. This packet included a Flight Evaluation Sheet, a Flight Plan, and a flight map.

The flight evaluation sheet, shown in Figure B-4, was designed to provide identification of and general information about the flight. The flight number and objectives were supplied at the top of the sheet, with operational data in the box at the center of the page. Operational data includes such parameters as time and date, a general description of flight route and duration, participants, and summary weather information. On the bottom of the sheet were data recording requirements, contingency plans, and special requirements. These three provided information to make a go/no-go decision based upon flight test objectives.

The flight plan is shown in Figure B-5. This sheet was in a format standard for pilot usage and completely specified the test flight profile. Distances, headings, times, and Omega receiver settings were all included. In addition, Omega receiver settings for additional LOP selections were included so that station outage would not require termination of data collection.

A map of the proposed flight (Figure B-6) was included in the flight test packet with the desired flight path marked. This provided a quick-look at the desired profile and was helpful in aircraft orientation on the charts

Flight No.: 1-20 Test Description

Test Objective: Provide S/N data in the vicinity of SWL VOR enroute to WAL, and along power lines.

| Item | Planned | Actual |
|---|---|---|
| Date | 3-6-75 | 3-7-75 |
| Departure | 1 p.m. | 1:55 p.m. |
| Duration | .4 | .6 |
| Area/Route | SBY-WAL | Same |
| Pilot | W. C. Hoffman | Same |
| Omega Operator | P. V. Hwoschinsky | Same |
| Other Participants | J. D. Howell | Same |
| Weather | VFR | Same |
| Winds at Cruise | 10 N | 10 S |

Data Recording Procedures: CIU on tape.
Voice tape log.

Contingency Plans: Non precision approach to WAL if IFR.
If Omega or CIU inoperative, pick up radar plots, return SBY.

Special Requirements: Above minimums for WAL approach.

Figure B-4. Sample Flight Evaluation Sheet.

FLIGHT NO.: 1-20 DATE: 3/7/75

| CHECK-POINT | HDG CN / MH | ΔLOP STATION A-B | ΔLOP STATION A-D | LEG DIST / GROUND SPD | TIME PT-PT | TIME ETA |
|---|---|---|---|---|---|---|
| | | B-D | B-C | | ALT | ATA |
| 0 | | 0 | | | | |
| SBY | | 0 | | | | |
| 1 | 096 | +1.8 | +0.2 | 18 | 9 | |
| SWL | 181 | -1.8 | -1.4 | | 1500 | |
| 2 | 086 | +2.6 | +0.4 | 8 | 4 | |
| WAL | 193 | -2.4 | -1.9 | | 1500 | |
| | | | | | | |
| | | | | | | |
| | | | | | | |
| | | | | | | |
| | | | | | | |
| | | | | | | |
| | | | | | | |
| | | | | | | |
| | | | | | | |
| | | | | | | |
| | | | | | | |
| | | | | | | |

Figure B-5. Omega Flight Plan.

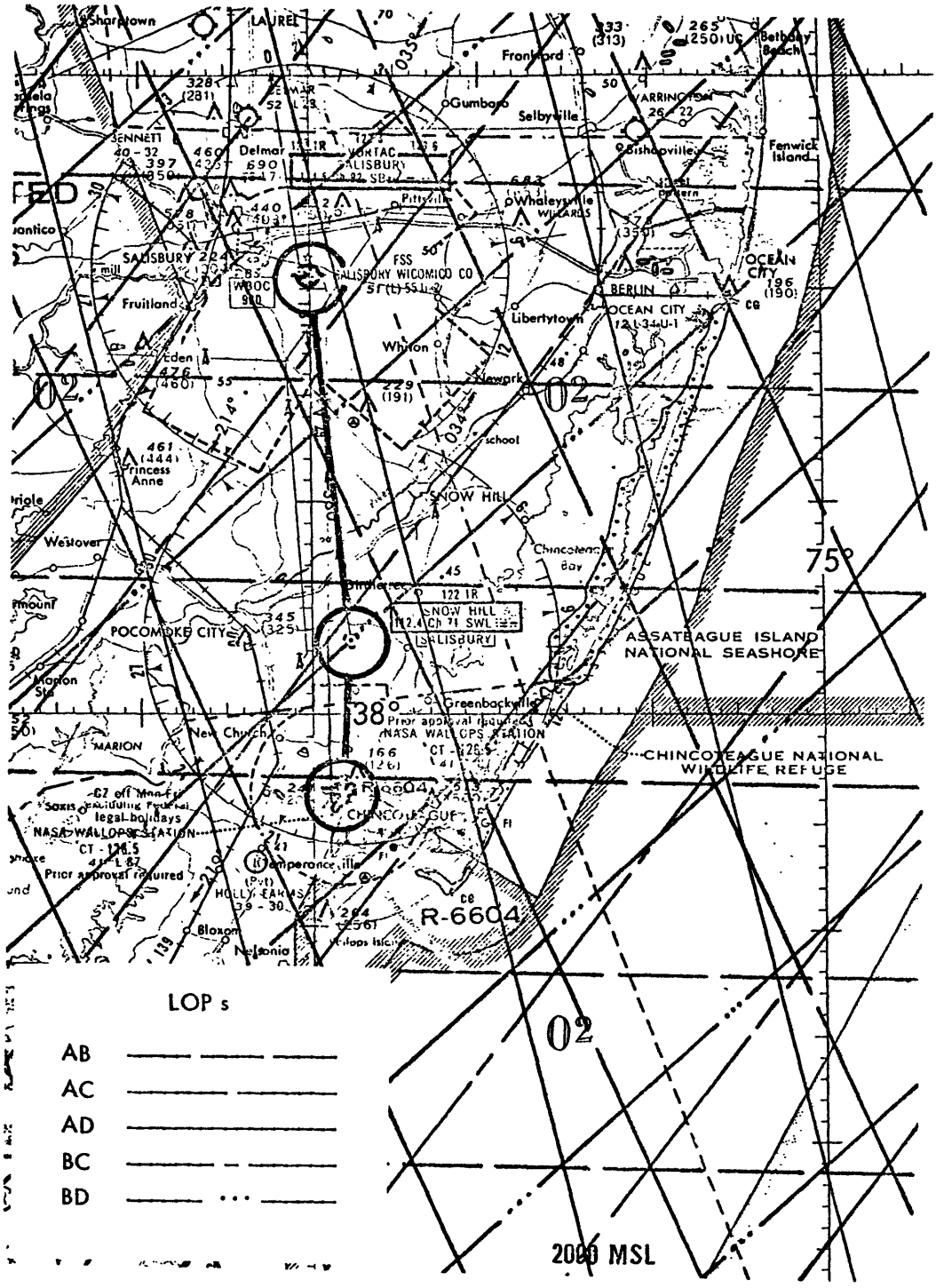


Figure B-6. Sample Flight Map.

actually used for navigation. In addition, it provided a convenient chart for clipboard use by observers.

B.3.1.2 Check Lists

A complete set of operational check lists was made to reduce errors in the flight program. The check lists are largely self-explanatory and are included as Figures B-7 through B-15.

B.3.2 Data Recording

Data were recorded in the aircraft on two airborne tape recorders and on maps. Ground data consisted of FPS-16 radar tracking at Wallops Island when available. Tape recorded data included the digital output of the CIU and voice records. Map records and radar data were used for position plotting.

B.3.2.1 Omega Data

As described in Section B.2.2, various Omega receiver parameters were recorded on a portable cassette recorder. During data reduction, it was discovered that the Omega/CIU/recorder system also recorded transmissions from the aircraft VHF transceivers. Most Omega data flights were made with the radios off, however, and very few transmissions were made on flights with the radios on. Thus, little data was lost.

Tapes used for the recording were standard audio quality tapes. Because of memory limitations in the processor, the standard tape length was 30 minutes per side. However, some recordings were made on 45-minute tapes, which were processed in two parts. Performance of standard tapes was adequate, and there was no requirement for any high fidelity tapes, such as $CrO_2$

1. Aircraft Keys
2. Standard Instrument Charts
3. Clipboard and Data Forms
4. Flight Plans and Charts
5. Custom Interface Unit
6. Two Tape Recorders Plus Cassettes
7. Connecting Cables
8. MIC and PWR Cable
9. Clip Leads; Masking Tape

Figure B-7. Flight Equipment Check List

1. Connect BNC-Mini cable from TO REC on CIU to MIC on recorder.
2. Connect BNC-Power cable from PWR on CIU to 6V on recorder.
3. Recorder Volume - set at 3.
4. 50 pin harness from receiver - plugged into either 50 pin socket.
5. Front PWR switch - up for DC power.
6. Enable/Disable switch - DISABLE for count of 5 on tape counter; then ENABLE.
7. Event Marker - initialize.
8. Note completion of this checklist on voice tape recorder.

Figure B-8. CIU Setup Checklist

1. T/B circuit breaker - OFF.
2. A/C master - ON.
3. PWR - ON.
4. SYNC sw - ON.
5. Adj SENS as required.
6. Chk format; record sta strength Str, Mod, Wk on voice tape.

Figure B-9. Omega Turn On Check List

AUTO SYNC

1. SYNC sw-ID.
2. SYNC-select D (or other).
3. Depress HOLD momentarily.
4. SYNC when REF light on and off (w/in 30 sec).
5. SYNC sw-ON.
6. Check sync.

MANUAL SYNC

1. SYNC sw-ON.
2. SYNC select-D (or other).
3. Depress HOLD when REF light goes off.
4. Release HOLD when proper RCV light goes off.
5. Adj ADV/RTD sw.
6. Insert LOP letters.
7. Insert LOP numbers for WPT.
8. Reset lane accumulators.
9. Display MTG, flag on FROM.
10. Adj MILES SET for distance.

Figure B-10. Receiver Synchronization Check Lists.

START ENGINE

1. T/B circuit breaker-ON.

TAXI

1. Check sync (SYN sw ON).
2. Check weak signal light no flashing.
3. Reset vector at airport ref. pt. during E through H slots.
4. Start DATA tape recorder.
5. Record completion on voice tape.

Figure B-11. Ground Operations Check List.

AFTER TAKEOFF

1. Auto zero indicator during E through H slots.
2. Verify course number.
3. Check CDI centered.
4. Record on voice tape.

AT WAYPOINT

1. Set in new LOP numbers from reset point.
2. Auto zero ind. on E through H slots.
3. Adjust distance scaler.
4. Record on voice tape.

Figure B-12. Inflight Operations Check Lists

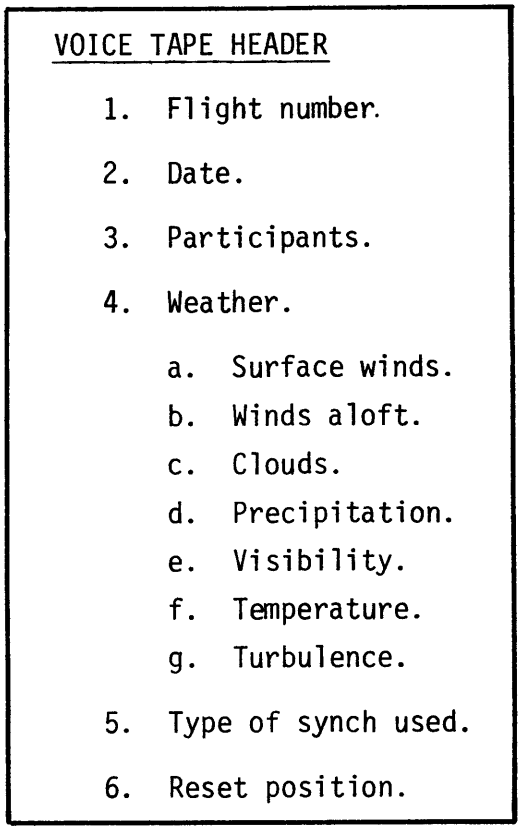


Figure B-13. Voice Recorder Check List for Initial Record on Tape.

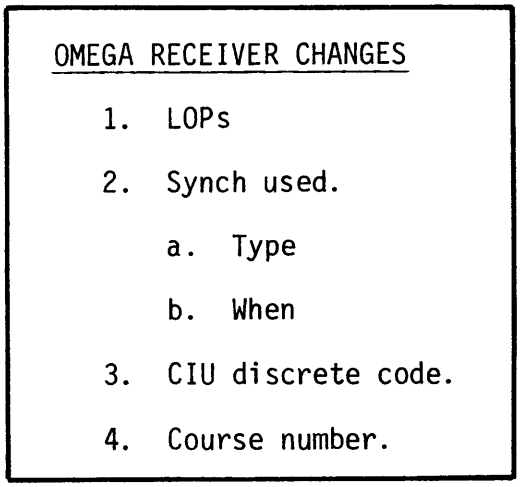


Figure B-14. Voice Recorder Check List for Receiver Setting Changes.

1. Time.
2. Actual position.
3. Altitude (MSL).
4. CIU discrete code.
5. Waypoint in use.
6. Course number.
7. CDI.
8. MTG.
9. Weather.

Figure B-15. Voice Recorder Check List: General.

tapes, or high fidelity recorders incorporating high-frequency noise reduction circuitry.

Time synchronization on the Omega data tapes was achieved by setting a new operator discrete code on the CIU at a known time. With this reference, the times of both previous and subsequent data strings could be determined, unless severely garbled data intervened. Few such problems were encountered.

B.3.2.2 Voice Recorder

During the flight evaluation program, pertinent information was verbally recorded on a cassette recorder. This provided the capability to process data later with extensive and complete notes of the events of the flight. The voice recorder was usually operated by the Omega receiver operator.

Figure B-16 shows a pocket size check list used for tape recorder operation. The first section was used to insure that the recorder itself was operating, and the second section of the check list was used to insure that entries on the tape were complete and appropriate. It was standard procedure for the person making the voice recording to do his own transcription. When this was done shortly after a flight, it was often possible to recall more

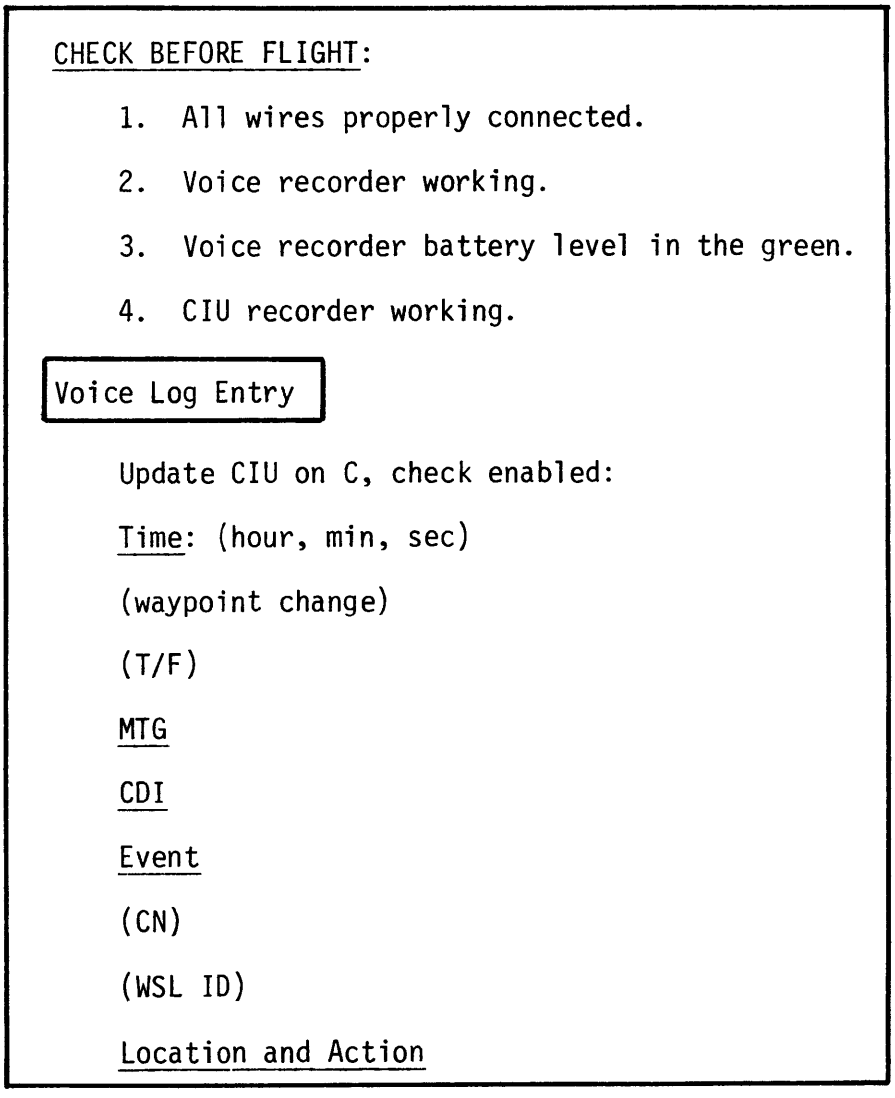


Figure B-16. Pocket Size Check List for Voice Recorder.

information than was recorded on the tape. A sample transcript is shown in Figure B-17.

Standard length audio cassettes were used in the recorder. With the microphone switch described in Section B-2.3, it was possible to record many flights on one side of the cassette. The time compression of the flights facilitated later transcription because it was not necessary to search the tape for voice records. A special tape recorder designed for transcription was used to play back the cassettes.

### B.3.3 Navigation Techniques

A variety of different navigation techniques were employed during the flight program so that comparisons could be made with a wide range of other test data and to assure reliability of measured accuracy. In both the Wallops area and the Northeast Corridor, all the tested forms of navigation were used in different flights over the same regions to provide corraborative data. The most common technique was navigation using Omega with visual position checks for confirmation. Occasionally, this was reversed by flying visually and recording Omega position information. Additinally, VOR radials and ILS localizers were used for navigation with the Omega position recorded for comparison. Finally, Omega routes were flown under radar tracking, with the radar position information supplied later for comparison.

#### B.3.3.1 Visual Navigation

The visual navigation mode consisted of contact flying with voice reports at regular intervals recording actual position relative to known landmarks. This information was then reduced with CIU supplied information for verification and comparison with the Omega indication of position.

OMEGA FLIGHT O-2Z-1 NOTES (December 20, 1974)

Route Z1 NYC-BOS (with Farmingdale and Bedford connectors)

| TIME | DISCRETE CODE | LOCATION | DESCRIPTION |
|---|---|---|---|
| 3:30 | 0 | T-O roll FRG | Weak A and weak BC, strong D |
| 3:35 | | 1 mi E FRG | Switched on tape, CDI centered MTG 11 CN 489 |
| 3:36 | | | Enable CIU |
| 3:37 | 1 | 3 NNE FRG | On direct course for WPT 2 CDI 3½ L MTG 11 ALT 5500 |
| 3:41 | 2 | | Jiggled tape, drive was erratic |
| 3:43 | 3 | WPT 2 | Set in WPT 3 |
| 3:45 | | | CDI 4½ L MTG 38 counting down |
| 3:53 | 4 | Bridgeport Apt. | CDI 3L MTG 16 |
| 3:58 | 5 | 35 N. Haven Apt. | CDI ½R MTG 2 "FROM" |
| 4:05 | 6 | Griswold Apt. (WPT 3) | CDI 1R MTG 7 "FROM" Good ABCD signals, set in WPT 4 |
| 4:15 | 7 | 4 lane Hwy | CDI ½R MTG 24 |
| 4:18 | 8 | 3 W Norwich, Hwy | CDI centered MTG 18 Switched tape sides |
| 4:20 | 9 | | Enabled CIU |
| 4:25 | 10 | Moosup, WPT 4 | CDI centered MTG 8 |
| 4:30 | 11 | S. of Lake 7 mi @ 166° from PUT | (41°50'/71°45'W) CDI centered MTG 0 "TO" → "FR" PUT 166° PVD 040° |
| 4:35 | 12 | 5W Woonsocket | PVD-WOS HWY PUT 071° CDI 2R MTG 10 |

Figure B-17. Sample Voice Transcript.

Examples of flight segments where visual navigation was the preferred mode included: flying under the New York TCA along the Hudson River, flying along a straight section of railroad on the Delmarva peninsula, and crossing expanses of water at low altitude. The main advantage of contact flying was the ability to navigate without the VOR receivers on, which was the major source of intereference for the Omega receiver.

B.3.3.2 VOR/ILS Navigation

Many flights were conducted using VOR as the primary navigation source, with the Omega recorded position used for comparison with a known ground track. In the Northeast Corridor, VOR was used for enroute navigation; and in the Wallops area, VOR was used to provide navigation for flying precise patterns in the Snow Hill area. Omega was used to navigate the aircraft to an ILS approach path, and Omega was monitored during the approach.

On most of the Northeast Corridor flights, the Omega receiver was used as the primary navigation source. However, IFR operations and some Boston area local flights used VOR for primary navigation, and the position recorded by the Omega set was analyzed for comparison.

At Wallops, the Snow Hill VOR was used for primary navigation on many flights. The VOR was used to define radials along which the aircraft was flown. By comparing the Omega indicated position to the known path, anomalies were revealed, and navigation information was provided through areas where Omega interference was suspected.

ILS paths were followed on flights 2-11 and 1-24. On these flights, the Omega set was adjusted to correspond to the ILS readout, but the ILS was used

for primary navigation. Again, the Omega position was later compared with the assumed aircraft path.

B.3.3.3 Omega Navigation

On many flights, including most of the Northeast Corridor flights, the aircraft was flown using the Omega receiver as the primary navigation device. This provided data on how well the pilot was able to follow the Omega generated needle deflections, and also gave data on pilot reactions to the needle and required techniques. Position reports were entered on the voice tape for statistical analysis of the errors. One major advantage of this mode of navigation was that it allowed the major noise source in the flight evaluation program, the aircraft VHF radios, to be turned off.

B.4 Post-Flight Data Processing

A very large volume of data was recorded during the 60-hour flight evaluation program. Thus, it was essential that an efficient computerized data processing and plotting system be developed to provide rapid reduction of the data for subsequent analysis. This section includes brief descriptions of the post-flight data reduction system including the data processing equipment, the data reduction software, and plotting routines.

B.4.1 Data Processing Equipment

A functional block diagram of the post-flight data processing system is shown in Figure B-18. As shown in Figure B-18, the data processing equipment consisted of a Wang 2200B mini-computer with peripherals including an output typewriter, an analog plotter, a cassette tape, and a teletype interface board. The elements of the ASI Wang 2200B mini-computer installation are indicated in Table B-3.

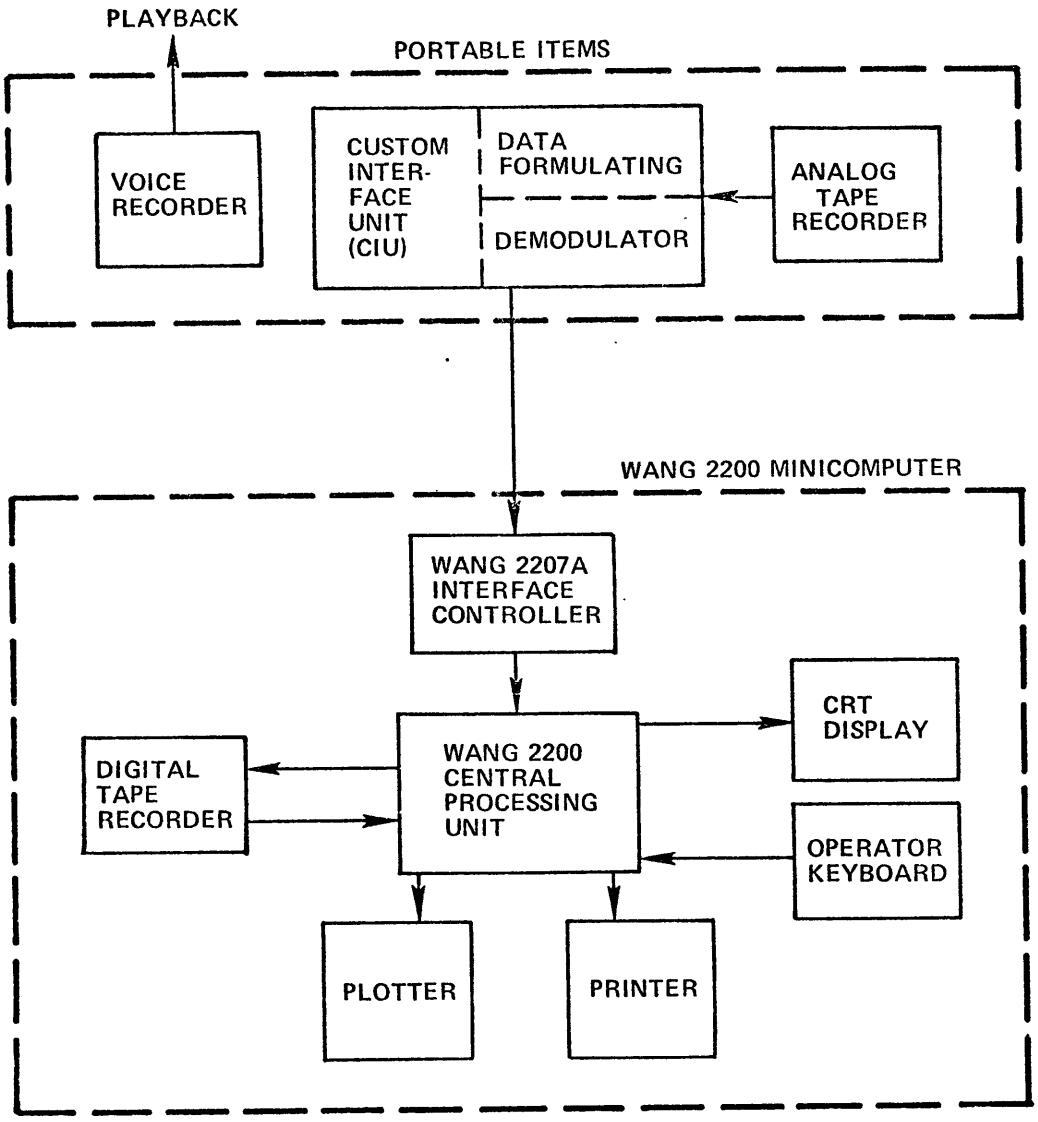


Figure B-18. Post-Flight Data Processing Functional Diagram.

Table B-3. ASI Wang 2200B Mini Computer.

| |
|---|
| 2200B-1 Central Processor |
| 2216/2217 Combined Display/Cassette Drive |
| 2222 Keyboard |
| 2201 Output Writer |
| 2290 CPU Stand |
| 2212 Analog Flatbed Plotter |
| 2207A I/O Interface Controller |
| 4096 Step Memory Option |
| OP-1 Option 1-Matrix ROM |
| OP-3 Option 3-Character Edit ROM |

The 2200B is programmed entirely in BASIC, thus simplifying program writing and debugging. Arithmetic operations are easily handled, and standard system routines include natural log, sine, cosine, tangent, and their inverses; square foot function, absolute value, greatest integer function, signum function, random number generator, etc. The logical functions and character string manipulation functions available are particularly useful for the Omega data reduction and processing tasks.

The small processor has several advantages for processing the type of data obtained on the Omega flight program. First, it can be dedicated to data reduction, eliminating waiting time for processor availability. Secondly, with a small, easy to use machine, errors are easily detected and cor-

rected. Lastly, the use of a small machine allows data processing at low cost.

With the processor dedicated to data reduction, flight test data could be re-written onto the processor's cassettes, processed, and parameters plotted at the rate of three hours of processing per hour of data, with no time lost accessing a distant machine or waiting for plots. Thus, it was possible to perform the data reduction well within the allotted time and even perform additional services to facilitate data interpretation and presentation.

Error detection was easily performed with the small machine. Because each data string was displayed as it was read in, errors caused by faulty tape recorders and interference between the CIU and tape recorders were detected before time was wasted processing bad data. In addition, programming bugs were easily detected and corrected, and program optimization for speed was simplified.

These advantages made up for the constraints of slow speed, small memory, and awkward bulk storage of capabilities of the machine.

B.4.2 Data Transcription

In the air, data were recorded on the portable cassette recorder by the custom interface unit as described in Section B.2.3. On the ground, the cassette recorder was played back through the CIU to generate RS232C teletype data for input to the Wang processor through a teletype interface board. The data at this point of a string of ASCII characters, followed by a carriage return (hex OD) and a line feed (hex OA).

Several anomalies were observed during the transcription. One anomaly was illegal character strings, i.e., strings containing characters not in the repertoire of the CIU. The other types of anomaly caused execution of the transcription program to stop.

The CIU expressed data as four-bit bytes, preceded by high order and parity bits so that the data were presented as the ASCII characters 0,1,...,9,:,;,[,=,], and ?. Occasionally, garbled data appeared, recognizable as characters not in this 16 character set. It was discovered that transmissions from the aircraft VHF transceivers were recorded on the cassette recorder along with the data. Because the data were within the human voice spectrum, garbled data resulted.

The second type of error was harder to discover because processing stopped. It was discovered that the "reset" instruction used to stop processing is an ASCII character (hex 03), and it was hypothesized that data garbled by voice overlay resulted in the interfaces considering a reset instruction to be present.

The actual program used for reading the data was "TRNSFR7+." This program read data into memory in real time and later stored the data onto the processor cassette. Because almost all of the memory of the processor was used for data storage, no processing of the raw data was undertaken in this program. File statistics were generated and printed for the various data logs maintained.

B.4.3 Data Checking

Although data was displayed as it was read in, it was decided to obtain the capability to check unprocessed data as stored on the processor cassette tapes. This served several functions: checking for anomalies in other than

real time, confirmation of data transfer, checking of log parameters, detection of errors in tape management, and checking for anomalies not easily discernible in real time. Two programs, TRNSCHK and DATACHK, were written for data verification.

B.4.3.1 TRNSCHK

TRNSCHK reads individual records from the data tapes, each record containing seven character strings. These strings were then printed on the processor CRT. With the strings displayed thus, strings containing illegal characters could be observed, as could strings which were over- or underlength. With practice, seven character strings could be verified in less than three seconds.

B.4.3.2 DATACHK

In order to detect hardware failures, DATACHK observed the eventual occurrence of a "1" and a "0" in each bit of the character strings. This program was written after a chip failure went undetected until final data processing, depreciating much of the data. DATACHK took each character string in a data file, checked that only strings of proper length and character content were processed, and "ANDed" and "ORed" each string with strings initially set to all zeroes and all ones, respectively. Thus, each bit which had failed and was identically either one or zero was detected. Further, the program had the capability to combine the results of more than one data file so as to provide a larger sample set.

Using DATACHK, the above-mentioned failure of four bits of the LOP 1 readout was confirmed. In addition, it was discovered that the least significant bit of the S/N counter had failed, but this error was determined to be insignificant and was not corrected. One known anomaly detectable with

TRNSCHK was the result of moving a defective chip on the CIU data bus. Because the CIU circuitry on the data bus was CMOS, the capacitance of the bus receiver duplicated the preceding byte of data during the time slot of the removed chip.

B.4.4 Plotting Routines

The recorded data were processed to yield several different types of plots. These plots included S/N ratios, Omega estimates of aircraft position, miles-to-go (MTG), various status flags, and needle deflection. These are discussed in the following sections.

B.4.4.1 Miles-To-Go Plotting

The miles-to-go (MTG) was plotted on a linear scale of 0 to 75 miles, with tic marks on the y axis representing 25 mile steps. No filtering or special processing of any kind was done. Not all character strings were processed for MTG, however. Any string which was over- or under-length or which contained illegal characters was not processed. A blank space was left on the plot, however, indicating deleted data. In addition, space was left to indicate the lack of data acquisition while a cassette was being changed in the aircraft.

B.4.4.2 Status Flag Plots

Four status flags were recorded by the CIU: to/from flag, autozero, lane accumulator reset, and weak signal on any station used for navigation. With the exception of the to/from flag, which was plotted as a continuous line, each flag was plotted as a tic mark above the x axis when it occurred. Lables for these flags are shown on the plots. Invalid character strings were omitted as in the MTG plots.

B.4.4.3 Needle Deflection Plotting

Needle deflection plots recorded the deviation of the needle sampled every ten seconds, the deflection calculated from the phase measurements at the end of a ten-second Omega transmission sequence. In practice, the needle was prone to oscillations at frequencies higher than those recordable by the sampler. These oscillations were apparent to the pilot and required the pilot to manually filter the CDI readout. As in the miles-to-go plotting routine, breaks in the data result in discontinuous plots of needle deflection.

B.4.4.4 S/N Ratio Plots

The needle deflection plotting routine also plotted S/N ratios as a user selectable option. S/N was recorded as an 8-bit S/N count number between 0 and 255, which gave an estimate of the S/N ratio according to the formula

$$\text{Count number} = 128 + 100 \times (\text{broadcast time of Omega station}) \times \text{ERF}\sqrt{\text{S/N power}}$$

The plotting routine used code to limit the signal-to-noise ratios to a minimum of -30 dB. The maximum was based upon the transmission time of the station. Invalid strings were omitted as was the case with the MTG plots.

B.4.4.5 Map Plots

The lane accumulators were used by the internal Omega receiver processor to generate navigation information for display to the pilot. These accumulators were recorded by the CIU and were used for generating map plots. The map plot routine converted the accumulated lane change between last reset point and present position, with four valid bits per lane of LOP 1 (on the ASI flights only) and eight valid bits per line of LOP 2. The four low-

order bits of LOP 1 were noise, being the (fairly constant) four high-order bits of the Station C S/N readout.

The LOP accumulators were read out and converted to numerical form. A linearization based upon a circular earth model was then used to determine change of latitude and longitude from the last reset point and, thus, the present estimate of latitude and longitude was derived. These points were then plotted as a continuous line, breaks occurring when data were not consecutive, as was the case with invalid character strings. All plots submitted in this report were made on Mercator projection maps, although the capability was also developed to plot on Lambert conformal projection maps.

JEPPESEN SANDERSON

LIMITED PERMISSION TO REPRODUCE COPYRIGHTED MATERIAL

JEPPESEN SANDERSON, INC., owner of copyrights covering avigation, approach and airport charts in the Jeppesen Airway Manual, hereby grants to C. E. Wischmeyer, Research Assistant, Flight Transportation Laboratory, of Dept. of Aeronautics & Astronautics, Mass. Institute of Tech., Cambridge, Mass. limited permission to reproduce and modify Bedford, Massachusetts Instrument Approach Procedure Charts 11-1/Arpt., 13-1/16-1, 16-2/Blank, 10-3 per conversation of 6-5-75 EW
under the following terms and conditions:

1. The copyrighted material shall be used for the purpose of writing a thesis
and for no other purpose.

2. All reproductions of the copyrighted material shall bear the notice of copyright, "Copyright 19 * Jeppesen & Co. (or Jeppesen Sanderson,Inc.)", appearing on printed copies of the original material, and also shall be marked "Illustration only--not to be used for navigational purposes."
*Appropriate Date.

3. The copyrighted material shall not be reduced in size, altered, mutilated, or revised in any way or manner prior to or during the process of reproduction without the written consent of Jeppesen Sanderson, Inc.

4. C. E. Wischmeyer/Massachusetts Institute of Technology shall inform each and every artist, photographer, or other organization, or person who takes part in the reproduction of this material, of the terms of this agreement and shall furnish Jeppesen Sanderson, Inc., with two (2) copies of all reproductions made as a result of this agreement and two (2) copies of all material relating to such reproduction.

5. No other reproduction rights are granted nor can this agreement be construed as applying to any other purpose or organization without permission from an authorized representative of Jeppesen Sanderson, Inc.

6. C. E. Wischmeyer/Massachusetts Institute of Technology assents to the above terms and conditions by its written acceptance below.

JEPPESEN SANDERSON, INC.

By: Jack H. Dana

Date: April 21, 1975

ACCEPTED:

Massachusetts Institute of Technology

By: C.E. Wischmeyer

Date: 6-5-75

## REFERENCES


1. Omega Propagation Correction Tables. H.O. Pub. No. 224. Defense Mapping Hydrographic Center, Washington, D.C.

2. Baxa, E.G., and Piserchia, P.V. "Recent Results of Parameteric Analysis of Differential Omega Error." ION Second Omega Symposium, Washington, D.C. 1974.

3. Beukers, J.M. "VLF and LF for Navigation." Navigation 21, No. 2.

4. Sakran, F.C. "Accuracy Specifications for Automatic Omega Receivers." ION Second Omega Symposium, Washington, D.C. 1974.

5. Baker, J.D. "The Weibull Distribution as a Model for Radial Errors." Navigation 14, No. 2. Summer 1967.

6. Menon, M.V. "Estimation of the Shape and Scale Parameters of the Weibull Distribution." Technometrics 5, No. 2. May 1963.

7. HP-55 Statistics Programs. Hewlett-Packard Company. 1974.

8. Terzian, R.C. "Discussion of 'A Note on CEPs.'" IEEE AES-10, No. 5. September 1974.

9. Gallagher, R.C. Information Theory and Reliable Communication. John Wiley and Sons, 1968.

10. Hoffman, W.C., Hollister, J.D. "Guidance and Navigation Requirements for Commercial VTOL Operations." NASA CR-132423. January 1974.

11. Omega Mark III Navigation System Description and Operation Manual. Dynell Electronics Corporation, Melville, N.Y. 1974.

12. Burhans, R.W. "Phase-Difference Method Offers Low Cost Navigation Receivers." Electronics, Vol. 47. September 5, 1974.

13. Feldman, D.A. "An Atmospheric Noise Model with Application to Low Frequency Navigation Systems." Ph.D. Thesis, MIT. June 1972.

14. Chamberlin, K.A. "The Memory-Aided Digital Phase Lock Loop." ION Second Omega Symposium, Washington, D.C. 1974.

15. Cox, D.B., et al. "Digital Phase Processing for Low-Cost Omega Receivers." ION Second Omega Symposium, Washington, D.C. 1974.

16. Howell, J.D., Hoffman, W.C., Hwoschinsky, P.V., and Wischmeyer, C.E. "Flight Evaluation of Omega Navigation in a General Aviation Aircraft." NASA CR 132720.

17. Hwoschinsky, P.V. "Flight Test and Evaluation of a Low Cost Omega Receiver for General Aviation." Engineer in Aeronautics and Astronautics Thesis, MIT. June 1975 (NASA CR-132677).

18. Lubin, S.J., and Lewis, B.M. "Effects of Weather on Airborne Omega." Navigation 19, No. 2. Summer 1972.

19. Personal communication with Ray Gupta, The Analytic Sciences Corporation, Reading, MA. April 25, 1975.

20. Miller, I., and Freund, J.E. Probability and Statistics for Engineers. Prentice Hall, Englewood Cliffs, NJ. 1965.

21. Bortz, J.E., Gupta, R.R., Scull, D.C., and Morris, P.B. "Omega Signal Coverage Prediction." ION Second Omega Symposium, Washington, D.C. 1974.

22. Beukers, J.M. "VLF and LF for Navigation." Navigation 21, No. 2. Summer 1974.

23. Nard, G. "State of Experimentations and Program of Development of Differential Omega in France." ION Second Omega Symposium, Washington, D.C. 1974.

24. Gaon, B.N. "Hand-Held Calculator Technology Applied to an Advanced Omega Receiver." ION Second Omega Symposium, Washington, D.C. 1974.

25. Hazelrigg, G.A., "Omega Air Data Computer," ATC Memo No. 2 (unpublished) Aerospace Systems Laboratory, Princeton University, N.J. March 1975.

26. Lytle, C.D., and Bradshaw, E.S. "A Comprehensive Program for Investigation of Various Omega Operational Modes with Selected Data Analysis Results." ION Second Omega Symposium, Washington, D.C. 1974.

27. Pierce, J.A. "The Use of Composite Signals at Very Low Radio Frequencies." Harvard University Tech. Rep. 553. 1968.

28. Mactaggart, D. "An Empirical Computed Evaluation of Composite Omega." ION Second Omega Symposium, Washington, D.C. 1974.

29. U.S. Standard for Terminal Instrument Procedures. FAA Handbook 8260.3A. February 1970.

30. Dodge, S.M. "A Comparative Analysis of Area Navigation Systems for Navigation." MIT Flight Transportation Lab Report R-74-1. June 1973.

31. Miller, H.G. "Differential Omega in the Air Traffic Control Environment." ION Second Omega Symposium, Washington, D.C. 1974.

32. Bortz, J.E., Gupta, R.R., Scull, D.C., and Morris, P.B. "Omega Signal Coverage Prediction." ION Second Omega Symposium, Washington, D.C. 1974.

33. Swanson, E.R. "Omega." Navigation 18, No. 2. Summer 1971.

## BIOGRAPHY

Edward Wischmeyer was born July 19, 1949 in Houston, TX, where he attended St. John's School. After graduating in 1967, he attended Brown University in Providence, RI, where he earned the Sc.B. in Applied Mathematics, cum laude, in 1971. He then attended the Massachussetts Institute of Technology, earning the S.M. degree in 1973.

Dr. Wischmeyer is a member of Sigma Xi, the Institute of Navigation, and the Institute of Electrical and Electronics Engineers. He holds a commercial pilot's license with an instrument rating, and has more than 300 flight hours.